

**A DISSERTATION REPORT**

On

**“BLAST LOADING ON REINFORCED CEMENT  
CONCRETE BARRIER”**

Submitted in partial fulfilment of the requirements for the award of the  
degree

of

**MASTER OF TECHNOLOGY**

in

**STRUCTURAL ENGINEERING**

by

**SIDDHARTH SHARMA**

**(17523021)**



**DEPARTMENT OF CIVIL ENGINEERING  
INDIAN INSTITUTE OF TECHNOLOGY ROORKEE  
ROORKEE-247667 (INDIA)  
NOVEMBER, 2018**

## CERTIFICATE

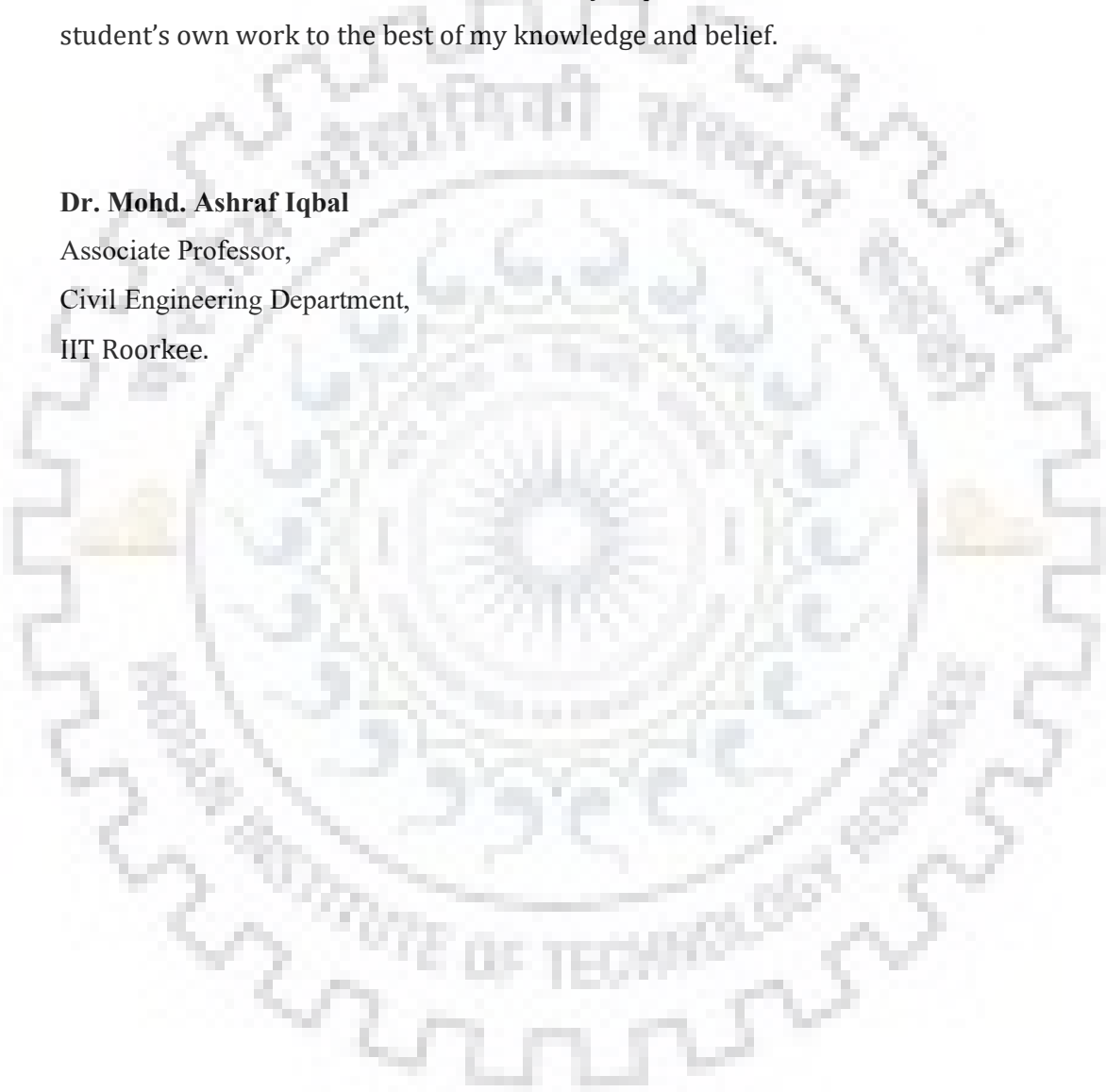
This is to certify that the project entitled BLAST LOADING ON REINFORCED CEMENT CONCRETE BARRIER submitted by Siddharth Sharma is partial fulfilment of requirements for award of the degree of Master of Technology (Civil Engineering) to IIT Roorkee has been carried out under my supervision and in authentic record of student's own work to the best of my knowledge and belief.

**Dr. Mohd. Ashraf Iqbal**

Associate Professor,

Civil Engineering Department,

IIT Roorkee.



## ACKNOWLEDGEMENT

I wish to express my deep sense of gratitude and sincere thanks to my supervisor, Dr. Mohd. Ashraf Iqbal, Associate Professor, Department of Civil Engineering, IIT Roorkee, for his consistent supervision and guidance in completing my dissertation report. I would like to thank all the teaching and non-teaching staff members of the department who have contributed directly or indirectly in successful completion of my dissertation work. I would also like to thank all my fellow friends for their help and encouragement.

Date: 03/06/2019

Place: Roorkee

Siddharth Sharma

(17523021)



## ABSTRACT

Blast loading on structures is an extreme event in which pressure pulse with overpressure many times above atmospheric and very high specific impulse impinges on surfaces of the structure. The effects of blast wave on RCC structures constitute damage in the form of cracks, spalling, scabbing and excessive deformation. The material behaviour in this stress range is essentially non-linear and affected by high strain rates.

In this work, numerical studies on Abaqus/explicit were performed to study effect of blast waves on 2 way simply supported RCC slab for different combinations of charge weight and standoff distances. The damage to the slab for different cases was observed. It was concluded that damage increases more rapidly with decreasing standoff distances as compared to increasing charge weight.

The conventional blast resistant design of structure constitutes idealising the structure as a single DOF system and blast loads as impulse loads. The design objective is to make the structure stiff and ductile enough to sustain a predefined deformation and damage level based on protection category.

In the presented work, design of cantilever and fixed blast barrier for protection categories type 1 and type 2 for a specified blast load has been presented.

The effect of presence of sacrificial cladding of cellular foam such as aluminium foam has shown promising results in protecting structures against effect of blast loads. Numerical studies to compare the performance of blast barriers with and without sacrificial cladding is undertaken.

The data for material models used for modelling the behaviour of concrete, steel and aluminium foam namely concrete damaged plasticity, Johnson cook hardening and crushable foam model respectively were taken from literature and validated by replicating experimental programs.

The numerical studies to compare the performance of blast barriers with and without foam cladding showed that foam cladding significantly reduced concrete damage and deformation. Foam claddings are effective in reducing damage by global response

reduction and attenuation of stress waves in solids. It was found that stiffer and lighter blast barriers are better suited for global response reduction using sacrificial foam.

Numerical studies were performed to compare the efficacy of sacrificial foams of two different thicknesses and of two different densities. It was concluded that increasing thickness of foam cladding beyond minimum design thickness is not beneficial and that foam of lower density is better suited for stress wave attenuation.

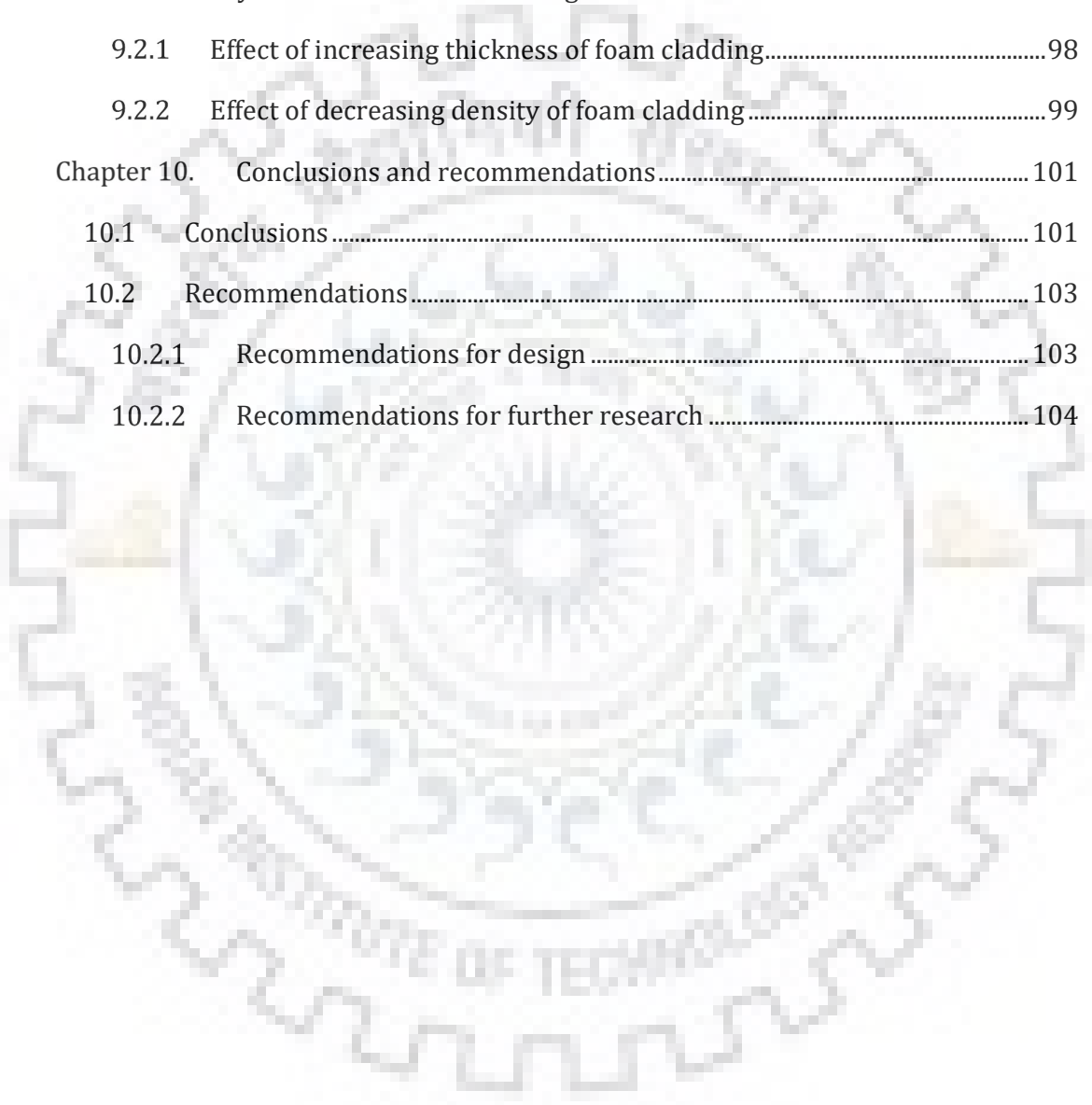


# Table of Contents

Chapter 1. Introduction .....	1
1.1 Properties of a blast wave .....	1
1.2 Effect of blast wave on structures .....	9
1.3 Blast resistant design of structures .....	15
1.4 Sacrificial cladding in blast resistant structures .....	24
1.5 Numerical analysis in Abaqus/Explicit.....	30
Chapter 2. Literature Review.....	34
2.1 General.....	34
2.2 Literature survey .....	34
Chapter 3. Objective and Methodology.....	39
3.1 Objective .....	39
3.2 Methodology .....	40
Chapter 4. Design of RCC blast barriers.....	41
4.1 Type 1 Cantilever blast barrier .....	41
4.2 Type 2 Cantilever blast barrier .....	45
4.3 Type 2 Fixed blast barrier .....	49
4.4 Aluminium foam sacrificial cladding.....	52
Chapter 5. Validation of material models used.....	54
5.1 Validation of material model for concrete and steel .....	54
5.1.1 Experimental program.....	54
5.1.2 Abaqus Model.....	54
5.1.3 Comparison of experimental and numerical result.....	58
5.2 Validation of material model for aluminium foam .....	59
5.2.1 Experimental programme .....	59
5.2.2 Abaqus Model.....	61

5.2.3	Comparison of experimental and numerical results.....	65
Chapter 6.	Parametric study .....	68
6.1	Abaqus model.....	68
6.2	Trends observed .....	69
Chapter 7.	Sacrificial cladding in blast barriers.....	71
7.1	Type 1 cantilever blast barrier.....	71
7.1.1	Without aluminium foam sacrificial cladding.....	71
7.1.2	With sacrificial cladding.....	73
7.1.3	Comparison of performance of barrier with/ without foam cladding ....	74
7.2	Type 2 cantilever blast barrier.....	76
7.2.1	Without aluminium foam sacrificial cladding.....	76
7.2.2	With sacrificial cladding.....	78
7.2.3	Comparison of performance of barrier with/ without foam cladding ....	78
7.3	Type 2 fixed blast barrier .....	81
7.3.1	Without aluminium foam sacrificial cladding.....	81
7.3.2	With sacrificial cladding.....	83
7.3.3	Comparison of performance of barrier with/ without foam cladding ....	84
Chapter 8.	Efficacy of sacrificial foam cladding .....	88
8.1	Effect of increasing thickness of foam cladding.....	88
8.1.1	Model details for revised foam cladding thickness.....	88
8.1.2	Comparison of performance of barrier for 200mm/100mm thick foam cladding.....	89
8.2	Effect of decreasing density of foam cladding .....	91
8.2.1	Foam cladding densities tested .....	91
8.2.2	Comparison of performance for 20%/10% relative density foam cladding	92
Chapter 9.	Interpretation of Results.....	94

9.1	Sacrificial cladding in Blast barrier.....	94
9.1.1	Type 1 cantilever blast barrier .....	94
9.1.2	Type 2 cantilever blast barrier .....	96
9.1.3	Type 2 fixed blast barrier .....	97
9.2	Efficacy of sacrificial foam cladding.....	98
9.2.1	Effect of increasing thickness of foam cladding.....	98
9.2.2	Effect of decreasing density of foam cladding .....	99
Chapter 10.	Conclusions and recommendations.....	101
10.1	Conclusions .....	101
10.2	Recommendations.....	103
10.2.1	Recommendations for design .....	103
10.2.2	Recommendations for further research .....	104





## List of figures

Figure 1-1: Pressure generated due to shock wave at a point.....	1
Figure 1-2: Blast wave propagation.....	2
Figure 1-3: Blast wave Pressure-Time profile.....	3
Figure 1-4: Parameters of the positive phase of a spherical wave from a free-air burst .....	7
Figure 1-5: Parameters for the positive phase of a hemispherical wave from a surface burst.....	8
Figure 1-6: Structure idealised as a SDOF system.....	9
Figure 1-7: Blast load idealised as triangular pulse.....	9
Figure 1-8: Quasi-static loading regime.....	11
Figure 1-9: Impulsive loading regime.....	12
Figure 1-10: Graphical representation of Quasi static (I), Impulsive (II) and Dynamic (III) Response.....	13
Figure 1-11: Typical strain rates for different types of loading.....	13
Figure 1-12: Structure and its equivalent SDOF system.....	15
Figure 1-13: Support rotation for structural elements.....	19
Figure 1-14: Typical resistance deflection curve of RCC.....	20
Figure 1-15: Bilinear idealisation of the deflection resistance curve of RCC section ..	21
Figure 1-16: Different materials in use as sacrificial cladding.....	25
Figure 1-17: Typical stress strain curve for aluminium foam.....	26
Figure 1-18: Idealised compression curve for aluminium foam.....	26
Figure 1-19: (a) Aluminium foam subjected to blast loading and (b) Blast load on the front cover of foam depicted as triangular pulse and pressure transferred through foam to the parent structure depicted as long duration low intensity rectangular pulse. .....	27
Figure 1-20: Hansen's model of foam compression under blast load.....	27
Figure 1-21: (a) Densification strain and (b) Assumed stress strain curve for the model .....	28
Figure 5-1: Wang et al. details of slab, reinforcement and support conditions.....	54
Figure 5-2: Experimentally observed damage on both faces of slab.....	58
Figure 5-3: Numerically obtained Tension damage on both faces of slab.....	58

Figure 5-4: Deflection vs time curve for centre of slab.....	59
Figure 5-5: Apparatus used for experiments by Langdon et al. ....	61
Figure 5-6: Foam hardening data for 10% and 20% relative density foam.....	63
Figure 5-7: Displacement contours for bonded aluminium foam.....	65
Figure 5-8: Displacement VS time curve for cover plate bonded with aluminium foam. .....	65
Figure 5-9: Displacement contours for unbonded aluminium and cover plate.....	66
Figure 5-10: Displacement time curve for top of unbonded aluminium foam.....	66
Figure 6-1: Effect of charge weight on concrete damage .....	69
Figure 6-2: Effect of standoff distance on concrete damage .....	70
Figure 6-3: Effect of both charge weight and standoff distance on concrete damage.	70
Figure 7-1: Assembly details of Type 1 blast barrier .....	73
Figure 7-2: Deflection of type 1 blast barrier .....	74
Figure 7-3: Comparative deflection vs time curve.....	74
Figure 7-4: Concrete tension damage for type 1 cantilever blast barrier .....	75
Figure 7-5: Deflection contours for type 2 blast barrier.....	79
Figure 7-6: Deflection VS time curve for type 2 cantilever blast barrier.....	79
Figure 7-7: Concrete tension damage for type 2 cantilever blast barrier.....	80
Figure 7-8: Assembly of type 2 fixed blast barrier.....	84
Figure 7-9: Deflection contours of fixed blast wall.....	85
Figure 7-10: Deflection VS time curve for fixed blast barrier .....	85
Figure 7-11: Concrete tension damage contours for fixed blast barrier.....	86
Figure 8-1: Assembly details of model with different foam cladding thicknesses (type 2 cantilever blast barrier).....	89
Figure 8-2: Deflection VS time curve for 2 thicknesses (type 2 cantilever blast barrier) .....	89
Figure 8-3: Concrete damage for type 2 cantilever blast barrier (effect of thickness of foam).....	90
Figure 8-4: Concrete damage for different foam density (Type 2 cantilever blast barrier).....	92
Figure 8-5: Deflection vs time curve for different densities (type 2 cantilever blast barrier).....	93

## List of tables

Table 1-1: DIF for concrete and reinforcing bars .....	18
Table 1-2: Support rotations and ductility ratios as per protection categories .....	19
Table 5-1: CDP values for plasticity parameters.....	55
Table 5-2: CDP stress strain data for compression .....	55
Table 5-3: CDP damage data for compression .....	55
Table 5-4: CDP stress strain data for tension.....	56
Table 5-5: Damage data for tension.....	56
Table 5-6: J-C strength parameters for DP-590 steel .....	56
Table 5-7: J-C strength parameters for mild steel.....	57
Table 5-8: J-C parameters common to both mild steel and DP-590 steel.....	57
Table 5-9: Partwise details of Abaqus model .....	57
Table 5-10: Experimental Vs numerical deflection at centre of slab.....	59
Table 5-11: Blast tests chosen to be replicated.....	60
Table 5-12: Density and elasticity modulus for two foam densities .....	62
Table 5-13: Part details for bonded aluminium foam model.....	63
Table 5-14: Part details for bonded aluminium foam model.....	64
Table 5-15: Comparison of experimental and numerical crushed thickness .....	67
Table 6-1: Partwise details for Abaqus model .....	68
Table 6-2: List of tests with different charge weight and standoff distance .....	69
Table 7-1: Part details of type 1 cantilever blast barrier.....	72
Table 7-2: Additional part details for foam cladding (type 1 cantilever) .....	73
Table 7-3: Deflection reduction for Type 1 cantilever blast barrier .....	76
Table 7-4: Part details for type 2 cantilever blast barrier.....	77
Table 7-5: Additional part details for foam cladding (type 2 cantilever) .....	78
Table 7-6: Deflection reduction due to foam cladding (Type 2 fixed barrier) .....	81
Table 7-7: Part details for fixed blast barrier .....	82
Table 7-8: Additional part details for foam cladding (type 2 fixed blast barrier) .....	83
Table 7-9: Deflection reduction for type 2 fixed blast barrier .....	87
Table 8-1: Revised part details for foam cladding .....	88
Table 8-2: Deflection for different foam thicknesses (type 2 cantilever blast barrier) .....	91

Table 8-3: Foam cladding density and thickness used .....91

Table 8-4: Deflection for 2 foam densities (type 2 cantilever blast barrier) .....93



### 1.1 Properties of a blast wave

A blast wave is the result of an explosion. An explosion is the sudden release of energy in the form of rapidly expanding gasses due to the process of combustion of combustible materials of high calorific value in the presence of sufficient oxygen.

When an explosion occurs, the rate at which heat is generated due to combustion is very high. It leads to quick build-up of pressure and the air in the vicinity of the explosive is subject to a high pressured expansion in the radial direction.

In the case of high explosives, this pressure increase is tremendous and leads to the formation of a shock wave lead by a shock front. This shock front travels at supersonic velocities and has a very high overpressure i.e.: pressure over and above atmospheric pressure, temperature and density as compared to ambient [1].

This shock front is followed by rapid decrease in pressure, density and temperature with increasing distance from shock front. The pressure and density falls below ambient before reducing to zero creating a negative or suction region. This shock front along with its tail moves in the atmosphere as a mechanical wave of pressure disturbance using energy from the explosion [1].

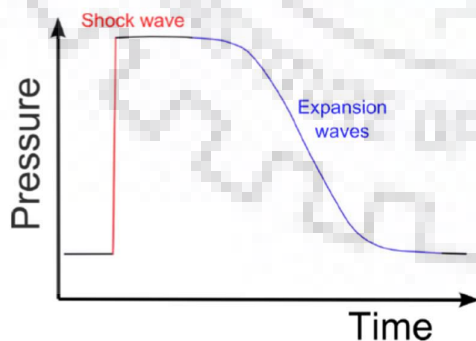


Figure 1-1: Pressure generated due to shock wave at a point.

Here, the focus is on high explosives that cause the generation of a blast wave which is a radial shock wave with a shock front having overpressure many times above the atmospheric pressure, high temperature, density and which advances at speeds many times above the speed of sound in that medium.

The pressure, density, temperature and velocity of advancement of the gasses decreases approximately exponentially with increasing distance from the shock front [2].

As the blast wave advances through the medium, its energy per unit volume decreases and hence the velocity of advancement, the overpressure at the shock front and the density and temperature decrease. In the far field, the shock wave losses most of its energy and turns into an acoustic wave and the blast is heard as a loud 'Thud' sound from a large distance [2].

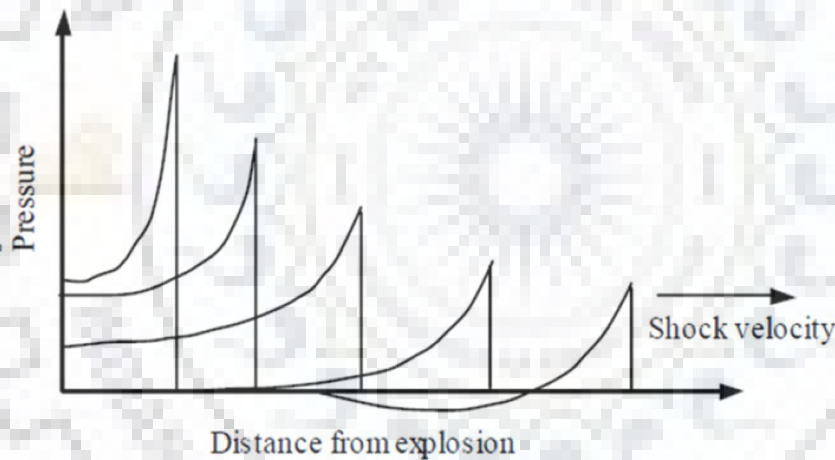


Figure 1-2: Blast wave propagation

The pressure time profile of a shock wave due to blast has two phases. One is the positive phase duration  $t_d^+$ , in which overpressure is positive or the pressure is more than atmospheric pressure and the negative phase duration  $t_d^-$ , wherein overpressure is negative or the pressure is less than atmospheric pressure [1].

As the shock wave propagates in the air, its energy density decreases which causes the peak overpressure and impulse to reduce and the time duration of the pressure pulse to increase [1].

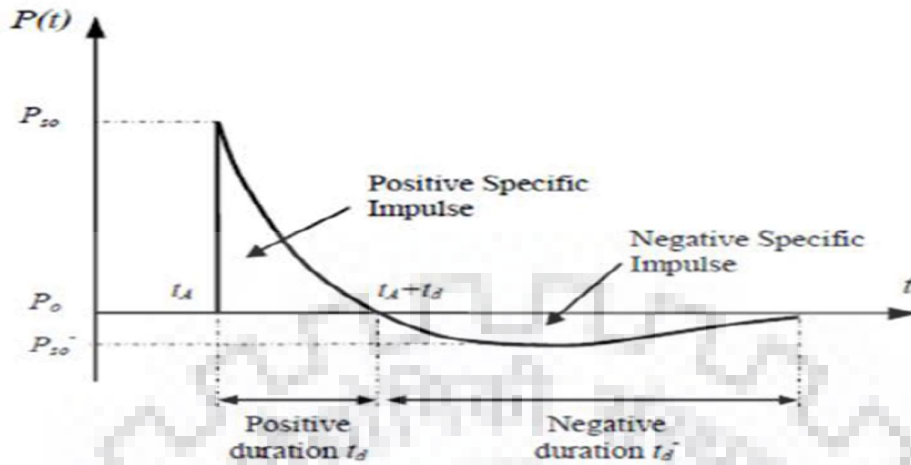


Figure 1-3: Blast wave Pressure-Time profile

In a blast wave, parameters such as overpressure, impulse etc. are usually given in terms of a quantity known as scaled distance Z.

$$Z = \frac{R}{W^{\frac{1}{3}}}$$

Where,

Z= Scaled Distance.

R= Standoff distance from point of Detonation.

W= TNT equivalent mass of the explosive.

Broude (1955) estimated the peak overpressure due to a spherical blast for different range of overpressures. The overpressures as given by Broude (in bar) are:

$$P_{so} = \frac{6.7}{Z^3} + 1 \quad (\text{For } P_{so} > 10 \text{ bar})$$

$$P_{so} = \frac{0.975}{Z} + \frac{1.455}{Z^2} + \frac{5.85}{Z^3} - 0.019 \quad (\text{For } 0.1 \text{ bar} < P_{so} < 10 \text{ bar})$$

These relations are valid for spherical wave front, which take place when the point of detonation is situated in free air away from any reflecting surfaces. Hence, these blasts are known as free air bursts or air bursts [1].

When the point of detonation is at the ground or close to the ground, the bottom half part of the spherical wave front that would have otherwise formed quickly gets reflected from the ground surface and a hemispherical wave front of almost double the energy intensity is formed. Since the ground is not a perfect reflector, some energy of the blast gets absorbed in the ground and around 0.8 times the energy is reflected. The hemispherical wave front thus formed is around 1.8 times stronger than the spherical wave front resulting from a detonation of equal charge weight.

When the point of detonation is neither in free air nor close to the ground, the reflection and interference of the blast wave presents a more complex situation which involves Mach stem formation.

The overpressure at a point as the blast wave crosses it, rises suddenly to  $P_{so}$  at a time  $T_A$  after which it decreases almost exponentially to zero at a time  $T_A + T_D^+$ , now it attains negative value (suction pressure) and at a time  $T_A + T_D^+ + T_D^-$ , it becomes zero.

Here,

$T_A$  = Arrival Time.

$T_D^+$  = Positive phase duration.

$T_D^-$  = Negative phase duration.

This variation of overpressure is closely approximated by Friedlander's curve. Friedlander's curve represents variation of blast overpressure with time [3].

$$P(t) = P_s e^{-\frac{\alpha t}{t^*}} \left( 1 - \frac{t}{t^*} \right)$$

Here,  $t^*$  represents the time after which the blast pressure first becomes zero after arrival. Or it is the positive phase duration  $T_D^+$ .  $\alpha$  is a multiplier that determines how quickly the blast pressure decays.



The impulse per unit area in a blast wave may be arrived upon by integrating the pressure as per Friedlander waveform over a time interval from  $T_A$  (arrival time) to  $T_A + T_D^+ + T_D^-$  (Arrival time + total phase duration)

The positive phase specific impulse i.e.: impulse per unit area of positive phase is given by:

$$I_S^+ = \int_{t_a}^{t_a + t_d^+} P_s \cdot dt$$

Similarly, the negative phase specific impulse, ie: the impulse per unit area of the negative phase is given by:

$$I_S^- = \int_{t_a + t_d^+}^{t_a + t_d^+ + t_d^-} P_s \cdot dt$$

Like any mechanical wave, blast wave gets reflected of the rigid boundaries of the material medium in which it traverses. The result is an increase in the overpressure in the vicinity of the surface from which the blast wave gets reflected and the formation of a reflected blast wave. The reflected overpressure is given by [1]:

$$P_r = 2P_{so} \left\{ \frac{7P_o + 4P_{so}}{7P_o + P_{so}} \right\}$$

Where,

$P_r$  = Peak Reflected overpressure.

$P_{so}$  = Peak side on (Unreflected) overpressure.

$P_o$  = Atmospheric overpressure.

The reflected Impulse per unit area may be likewise calculated by substituting reflected overpressure in place of side on overpressure in the impulse calculation formulae.

A readymade expression to solve for specific impulse using pressure from the following Friedlander waveform [3]:

$$P_s(t) = P_{so} \left( 1 - \frac{t}{t_o} \right) e^{-b \frac{t}{t_o}}$$

is given by:

$$i_s = \int_{t_A}^{t_A+t_o} P_s(t) dt = \frac{P_{so} t_o}{b} \left[ 1 - \frac{(1 - e^{-b})}{b} \right]$$

Here,

$P_{so}$  = Peak side on overpressure.

$t_o$  = Positive phase duration.

$b$  = Decay coefficient.

Though this expression is meant for specific impulse, it may be used for calculating reflected impulse by replacing peak side on overpressure with peak reflected impulse. It may be noted that the time period here is the positive phase duration, hence, the impulse calculated is for the positive phase duration only. The impulse transferred in the negative phase duration is insignificant and inconsequential for most cases of blast loading.

The technical manual of Kingery and Bulmash is the most widely used and accepted approach for the determination of blast wave parameters. One of the most useful characteristics in this manual, is that it contains polynomial formulations for both spherical and hemispherical blast waves. These formulations may be used to calculate the peak overpressure, the resulting impulse and the positive phase duration [3]. These equations have already been incorporated in various computer explicit codes including the CONWEP code in ABAQUS/EXPLICIT which was used for the present work. Figure 1-3 shows such a diagram for the positive phase of a free-air burst and Figure 1-4 for the positive phase of a surface burst.

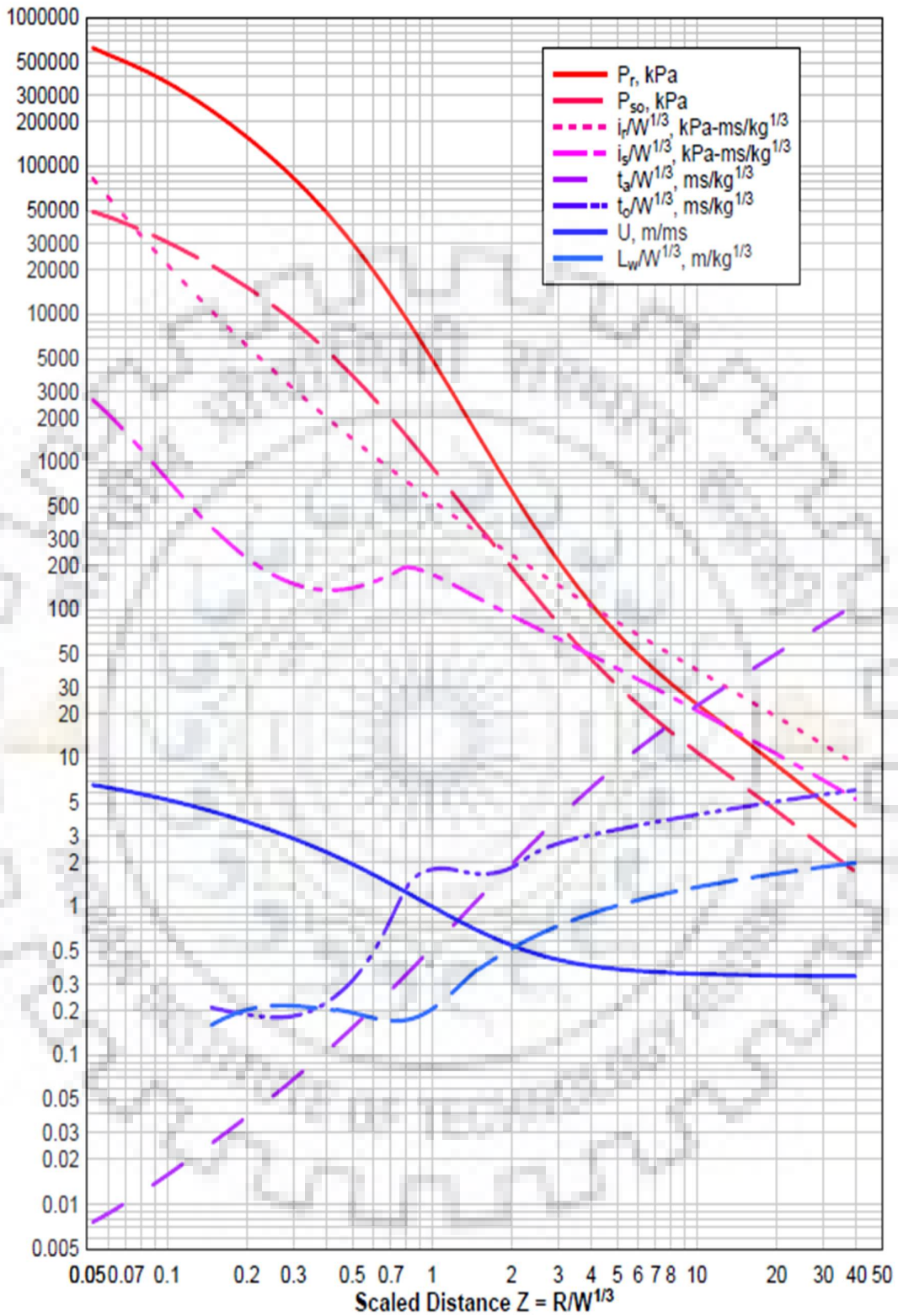


Figure 1-4: Parameters of the positive phase of a spherical wave from a free-air burst

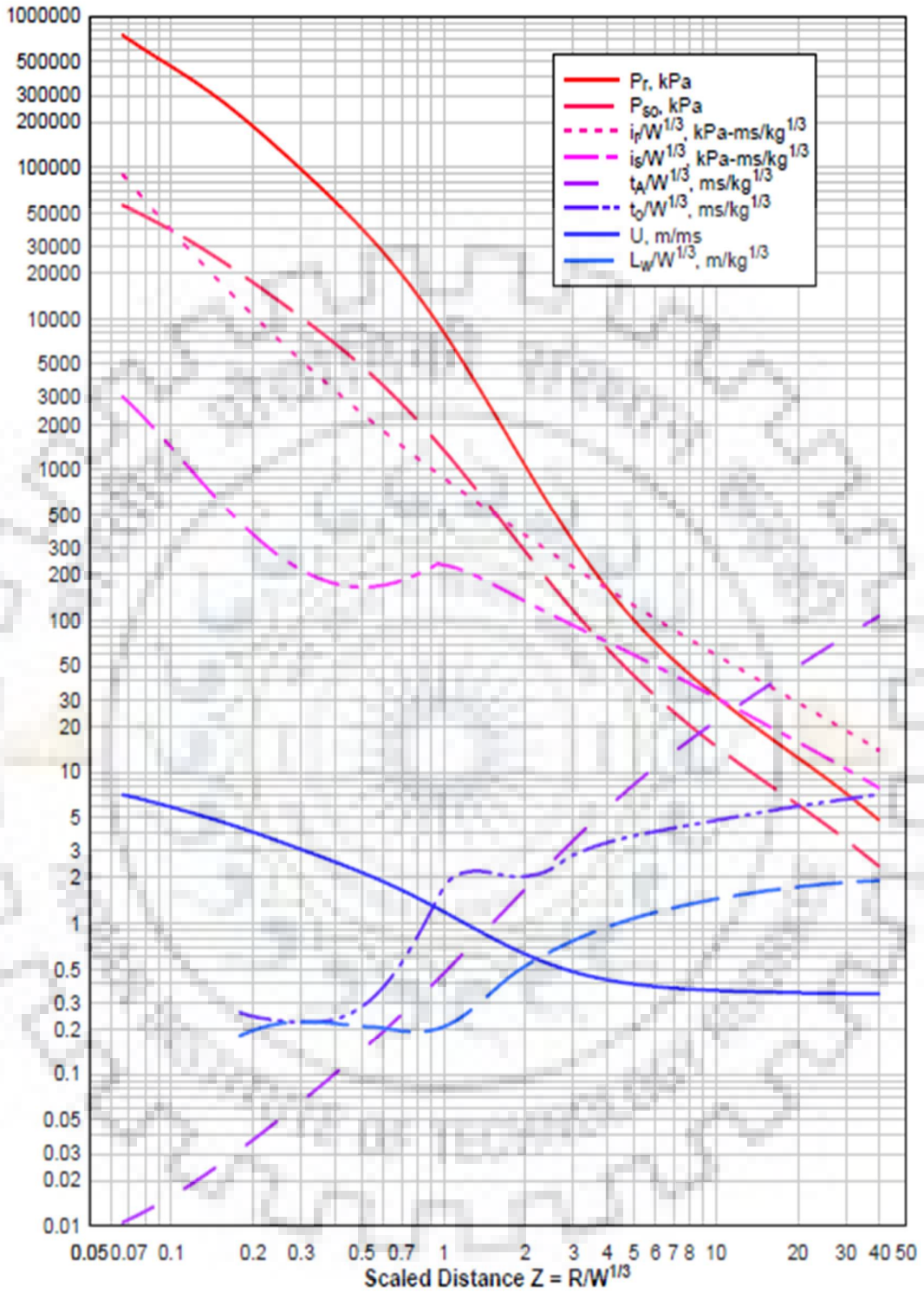


Figure 1-5: Parameters for the positive phase of a hemispherical wave from a surface burst.

## 1.2 Effect of blast wave on structures

Structures are frequently idealised as single degree of freedom systems in order to assess their response to blast load, while the blast loads are idealised as a triangular pulse with a peak force [4].

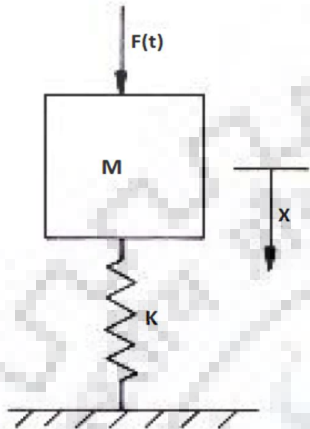


Figure 1-6: Structure idealised as a SDOF system

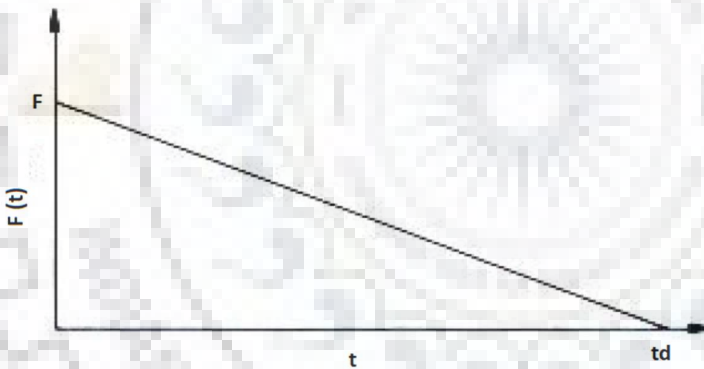


Figure 1-7: Blast load idealised as triangular pulse

The forcing function for this triangular pulse is:

$$F(t) = F \left( 1 - \frac{t}{t_d} \right)$$

And the impulse transferred by such load of triangular pulse is given by area under the curve.

$$I = \frac{1}{2} F t_d$$

The equation for motion of this structure is given by:

$$M\ddot{x} + Kx = F\left(1 - \frac{t}{t_d}\right)$$

For such forced vibration, the ratio of maximum dynamic to static displacement, also known as dynamic load factor (DLF), depends on the ratio of time of decay of the forcing function and the time period of natural vibration of the system. This is mathematically expressed as [4]:

$$\frac{x_{\max}}{F/K} = \psi(\omega t_d) = \psi\left(\frac{t_d}{T}\right)$$

Where  $\omega = \sqrt{K/M}$  is the angular frequency of free vibration of the system.

This ratio of maximum dynamic to static amplitude or displacement is categorised into 3 different regimes based on the limits of ratio of decay time of forcing function and time period of natural vibration of the system. They are [1]:

- $40 < \omega t_d$  -Impulsive loading regime
- $0.4 > \omega t_d$  -Quasi static loading regime
- $0.4 < \omega t_d < 40$  -Dynamic loading regime

In the case of quasi static loading regime, the decay time of forcing function is much larger than the time period of natural vibration of the system.

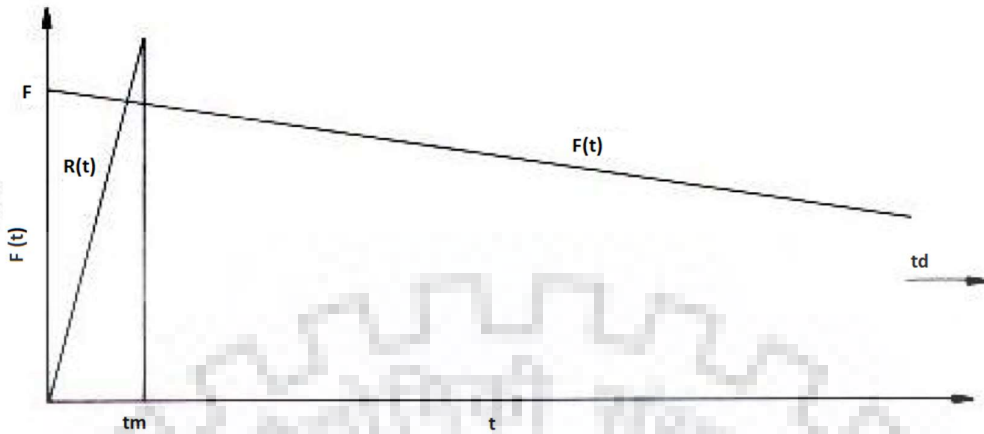


Figure 1-8: Quasi-static loading regime

In this case, the work done by the external force is equal to the force times displacement of the system.

$$WD = Fx_{\max}$$

And the strain energy of the system is equal to area beneath the resistance displacement curve.

$$U = \frac{1}{2} Kx_{\max}^2$$

Equating the work done by external force to the strain energy acquired by the system (after some rearrangement) gives:

$$\frac{x_{\max}}{(F/K)} = \frac{x_{\max}}{x_{st}} = 2$$

This represents the quasi static asymptote in the DLF curve.

In the case of impulsive loading regime, the decay time of forcing function is much lesser than the time period of natural vibration of the system.

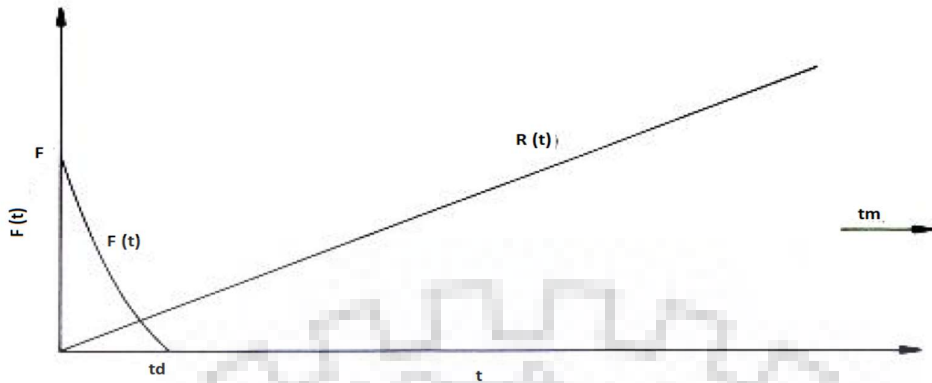


Figure 1-9: Impulsive loading regime

This means that the impulse transferred in the impulsive loading regime instantly provides momentum to the mass of the structure which is seen as a kinetic energy.

$$KE = \frac{1}{2} Mx_0^2 = \frac{I^2}{2M}$$

At maximum displacement, this kinetic energy turns into strain energy.

Hence, equating the strain energy with kinetic energy and in turn energy acquired by impulse:

$$\frac{1}{2} Kx_{\max}^2 = \frac{I^2}{2M}$$

Comparing the maximum displacement above with static displacement with a little rearrangement gives:

$$\frac{x_{\max}}{F/K} = \frac{x_{\max}}{x_{st}} = \frac{1}{2} \omega t_d$$

This represents the impulsive amplitude in the DLF curve.

These asymptotes mark the response for impulsive and quasi static loading regimes. If the regime is dynamic, the solution isn't this simple and may involve actually solving the differential equation of motion of the structure to ascertain its maximum displacement [4].



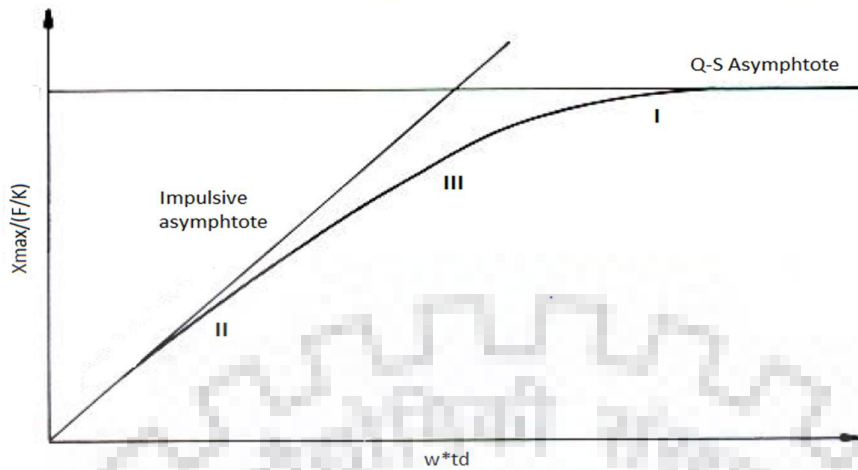


Figure 1-10: Graphical representation of Quasi static (I), Impulsive (II) and Dynamic (III) Response.

This discussion summarises the response of a structure to the type of loading. In case of blast loads, maximum close range blasts have decay time of the order of a few milliseconds while most structures have time period of the order of a few hundred milliseconds. So, invariably blast loads act as impulsive loads wherein all the energy of the impulse is transferred at once and is dissipated slowly in the form of damage to structure or damping etc.

**Effect of high strain rates:**

The strain rates produced by blast loading is of the order of  $10^2 - 10^4 s^{-1}$ . This strain rate is extremely high as compared to strain rate encountered in other types of loading.

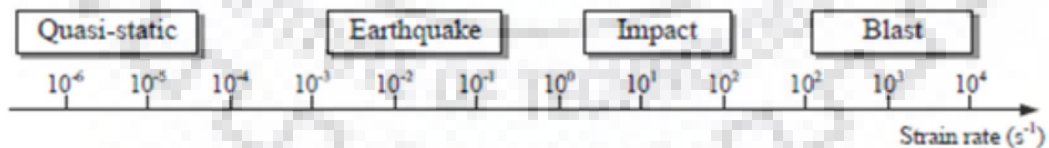


Figure 1-11: Typical strain rates for different types of loading

Figure 1-11 shows the range of strain rates associated with typical loadings, it can be seen that strain rates associated with blast loads is several magnitudes higher than that with earthquake or impact loads. Such high strain rates alter the response behaviour of most materials including their modulus of elasticity, failure strength and

damage mechanism. Significant change in the properties of concrete and steel are reported at strain rates comparable with blast loads.

### **Changes in material properties due to high strain rates:**

Concrete:

Significant change in the properties of concrete is observed under dynamic loads as compared to static loads. The compressive strength may increase by 4 times whereas the tensile strength may increase by 6 times for strain rates of the order of  $10^2 - 10^3 s^{-1}$ . Though, no appreciable change in the modulus of elasticity or stiffness is observed under dynamic loading conditions as compared to static loading conditions [1].

Steel:

Compressive and tensile strength, both are increased by 10% to 25% for a strain rate of  $10^5 - 10^6 s^{-1}$ . The lower yield strength increases by 50% whereas the ultimate tensile capacity becomes 200%. It is also observed that the ultimate tensile strain at failure decreases with increasing strain rate [1].

### **Failure modes of blast loaded structures:**

The damage and failure of reinforced concrete structures subject to blast loads may be divided into two categories. They are global failure due to global structural response and local failure due to local structural response.

The global structural response to blast loading is the development of flexural and shear resistance in structural components due to impulse transmitted by blast. On the exceedance of compressive, tensile or shear strength of concrete, failure may occur at the most stressed part and the structure starts losing its moment or shear capacity.

Local failure is due to the propagation of stress waves in concrete that are generated when blast waves impinge on the proximal face of the structure. Stress waves are powerful compression and tension waves that propagate, reflect, interfere and amplify inside the concrete member and has amplitude frequently surpassing the failure strength of concrete. Local tensile failure, cracks and their propagation and spalling and scabbing on distal side are mostly a result of local failure due to stress waves. It

may also cause flying fragments and debris that can injure persons or equipment on the distal side meant to be protected from the blast.

### 1.3 Blast resistant design of structures

In this section, a simplified approach to blast resistant design of RCC elements has been presented.

#### Idealised SDOF lumped mass system

In order to analyse and assess the response, the structure is modelled as a single degree of freedom lumped mass system having a single equation of motion. The actual structure is a multi-degree of freedom system with each particle having its own equation of motion. In a lumped mass system, the mass of the original structure undergoing vibration is replaced by an equivalent mass. The original stiffness of the system is replaced by an equivalent stiffness of the SDOF system and the load applied on the system is replaced by the equivalent load on the SDOF system [4]. How this equivalent mass, stiffness and load is selected is briefly described here.

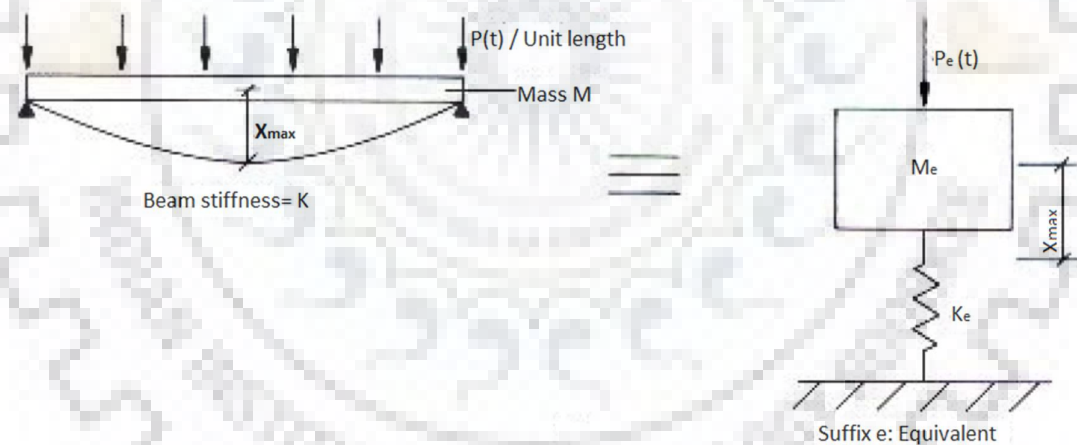


Figure 1-12: Structure and its equivalent SDOF system

The maximum deformation at a selected point in the structure is taken as reference, in this example  $X_{max}$ .

The total work done by external loads on the structure is described in terms of  $X_{max}$  and equated with work done on SDOF lumped mass system.

$$\frac{2}{3}PX_{max} = P_eX_{max}$$

$$\frac{P_e}{P} = 0.66 = K_l$$

Hence, the relation between load and equivalent load is obtained.

Similarly, Equating the strain energy absorbed by the structure to the strain energy absorbed by SDOF system, both expressed in terms of  $X_{\max}$ , Relation between stiffness and equivalent stiffness is obtained.

$$0.64 \times \frac{1}{2} \times K X_{\max}^2 = \frac{1}{2} \times K_e X_{\max}^2$$

$$\frac{K_e}{K} = 0.64 = K_k$$

Equating initial kinetic energy of the structure to the initial kinetic energy of SDOF system:

$$0.50 \times \frac{1}{2} \times M V^2 = \frac{1}{2} \times M_e V^2$$

$$\frac{M_e}{M} = 0.50 = K_m$$

Relation between equivalent mass and mass of structure is obtained.

Hence, the method to obtain Load factor, stiffness factor and mass factor is demonstrated.

Now, the equation of motion of this SDOF lumped mass system will represent the motion of the actual structure. For any system having a mass and a stiffness loaded with time varying force the governing differential equation of motion is given by:

$$M\ddot{X} + Kx = P(t)$$

Where,

M= Mass of system

K= stiffness of the system

P (t) = Load on the system.

In order to represent the actual structure using this SDOF system, making use of load factor, stiffness factor and mass factor, we have:

$$K_M M \ddot{X} + K_k K x = K_L P(t)$$

The stiffness and load factor are approximately same and it is general practice to take them as equal. The ratio of mass factor to load factor is called load-mass factor.

$$\frac{K_M}{K_L} = K_{LM}$$

Hence, we get:

$$K_{LM} M \ddot{X} + K x = P(t)$$

The value of this load mass factor is available for a number of boundary conditions and loading in the literature.

Hence, the structure may be analysed using this idealised SDOF lumped mass system approach.

### **Design objective**

The primary objective of blast resistant design is to provide sufficient ductility to the structure or part thereof so that deformations consistent with the degree of damage permitted are allowed to take place. The structure must not fail prematurely in going through the said deformations due to shear or local instability. This leads to a design based on extensive flexural plastic deformation [4]. The structure, unless it is to be subjected to repeated blast loading (for example in a test facility) is to be designed based on the ultimate limit state.

### **Design loads**

The blast loading for which the structure is to be designed is likely to be an extreme event and as such has a low probability of occurrence. Hence, the partial safety factor with respect to loads is taken as unity [4].

### **Design strength**

The design should be based on characteristic strength of materials with a partial safety factor of unity. Blast loads have very high strain rates of the order of  $10^2$ - $10^4$ /s. such high strain rates may cause a marked increase in the design strength of materials. The factor by which the design strength of the materials increase is known as dynamic increase factor (DIF) [4]. The DIF of reinforcing bars and concrete is given in table 1-1.

Table 1-1: DIF for concrete and reinforcing bars

Type of stress	Concrete	Reinforcing bars	
	$\frac{f_{dcu}}{f_{cu}}$	$\frac{f_{dy}}{f_y}$	$\frac{f_{du}}{f_u}$
Bending	1.25	1.20	1.05
Shear	1.00	1.10	1.00
Compression	1.15	1.10	-

### Deformation limits

The controlling criteria in blast resistant design of structural elements is the allowable deformation or limiting deformation. By prescribing limits on the allowable deformation, the damage to the structural element as a result of the blast load is restricted to an acceptable value. The limit on allowable deformation is given in 2 ways. They are ductility ratio and support rotation.

Ductility ratio is the ratio of total deformation to deformation at elastic limit.

$$\mu = \frac{\text{total deflection}}{\text{deflection at elastic limit}} = \frac{X_m}{X_E}$$

Support rotation is the rotation at the support that will effect a given deformation at the specified location in the structural element.

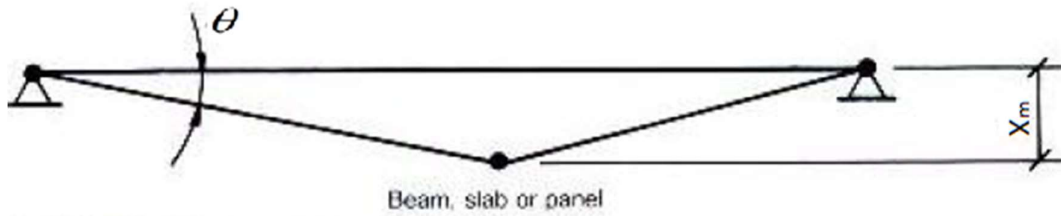


Figure 1-13: Support rotation for structural elements

$$\theta = \frac{\text{Total deflection}}{\text{Distance from support}}$$

The limits of ductility ratio and support rotation are specified based on what is to be protected and the degree of protection intended. These are specified in protection categories wiz type 1, type 2 etc. [4]. In RCC design the limits are specified in terms of support rotations. Ductility ratio is used in structural steel design.

Type 1 protection category entails the protection of equipment and personnel from blast overpressures and secondary fragments and falling parts of the structure. Type 2 protection category entails the protection of the structure itself from collapse under the action of blast loads [4].

Table 1-2: Support rotations and ductility ratios as per protection categories

Structural element	Protection category			
	1		2	
	$\theta$	$\mu$	$\theta$	$\mu$
Reinforced cement concrete	2°	-	4°	-
Structural steel	2°	10	12°	20

### Idealised resistance curve of reinforced concrete

The resistance offered by RCC to blast loads is expressed in the form of force per unit length. This force is related to the moment of resistance of the RCC section. This resistance is related to the deformation measured at a given location which is related to the support rotation. Hence the relation between moment of resistance and support rotation is expressed as relation between resistance and deformation.

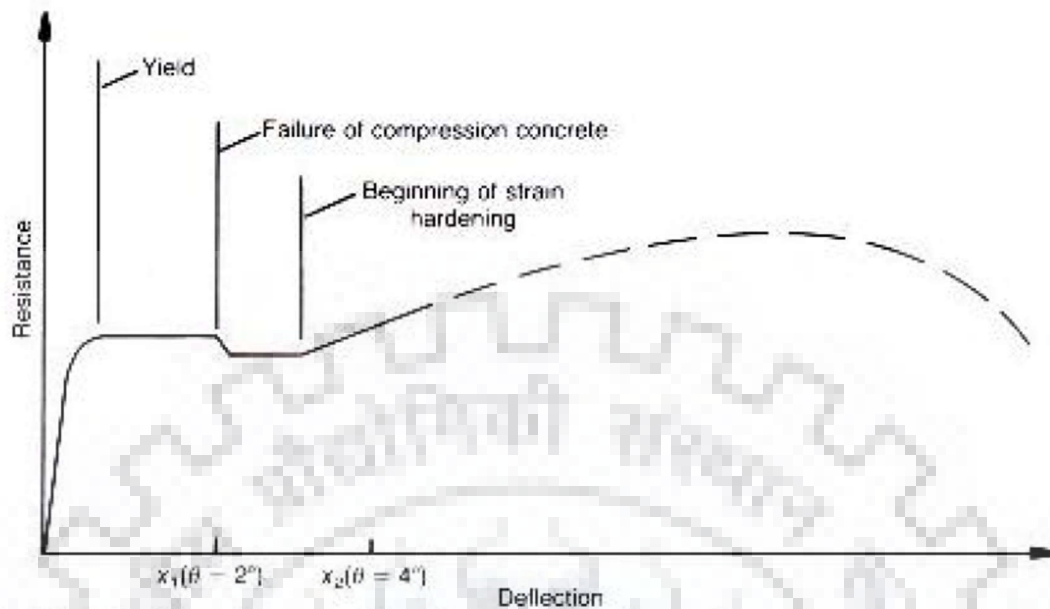


Figure 1-14: Typical resistance deflection curve of RCC

A typical resistance deflection curve of RCC is shown. The trends are as discussed. The resistance increases linearly with deflection until the yield point is reached wherein the yielding of tension reinforcement occurs. After this point resistance does not grow further and deflection increases at constant resistance up to a point where concrete starts getting crushed in compression ( $\theta = 2^\circ$ ). This causes a slight reduction in moment of resistance and then the compression steel takes up the stresses from concrete and gets yielded. This resistance due to yielding of both tension and compression reinforcement continues up to a point ( $\theta = 4^\circ$ ) where steel enters strain hardening zone and the resistance starts increasing.

Type 1 sections are section designed to develop resistance up to crushing of compression concrete, i.e. up to a rotation of  $2^\circ$ . The ultimate moment of resistance calculated for type 1 section is corresponding to the ultimate limit state of crushing of compression concrete [4].

Type 2 sections are sections designed to develop resistance up to yielding of both compression and tension steel, i.e. up to a rotation of  $4^\circ$ . The ultimate moment of resistance calculated for type 2 section is corresponding to ultimate limit state of yielding of both compression and tension steel [4].



For design purposes, the idealisation of resistance deflection curve of reinforced concrete is a bilinear idealisation wherein resistance develops linearly up to a deflection given by initial stiffness and then increasing deflection at a constant resistance up to limiting deflection [4].

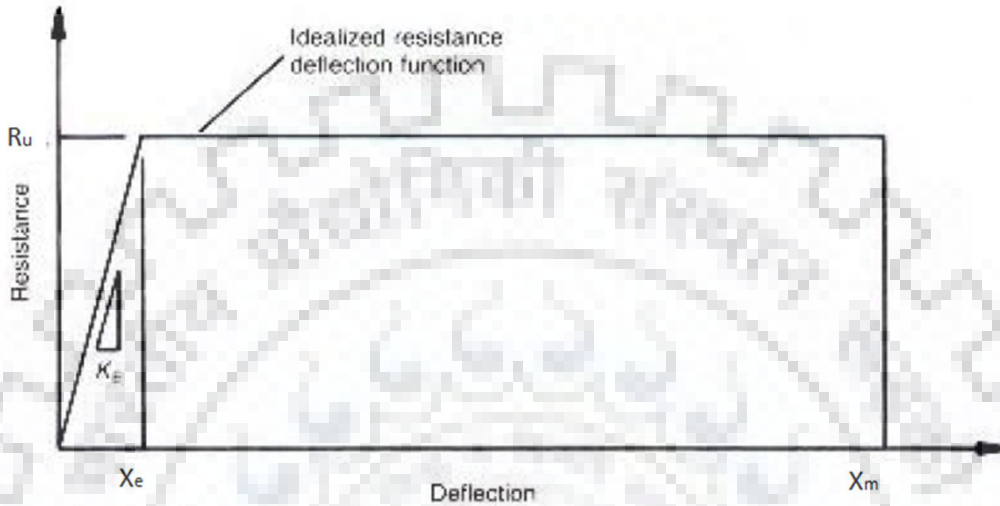


Figure 1-15: Bilinear idealisation of the deflection resistance curve of RCC section

### Design procedure

Blast resistant sections designed in this work are of such time period that the blast loading acts as impulsive loading regime. Hence, the kinetic energy gathered by the system converts to strain energy and energy of permanent deflection. This is expressed in the following deflection equation [4].

$$\frac{i^2}{2K_{LM}m} = \frac{r_u X_E}{2} + r_u (X_m - X_E)$$

Where,

I= reflected specific impulse for given standoff distance and charge weight. (As calculated from manual of Kingery and Bulmash or TM 5-1300)

M= Mass per unit area for structural element

$K_{LM}$  = Load mass factor

$r_u$  = ultimate resistance (in  $N/m^2$ )

$X_m$  = Maximum permitted deflection as per support rotation.

$X_E$  = Elastic deflection

Step 1: Assume reinforcement percentage and calculate  $M_u$  for required section in terms of depth  $d$ . For type 1 section:

$$M_U = 0.675 f_{ck} b d^2 \cdot \frac{x_u}{d} \cdot \left(1 - 0.42 \frac{x_u}{d}\right)$$

$$\frac{x_u}{d} = \frac{1.2 f_y}{0.675 f_{ck}} \cdot \frac{A_{st}}{b d}$$

For type 2 section:

$$M_U = 1.2 f_y \cdot \frac{A_{st}}{b d_c} \cdot b d_c^2$$

Here,

$f_{ck}$  = Characteristic strength of concrete.

$f_y$  = Yield strength of steel

$b$  = width of section

$d$  = depth of section

$d_c$  = Centre to centre distance between reinforcement on opposite faces

$\frac{A_{st}}{b d}$  = Reinforcement ratio

$\frac{x_u}{d}$  = Neutral axis depth ratio

Step 2: Calculate the ultimate resistance of structural element in terms of assumed reinforcement ratio and depth of section.

$$R_u = f(M_u, L)$$

Step3: Calculate elastic stiffness in terms of assumed reinforcement ratio and depth of section.

$$K_E = f(E, I, L)$$

Step 4: Calculate maximum elastic deflection.

$$X_E = \frac{R_u}{K_E}$$

Step 5: Calculate maximum total deflection.

$$X_M = f(\theta, l)$$

Step 6: Use these quantities obtained in step1-5 in the basic impulse equation and solve for depth d.

$$\frac{i^2}{2K_{LM}m} = \frac{r_u X_E}{2} + r_u (X_m - X_E)$$

Step 7: Obtain depth of section and provide reinforcement as per assumed reinforcement ratio.

Step 8: Design for shear; Shear resistance is required to fully develop requisite resistance  $R_u$ . A shear resistance of value  $V_u = f(R_u, l)$  is required and hence shear reinforcement required is:

$$A_v = \frac{(v_u - v_c)bs}{f_{ds}}$$

Shear reinforcement is to be provided in the form of closed 'blast' links. In type 2 sections, diagonal bars are required at the ends to develop shear as entire concrete is crushed. Hence, diagonal bars of area given is required.

$$A_d = V_s b / f_{ds}$$

This completes the design procedure of structural elements for blast resistance.

## 1.4 Sacrificial cladding in blast resistant structures

Sacrificial cladding in blast resistant design of structures is a relatively new concept. This involves applying a cladding of a material that can absorb sudden impact and shocks due to blast loading and take up the energy in the form of damage to itself while protecting the structure on which it is applied [5]. Different types of materials are used in sacrificial cladding design and numerous research has been done to investigate and improve their efficacy [6].

### Types of sacrificial cladding

The materials used in sacrificial cladding are categorised into 3 main types [6] [7]:

1. Cellular foams: for example – Aluminium foams.

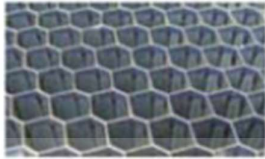
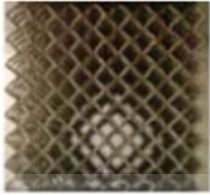
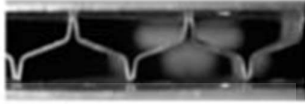



Such materials can absorb significant amount of energy by undergoing large plastic deformations. These deformations are possible because of their cellular structure wherein pores make up large fraction of volume and are surrounded by solid materials. Such ability to absorb large amounts of energy at relatively low plateau stress make them suitable as shock absorbents and find applications in blast and impact loading.

2. Micro-architectural Cores: Materials having microstructure of regular lattices such as honeycomb.

Such materials absorb impact energy by virtue of undergoing large deformation through collapse mechanisms of the regular lattices at microstructure level. The result is a large strain range at constant plateau stress that can absorb considerable amount of energy.

3. Macro-architectural Cores: Materials having macrostructure of corrugated aluminium sheet packed in cover plates such that individual macro structural lattice is capable of undergoing collapse mechanism and absorb energy.

These are built with geometries such that shock loading on the front plate causes several plastic hinges to form in the core geometry of these cladding. Through excessive rotations considerable energy is absorbed in these structures leading to reduction in the damage and deflection of structures they protect.

Cellular Material	Micro-architectural	Macro-architectural
 <p>Honeycomb</p>	 <p>±45° lattice</p>	 <p>BRAS</p>
 <p>Aluminium Foam</p>	 <p>Pillar-octahedral lattice</p>	 <p>Y-Web corrugations</p>

*Figure 1-16: Different materials in use as sacrificial cladding*

### **Aluminium foam as sacrificial cladding**

As remarked earlier, aluminium foams have the capacity to undergo large deformation at nearly constant nominal stress, making them suitable materials for construction of sacrificial cladding panels [7] [8]. The stress strain behaviour of aluminium foams is briefly discussed here:

Aluminium foams when subjected to compressive stresses behave elastically, at first for a very small range of strains after which it enters its yield stress at which it undergoes significant strains at almost constant stress up to its densification strain at which point the foam has densified to such extent that a sharp increase in stress with further straining is observed [6].

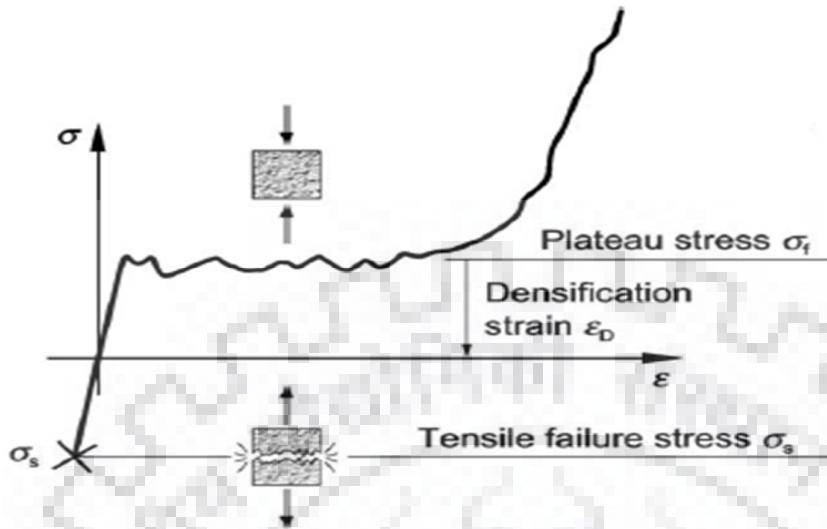


Figure 1-17: Typical stress strain curve for aluminium foam

The densification strain is of the order of 100 times the yield strain. This range signifies the zone over which foam absorbs energy at nominal constant stress. An idealised stress strain curve for aluminium foam that can be used for the purpose of design and analysis is shown.

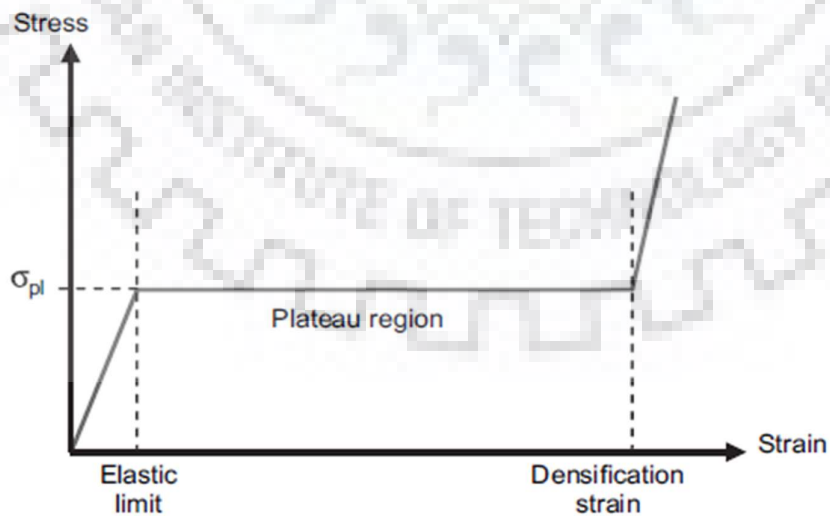


Figure 1-18: Idealised compression curve for aluminium foam

The impulse transferred to the foam by the blast wave is a short duration high pressure impulse, which is converted to a longer duration low pressure impulse by the foam. In effecting this conversion, the foam goes through compression and densification.

Seen in terms of energy, the aluminium foam absorbs the energy of the blast wave by getting compressed itself while shielding the parent structure so that only a portion of the energy is available to cause damage to the parent structure [7].

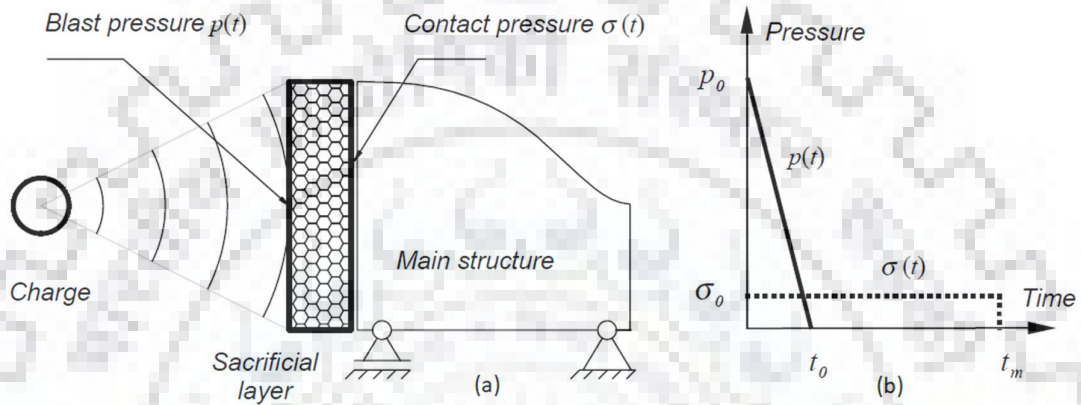


Figure 1-19: (a) Aluminium foam subjected to blast loading and (b) Blast load on the front cover of foam depicted as triangular pulse and pressure transferred through foam to the parent structure depicted as long duration low intensity rectangular pulse.

### Design parameters in sacrificial cladding

Hansen et al (2002) has developed differential equations and their solutions for a cellular foam subject to sudden impact load of a blast [7].

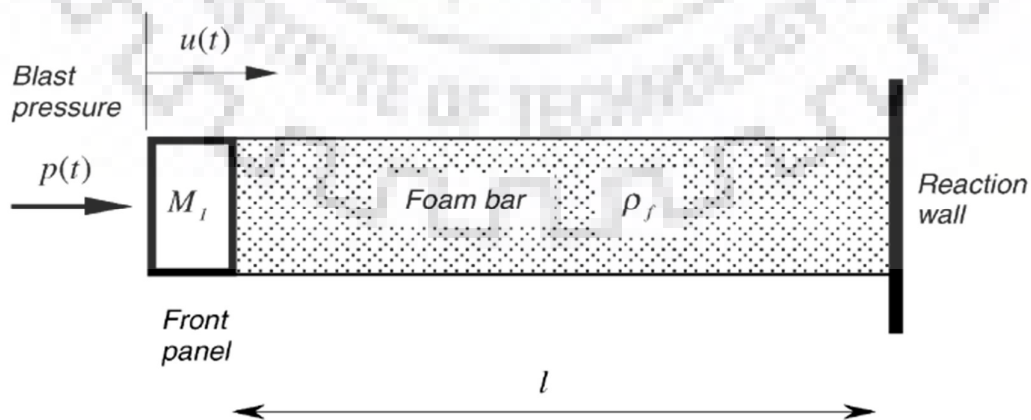


Figure 1-20: Hansen's model of foam compression under blast load.

In this model:

$P(t)$  = Triangular blast pulse

$U(t)$  = Displacement of cover plate with time

$l$  = Uncompressed thickness of foam panel

$\rho_f$  = Uncompressed density of foam

$\rho_{f0}$  = Compressed density of foam

$A$  = Area of foam

$M_0 = \rho_f \times l \times A$  = Mass of foam

$M_1$  = Mass of cover plate.

$\varepsilon_d$  = Densification strain of the foam

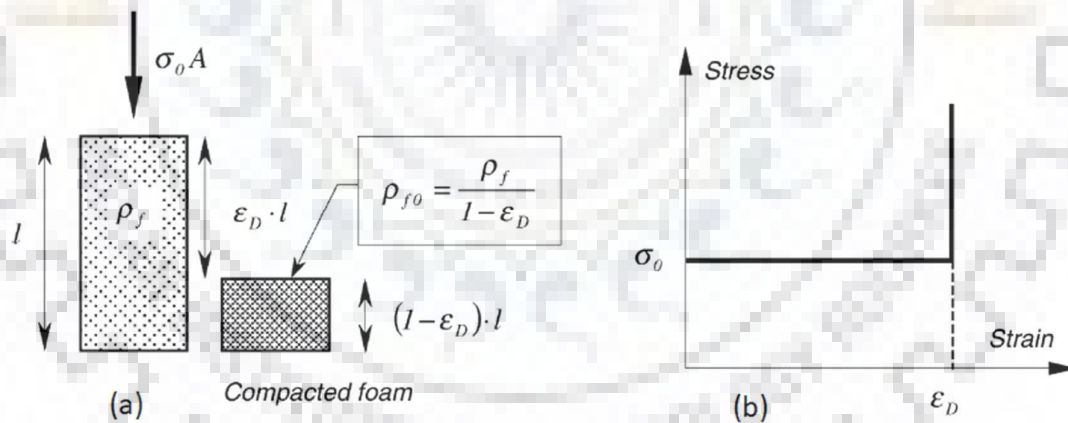


Figure 1-21: (a) Densification strain and (b) Assumed stress strain curve for the model

Using the equilibrium condition of impulse equal to stress generated in the foam, compatibility condition of displacement of the cover equal to densification of the foam and constitutive relation between stress and strain, Hansen developed the following differential equation.

$$\left[ 1 + \frac{\rho_f A}{M_1 \varepsilon_D} u \right] \ddot{u} + \frac{\rho_f A}{M_1 \varepsilon_D} \dot{u}^2 + (\sigma_0 - p(t)) \frac{A}{M_1} = 0$$



He used commercially available software Maple to solve this equation. The solution is presented:

For a time varying pressure pulse defined by:

$$p(t) = \begin{cases} p_0 \left(1 - \frac{t}{t_0}\right), & t \leq t_0 \\ 0, & t > t_0 \end{cases}$$

The displacement is calculated as:

$$\frac{u}{\varepsilon_D l} = 0, \quad t \leq 0 \text{ or } \frac{p_0}{\sigma_0} \leq 1$$

$$\frac{u}{\varepsilon_D l} = -m + \sqrt{m^2 + 4\xi \left\{ \left(1 - \frac{\sigma_0}{p_0}\right) \left[\frac{t}{t_0}\right]^2 - \frac{1}{3} \left[\frac{t}{t_0}\right]^3 \right\}}, \quad 0 < t \leq t_0 \text{ and } \frac{p_0}{\sigma_0} > 1$$

$$\frac{u}{\varepsilon_D l} = -m + \sqrt{m^2 + 4\xi \left\{ -\frac{1}{3} + \left[\frac{t}{t_0}\right] - \frac{\sigma_0}{p_0} \left[\frac{t}{t_0}\right]^2 \right\}}, \quad t_0 < t \leq \frac{1}{2} \frac{p_0}{\sigma_0} t_0 \text{ and } \frac{p_0}{\sigma_0} > 2$$

$$\frac{u}{\varepsilon_D l} = -m + \sqrt{m^2 + \xi \left\{ \frac{p_0}{\sigma_0} - \frac{4}{3} \right\}}, \quad t > \frac{1}{2} \frac{p_0}{\sigma_0} t_0 \text{ and } \frac{p_0}{\sigma_0} > 2$$

Two dimensionless terms have been introduced. They are the ratio between mass of front cover to mass of foam.

$$m = \frac{M_1}{M_0}$$

And an impact factor  $\xi$  (I is the impulse due to blast loading)

$$\xi = \frac{I^2}{M_0 p_0 \varepsilon_D l}$$

The solutions indicate that:

- There will be no displacement if  $\frac{p_0}{\sigma_0} \leq 1$ ,

- The displacement will stop before  $t_0$  if  $1 \leq \frac{p_0}{\sigma_0} \leq 2$ ,
- The maximum displacement will occur at time given by  $t_m = \frac{1}{2} \cdot \frac{p_0}{\sigma_0} \cdot t_0$ , for

$$\frac{p_0}{\sigma_0} > 2$$

The solutions also give a minimum thickness of foam below which the total impulse of blast wave cannot be dissipated.

$$l \geq \frac{I^2}{(M_0 + 2M_1) p_0 A \varepsilon_D} \left\{ \frac{p_0}{\sigma_0} - \frac{4}{3} \right\}, \quad \frac{p_0}{\sigma_0} > 2$$

This is the most important parameter from the point of view of design.

## 1.5 Numerical analysis in Abaqus/Explicit

Owing to difficulties and safety concerns with conducting blast experiments and difficulties in the logistics of obtaining explosives, the investigations and validations in this work are purely numerical studies performed in the commercial finite element software package Abaqus. The solver used is Abaqus/Explicit.

It is impertinent that the true nature of blast loading experiments on reinforced cement concrete elements be reflected in the numerical studies. The important peculiarities of such types of experiments and the properties of numerical model in Abaqus that make it possible to recreate them in numerical simulation has been discussed here.

### Material non linearity

The behaviour of 3 different materials is a point of interest here. They are concrete, steel and aluminium foam. Concrete is well known for its non-linear stress strain response and is expected to behave non linearly in blast loading experiments. Material behaviour of steel is usually idealised as bilinear elastic plastic in design but steel is also has a non-linear material response especially in the region where it shifts from elastic to plastic behaviour, this non linearity is quite well pronounced in high yield strength steels as they lack a well-defined yield point. Aluminium foam is similarly

assumed to have no hardening before reaching densification strain but in actuality hardening is seen throughout with increasing rate before densification and at much larger rate after densification [8].

### **Dynamic nature of loading**

Blast loads are short duration extreme loads that have a time duration of a few milliseconds in which very high impulse is transferred. Hence the response of structural elements to blast loading is dynamic involving time dependent displacements.

### **Effect of high strain rates**

As described earlier strain rates associated with blast loading can cause strength magnification factor of around 4 to 6 in concrete and 10% to 25% in steel.

Material models and solver used in Abaqus that capture the essentials of blast loading experiments viz material non linearity, effect of high strain rates and dynamic nature of problem have been briefly described here.

### **Concrete Damage Plasticity model (CDP)**

Concrete damaged plasticity model is a continuum, plasticity based damage model for concrete with a Drucker pager failure surface and non-associated flow rule. It takes up data in the form of uniaxial compression and tension test data comprising short term elastic modulus and tabular data linking compressive stress with inelastic strain and cracking strain. With the increase in inelastic strain, the stiffness degrades as per stiffness degradation factor. The compression and tension damage is linked with inelastic strain data which is in essence the damage suffered by concrete at that strain level [9].

The stress-strain relations for the general three-dimensional multiaxial condition are given by the scalar damage elasticity equation:

$$\boldsymbol{\sigma} = (1 - d)\mathbf{D}_0^{el} : (\boldsymbol{\varepsilon} - \boldsymbol{\varepsilon}^{pl})$$

Where  $\mathbf{D}_0^{el}$  the initial (undamaged) elasticity matrix and damage parameter  $d$  is depends on stress loading in 3 dimensions.

Based on input values the shape of failure surface, strength and flow rule can be defined. Material non linearity of concrete is appropriately captured in the compression and tension data. The data input can be opted to include strain rate dependent data which includes the effect of strain rate in modifying the compression and tension behaviour [9].

### **Johnson-Cook model (J-C)**

Johnson-Cook model is meant for ductile metals such as steel. It is a modified von Mises model with associated flow rule with analytical parts for hardening law, strain rate dependence and temperature dependence [9].

$$\bar{\sigma} = \left[ A + B (\bar{\epsilon}^{pl})^n \right] \left[ 1 + C \ln \left( \frac{\dot{\epsilon}^{pl}}{\dot{\epsilon}_0} \right) \right] (1 - \hat{\theta}^m)$$

This model is to be used in conjunction with linear elastic model and is suitable for use in high strain rate applications.

### **Crushable foam model**

The crushable foam model is used to model aluminium foams. In this model, Volumetric hardening is used, which is to say that evolution of yield surface depends on volumetric strains, compactive inelastic strains produce hardening while dilatant inelastic strains lead to softening. The, evolution of failure surface depends on a shape factor which in turn depends on the ratio of yield stress in uniaxial compression to the yield stress in hydrostatic compression and the yield strength in uniaxial tension to hydrostatic tension [8].

$$\alpha = 3k / \sqrt{(3k_t + k)(3 - k)}, \quad k = \sigma_c^0 / p_c^0, \quad k_t = p_t / p_c^0$$

Plastic hardening data is provided in tabular format that takes into account non-linear behaviour. Strain rate sensitivity of aluminium foams is found to be insignificant and hence not incorporated in this material model.

### **Modelling of blast load**

Blast loads on the surface of concrete wall has been modelled using CONWEP module in Abaqus. CONWEP is the conventional weapons effect computer program meant to

calculate blast pressures due to high explosives and has been extensively used in blast load computation. CONWEP uses TM 5-1300 curves (which are based on manual by Kingery and Bulmash) for blast overpressure, impulse, arrival time and positive phase duration calculation for reflected and unreflected blast waves. The blast pressure decay has been taken as Friedlander's waveform [3] [9].

### **Explicit solver in Abaqus**

Dynamic problems where the transmission of stress waves at sound speeds poses significant effects must be solved using the explicit solver in Abaqus. Explicit solver produces a stable time increment based on the time taken for the stress wave to advance through a single element and uses explicit numerical integration wherein the calculations of the next step are taken directly from the previous step [9].

By contrast dynamic analysis in standard solver is iterative in which the solver tries to 'best fit' a solution without accounting for stress waves [9].

Blast loads produce strong stress waves capable of causing damage to the material. Hence, it is impertinent to account for them in the analysis and that is done using the explicit solver of Abaqus.

## Chapter 2. Literature Review

---

### 2.1 General

A considerable amount of work has been accomplished in describing the blast loads and blast effects on structures and on ways to understand the structural response to such loading. Of these, select material relevant to this work was referred through the course of this work. This includes books, papers published in journals and documentations of finite element software packages.

In this section, a literature survey of the papers published in peer reviewed journals that has been referred to for gaining information and developing background for this work has been presented.

### 2.2 Literature survey

Ngo et al., (2007) [1] presented a comprehensive overview of the effects of explosion on structures. The nature of explosions and the mechanism of blast waves in free air is explained. An introduction to different methods of blast load estimation and structural response was provided.

Smith (2009) [10] reviewed the studies concerning blast barrier performance in shielding the asset from the damaging effect of a blast wave. The study focused on the importance of the blast wall's location relative to the threat and the asset that is to be protected. Assessment of the damage that a blast wall might sustain, while still possessing its capabilities to provide protection against blast wave were discussed. Both permanent and temporary blast wall designs and constructions that are used by both civil and military organisations were included in the study.

Rose et al., (1995) [11] described a series of experiments in their research in which detailed measurements of the blast environment were made behind a one-tenth scale model of a vertical blast wall in front of which scaled blast charges were detonated at appropriate distances from the wall. Behind the wall, a space equal of six wall heights behind the wall and up to three wall heights above the ground was measured for the maximum overpressures and impulses. From the pressure-time histories thus obtained, contour plots of overpressure and impulse were developed. These were

compared with histories obtained in the same region for maximum overpressures and impulses when the wall was absent. The results in the form of spatial contour plots of max overpressure and impulse for the presence and absence of the wall were compared and a spatial plot of percentage reduction in overpressure and impulse histories due to presence of blast wall was generated. The regions gaining maximum benefit due to the presence of blast wall were identified.

Kingery and Bulmash (1984) [3] developed polynomial expressions for blast parameters like overpressure, impulse, reflected overpressure, reflected impulse, arrival time and positive phase duration for both spherical wave fronts due to free air bursts and hemispherical wave fronts due to surface bursts of TNT. The expressions developed by Kingery and Bulmash have since become the most widely used and accepted method for determination of blast wave parameters. All the proposed parameters are valid for distances from 0.05m up to 40m. These equations have already been incorporated in various computer explicit codes, and many blast design studies are performed based on them.

Karlos et al., (2015) [3] performed calculations of blast parameters due to an explosion with special emphasis on the blast wave decay coefficient needed for modelling the pressure-time curve with the Friedlander equation. Based on these calculations, a new set of equations for the calculation of the decay coefficient were developed for both incident and reflected blast waves for free-air and surface bursts. These expressions, which are of polynomial or exponential form, are dependent on the scaled distance and are the result of appropriate curve fitting of the Kingery-Bulmash data. The use of these equations within a consistent Kingery-Bulmash framework, allows a designer to produce the pressure-time history from a certain blast scenario and insert it into an explicit computer code for quantitatively assessing the effects of the explosion on a structure or structural component.

Erdik and Ucar, (2018) [12] investigated the method of simulating blast loads in LS-DYNA. Blast simulations were carried out through CONWEP, Arbitrary Lagrangian Eulerian (ALE), and hybrid CONWEP-ALE. The three blast loading approaches were comparatively evaluated in order to get better understanding on the requirements of computational effort, accuracy of blast loading scheme, and influence of element size.



A comparison was made between peak pressures calculated in simulations and maximum dynamic deformation measured in the field tests.

Wang (2012 & 2013) [13] [14] investigated the behaviour of fixed one-way RCC slabs of square shape subjected to a blast load through experiments and numerical simulations. In the first set of experiments slabs of different sizes were subjected to close range blasts from TNT of different charge weight and standoff distances such that scaled distance remained same. The damage and deflection levels were comparable for same scaled distances.

In the second set of experiments four 1000 mm\*1000 mm\*40 mm slabs under close-in blast loading. The blast loads are generated by the detonations of 0.2–0.55 kg TNT located at a 0.4 m standoff above the slabs. The variation in damage levels and modes were observed.

Jankowiak and Lodygowski (2005) [15] presented the requirements of the material parameters for the concrete damage plasticity constitutive model of Abaqus and a method for their identification. The laboratory tests, which are necessary to identify constitutive parameters of this model have been presented. The CDP parameters namely dilation angle, eccentricity,  $\sigma_{b0} / \sigma_{c0}$  ; the ratio of initial equibiaxial compressive yield stress to initial uniaxial compressive yield stress;  $K_C$ , the ratio of the second stress invariant on the tensile meridian,  $q(TM)$  , to that on the compressive meridian,  $q(CM)$  at initial yield, viscosity parameter and stress strain data along with damage parameters in the form of tabular data have been presented.

Vedantam et al., (2006) [16] characterized Mild and DP590 steel in tension using the quasi-static and split Hopkinson bar techniques at various strain rates ranging from  $\sim 10^{-3}/s$  to  $\sim 1800/s$ . Tension stress-strain data for both the steels are analysed to determine the Johnson-Cook Strength model constants. J-C model constants A, B, C, m and for mild steel and DP 590 steel are reported.

Guruprasad and Mukherjee, (2000) [17] [18] investigated the behaviour of layered sacrificial cladding subject to blast loading through both experimental and numerical studies. The sacrificial cladding layer was constructed as board of corrugated mild



steel sheet covered by plane mild steel sheet on either side. The corrugations were made such that the sheet could collapse by formation of plastic hinges at particular points and reduce into a more stable configuration whilst absorbing energy from the blast and reducing rate of impulse transfer. The layers collapse successively and the mode of collapse of the unit cell in any layer is the same. The numerical studies as well as the experimental programme demonstrated that under blast loading, layered sacrificial claddings effectively absorbed energy and behaved predictably. Hence, they can be reliably used in blast resistant design of structures.

Hansen et al. (2001) [7] conducted experiments to investigate the behaviour of aluminium foam subject to blast loading. A ballistic pendulum with its panel fixed with aluminium foam was subject to blast loads due to detonations of varying charge weights and standoff distances. The same charge weight and standoff distances were kept for detonations without the application of aluminium foam. The comparison of maximum swing of the pendulum with and without foam showed that application of foam unexpectedly increased the swing of pendulum. A differential equation describing the compression of aluminium foam under blast loading was also developed.

Yuen et al. (2009) [6] reviewed the materials currently in use for sandwich panels for protection against blast and impact loads. Three types of sandwich panels are identified, by core type: cellular core, such as aluminium foam, micro-architectural core, such as honeycomb and macro-architectural core such as corrugated aluminium sheets sandwiched in mild steel cover plates. Their relative performance under different blast loading cases as tested by various researchers is reviewed.

Langdon et al. (2009) [8] performed experiments to investigate the effect of core density and cover plate thickness on the blast response of sacrificial cladding panel with steel cover plates and aluminium foam cores. Three core densities were examined, with 10%, 15% and 20% nominal relative densities. Numerical simulations of the experiment performed in ABAQUS/Explicit provided insight into the response mechanism. It was observed that thicker cover plate caused more even compression of the foam. Cracking of the foam was more common in lower density

foams and bonded claddings. The findings of numerical analysis was consistent with the experimental observations.



## Chapter 3. Objective and Methodology

---

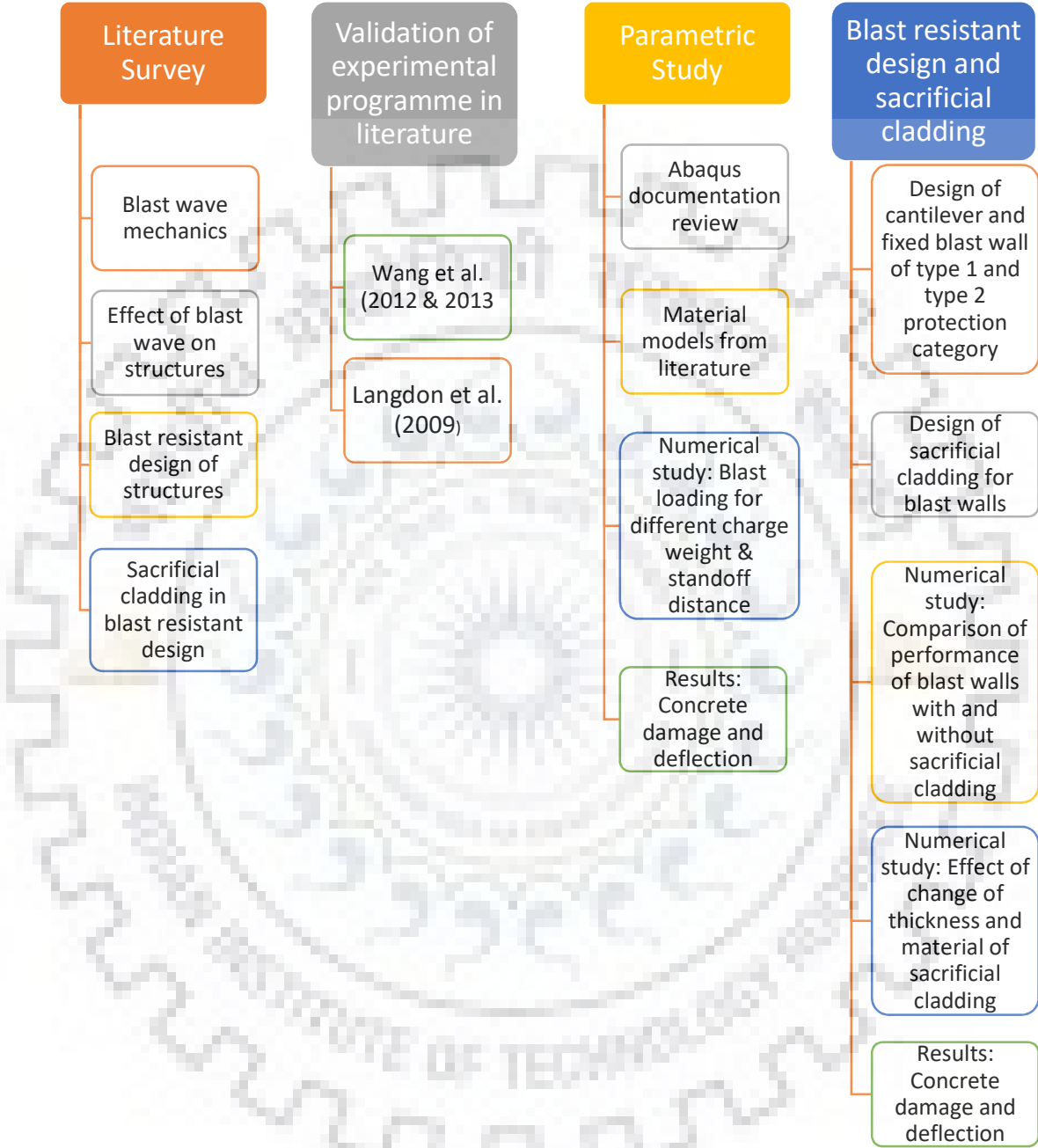
### 3.1 Objective

The objectives of the work presented in this thesis are:

1. To present design of blast resistant cantilever and fixed wall for type 1 and type 2 protection categories as per design method and design parameters outlines in TM 5-1300 and to design the aluminium foam sacrificial cladding for these walls.
2. To develop Abaqus models of cantilever and fixed blast walls and validate the material models used in these models with experimental work described in literature by replicating them in Abaqus simulation.
3. To perform a parametric study of blast load on a 2 way simply supported square blast wall for different charge weight and standoff distance and compare the concrete damage and deflection.
4. To perform numerical studies of blast loads on the blast walls with sacrificial claddings presented in the design and note the concrete damage and deflection and compare them with the damage and deflection on the walls without sacrificial claddings and to study the effect of change in thickness and material density of aluminium foam used as sacrificial cladding.

### 3.2 Methodology

The work presented in this thesis has been shown in the form of this flowchart.



## Chapter 4. Design of RCC blast barriers

---

In this chapter, the design of blast barriers and sacrificial cladding is presented. The design of blast wall is presented for a width of 1m. The design includes depth of section, reinforcement detailing including shear reinforcements in the form of closed blast links and diagonal stirrups for end shear (for type 2 cantilever). The design of aluminium foam is for its thickness.

The blast walls of height 3.0 m have been designed for a blast load corresponding to detonation of 180 Kg TNT at ground level at a distance of 5 meter from the blast barrier. The aluminium foam thickness has been obtained for the same

### 4.1 Type 1 Cantilever blast barrier

Height of blast barrier = 3.0 m

Width of blast barrier = 1.0 m

Loads:

Charge weight of TNT = 180 kg

Standoff distance = 5.0 m

Type of burst = Hemispherical surface burst

Reflected impulse =  $5800 \text{ N s} / \text{m}^2$  (from curve given in figure 1-4)

Partial safety factor wrt loads = 1.0

Material strength:

Characteristic Cube strength of concrete = 50 MPa

Usable strength of concrete =  $0.67 f_{ck} = 33 \text{ MPa}$

Yield strength of steel = 590 MPa

#### Flexural design

Moment of resistance of type 1 section:

$$M_u = 0.675 f_{ck} b d^2 \cdot \frac{x_u}{d} \cdot \left(1 - 0.42 \frac{x_u}{d}\right)$$

Where the neutral axis depth is given by:

$$\frac{x_u}{d} = \frac{1.2 f_y}{0.675 f_{ck}} \cdot \frac{A_{st}}{b d}$$

The reinforcement percentage has been assumed as 0.5%. Hence,

$$\frac{A_{st}}{b d} = 5 \times 10^{-3}$$

$$\frac{x_u}{d} = \frac{1.2 \times (590)}{0.675 \times (50)} \cdot \frac{A_{st}}{b d}$$

$$\Rightarrow \frac{x_u}{d} = 0.109$$

Writing moment of resistance in terms of effective depth  $d$  (in mm):

$$M_u = 0.675 \times (50) \times 1000 \times d^2 \times 0.109 \times (1 - 0.42 \times 0.109) \text{ Nmm}^2 = 3.38 \times d^2 \times 10^{-3} \text{ KNm}$$

The Resistance offered by the barrier is expressed in force per unit height of wall per metre width.

$$R_u = \frac{2 \times M_u}{H^2} = \frac{2 \times 3.38 \times d^2 \times 10^{-3}}{3^2} = 0.75 \times d^2 \times 10^{-3} \text{ KN / m}$$

The elastic stiffness of the member is calculated by:

$$K_E = \frac{8EI}{H^4}$$

$$E_s = 2 \times 10^5 \text{ MPa}$$

$$E_c = 0.35 \times 10^5 \text{ MPa}$$

$$m = 5.714$$

For  $\frac{A_{st}}{b d} = 5 \times 10^{-3}$ ,  $I$  is calculated from standard chart for type 1 section.

$$I = 0.017 \times 10^3 \times d^3 m^4$$

$$\therefore K_E = \frac{8EI}{H^4} = 5.87 \times 10^{-5} \times d^3 KN / m / m$$

The maximum deflection in elastic region is calculated as:

$$X_E = \frac{R_u}{K_E} = \frac{16.2}{d} m$$

For protection category 1, maximum deflection is calculated as:

$$X_m = H \times \tan 2^\circ = 3.0 \times \tan 2^\circ = 104.76 \times 10^{-3} m$$

The load mass factor for cantilever wall is;

$$K_{LM} = 0.65$$

Mass per unit height per metre width for the wall in terms of section depth:

$$m = 2400 Kg / m^3 \times 1.0 m \times d \times 10^{-3} m = 2.4 \times d Kg / m$$

Putting these quantities in to the basic impulse equation for blast loading:

$$\frac{i^2}{K_{LM} \times m} = \frac{R_u \times X_E}{2} + R_u \times (X_m - X_E)$$

$$i = 5800 Ns / m^2$$

$$\frac{(5800 Ns / m^2)^2}{0.65 \times 2.4 \times d Kg / m} = \frac{(0.75 \times d^2 \times 10^{-3} KN / m) \times (\frac{16.2}{d} m)}{2} + (0.75 \times d^2 \times 10^{-3} KN / m) \times \left( (104.76 \times 10^{-3} m) - (\frac{16.2}{d} m) \right)$$

With some rearrangement we get:

$$d^3 - 55d^2 + 2502 \times 10^5 = 0$$

Solving for d, the only admissible solution is:

$$d = 607 mm$$

Hence, provide an effective depth of 610 mm

$$\text{Area of steel} = 3050 mm^2$$

Provide 20 mm diameter bars of yield strength 590MPa at 90mm c/c on tension face as the main reinforcement.

Provide 10 mm diameter bars of yield strength 590MPa at 90mm c/c on compression face as secondary reinforcement.

### Design for shear

The shear force to be resisted by the section depends on the concrete resistance and is maximum at a section  $d$  away from the face of support:

$$V_u = R_u \times (H - d)$$

$$V_u = 0.75 \times 610^2 \times 10^{-3} \text{ KN} / m \times (3.0 - 0.61)m$$

$$V_u = 625 \text{ KN}$$

The shear stress resisted by concrete alone is given by:

$$V_c = \tau_c \cdot b \cdot d = 0.51 \text{ N} / \text{mm}^2 \times 1000 \text{ mm} \times 610 \text{ mm} = 312 \text{ KN}$$

The design shear (for which shear reinforcement is designed) is provided for ultimate shear less shear strength of concrete:

$$V_d = V_u - V_c = 625 \text{ KN} - 312 \text{ KN} = 313 \text{ KN}$$

The cross section area of closed blast links (for shear is) given by:

$$A_{sv} = \frac{V_d \times s}{f_{ds} \times d}$$

$$s = 300 \text{ mm}$$

$$d = 610 \text{ mm}$$

$$f_{ds} = 1.1 \times 250 \text{ N} / \text{mm}^2 = 275 \text{ N} / \text{mm}^2$$

Takin the width of blast link as 90 mm:

$$A_{sv} = \frac{V_d \left( \frac{90}{1000} \right) \times s}{f_{ds} \times d} = \frac{(312 \times 10^3 \text{ N}) \times \left( \frac{90}{1000} \right) \times 300 \text{ mm}}{275 \text{ N} / \text{mm}^2 \times 610} = 50.21 \text{ mm}^2$$



Provide closed blast links of 10 mm diameter rebars and width 90mm of yield strength 250 MPa at a spacing of 300mm c/c.

The overall depth of the section is given by:

$$D = d + \frac{\phi_{main}}{2} + \phi_{shear} + \text{Clear cover}$$

$$D = 610mm + \frac{20mm}{2} + 10mm + 50mm = 680mm$$

Hence, provide an overall depth of 680 mm.

## 4.2 Type 2 Cantilever blast barrier

Height of blast barrier = 3.0 m

Width of blast barrier = 1.0 m

Loads:

Charge weight of TNT = 180 kg

Standoff distance = 5.0 m

Type of burst = Hemispherical surface burst

Reflected impulse = 5800  $Ns / m^2$  (from curve given in figure 1-4)

Partial safety factor wrt loads = 1.0

Material strength:

Characteristic Cube strength of concrete = 50 MPa

Usable strength of concrete =  $0.67f_{ck} = 33$  MPa

Yield strength of steel = 590 MPa

### Flexural design

Moment of resistance of type 2 section:

$$M_u = bd^2 \cdot \frac{A_{st}}{bd} \cdot (1.2f_y)$$

The reinforcement percentage has been assumed as 0.5%. Hence,

$$\frac{A_{st}}{bd} = 5 \times 10^{-3}$$

Writing moment of resistance in terms of centre to centre distance between tension and compression side reinforcement  $d_c$  (in mm):

$$M_u = 1000 \times d_c^2 \times 5 \times 10^{-3} \times (1.2 \times 600) Nmm^2 = 3.54 \times d^2 \times 10^{-3} KNm$$

The Resistance offered by the barrier is expressed in force per unit height of wall per metre width.

$$R_u = \frac{2 \times M_u}{H^2} = \frac{2 \times 3.54 \times d^2 \times 10^{-3}}{3^2} = 0.80 \times d^2 \times 10^{-3} KN / m$$

The elastic stiffness of the member is calculated by:

$$K_E = \frac{8EI}{H^4}$$

$$E_s = 2 \times 10^5 MPa$$

$$E_c = 0.35 \times 10^5 MPa$$

$$m = 5.714$$

For  $\frac{A_{st}}{bd} = 5 \times 10^{-3}$ ,  $I$  is calculated from standard chart for type 2 section.

$$I = 0.021 \times 10^3 \times d^3 m^4$$

$$K_E = \frac{8EI}{H^4} = 7 \times 10^{-5} \times d^3 KN / m / m$$

The maximum deflection in elastic region is calculated as:

$$X_E = \frac{R_u}{K_E} = \frac{11.3}{d} m$$

For protection category 2, maximum deflection is calculated as:

$$X_m = H \times \tan 4^\circ = 3.0 \times \tan 4^\circ = 209.05 \times 10^{-3} m$$

The load mass factor for cantilever wall is;

$$K_{LM} = 0.66$$

Mass per unit height per metre width for the wall in terms of section depth:

$$m = 2400 \text{ Kg} / \text{m}^3 \times 1.0 \text{ m} \times d \times 10^{-3} \text{ m} = 2.4 \times d \text{ Kg} / \text{m}$$

Putting these quantities in to the basic impulse equation for blast loading:

$$\frac{i^2}{K_{LM} \times m} = \frac{R_u \times X_E}{2} + R_u \times (X_M - X_E)$$

$$i = 5800 \text{ Ns} / \text{m}^2$$

$$\frac{(5800 \text{ Ns} / \text{m}^2)^2}{0.66 \times 2.4 \times d \text{ Kg} / \text{m}} = \frac{(0.80 \times d^2 \times 10^{-3} \text{ KN} / \text{m}) \times \left(\frac{11.3}{d} \text{ m}\right)}{2} + (0.80 \times d^2 \times 10^{-3} \text{ KN} / \text{m}) \times \left((209.05 \times 10^{-3} \text{ m}) - \left(\frac{11.3}{d} \text{ m}\right)\right)$$

With some rearrangement we get:

$$d^3 - 55d^2 + 59.7 \times 10^6 = 0$$

Solving for d, the only admissible solution is:

$$d = 400 \text{ mm}$$

Hence, provide a centre to centre distance between main reinforcing bars on tension and compression face as 400 mm

$$\text{Area of steel} = 3050 \text{ mm}^2$$

Provide 20 mm diameter bars of yield strength 590MPa at 150 mm c/c on both faces equally.

### Design for shear

The shear force to be resisted by the section depends on the concrete resistance and is maximum at a section d away from the face of support:

$$V_u = R_u \times (H - d)$$

$$V_u = 0.80 \times 400^2 \times 10^{-3} \text{ KN} / \text{m} \times (3.0 - 0.40) \text{ m}$$

$$V_u = 332.8 \text{ KN}$$

The shear stress resisted by concrete alone is given by:

$$V_c = \tau_c \cdot b \cdot d = 0.51 \text{ N/mm}^2 \times 1000 \text{ mm} \times 400 \text{ mm} = 204 \text{ kN}$$

The design shear (for which shear reinforcement is designed) is provided for ultimate shear less shear strength of concrete:

$$V_d = V_u - V_c = 332.8 \text{ kN} - 204 \text{ kN} = 128.8 \text{ kN}$$

The cross section area of closed blast links (for shear is) given by:

$$A_{sv} = \frac{V_d \times s}{f_{ds} \times d}$$

$$s = 300 \text{ mm}$$

$$d = 610 \text{ mm}$$

$$f_{ds} = 1.1 \times 250 \text{ N/mm}^2 = 275 \text{ N/mm}^2$$

Takin the width of blast link as 150 mm:

$$A_{sv} = \frac{V_d \left( \frac{150}{1000} \right) \times s}{f_{ds} \times d} = \frac{(128.8 \times 10^3 \text{ N}) \times \left( \frac{150}{1000} \right) \times 300 \text{ mm}}{275 \text{ N/mm}^2 \times 400} = 52.69 \text{ mm}^2$$

Provide closed blast links of 10 mm diameter rebar and of width 150mm of yield strength 250 MPa at a spacing of 300mm c/c.

Type 2 section requires additional reinforcement for support shear as diagonal bars.

Hence, provide diagonal bars of 12 mm diameter and yield strength 590 MPa at 45° to the main reinforcement at the support

The overall depth of cross section will be:

$$D = d_c + 2 \times \frac{\phi_{main}}{2} + 2 \times \phi_{shear} + 2 \times \text{Clear cover}$$

$$D = 400 \text{ mm} + 2 \times \frac{20 \text{ mm}}{2} + 2 \times 10 \text{ mm} + 2 \times 50 \text{ mm} = 540 \text{ mm}$$

Hence, provide an overall depth of 540 mm.

### 4.3 Type 2 Fixed blast barrier

Height of blast barrier = 3.0 m

Width of blast barrier = 2.0 m

Support condition: The blast barrier is fixed on both sides on vertical unyielding supports from counterforts.

Loads:

Charge weight of TNT = 180 kg

Standoff distance = 5.0 m

Type of burst = Hemispherical surface burst

Reflected impulse =  $5800 \text{ Ns} / \text{m}^2$  (from curve given in figure 1-4)

Partial safety factor wrt loads = 1.0

Material strength:

Characteristic Cube strength of concrete = 50 MPa

Usable strength of concrete =  $0.67 f_{ck} = 33 \text{ MPa}$

Yield strength of steel = 590 MPa

#### Flexural design

Moment of resistance of type 2 section:

$$M_u = bd^2 \cdot \frac{A_{st}}{bd} \cdot (1.2 f_y)$$

The reinforcement percentage has been assumed as 0.5%. Hence,

$$\frac{A_{st}}{bd} = 5 \times 10^{-3}$$

Writing moment of resistance in terms of centre to centre distance between tension and compression side reinforcement  $d_c$  (in mm):

$$M_u = 1000 \times d_c^2 \times 5 \times 10^{-3} \times (1.2 \times 600) \text{ Nmm}^2 = 3.54 \times d^2 \times 10^{-3} \text{ KNm}$$

The Resistance offered by the barrier is expressed in force per unit height of wall per metre width.

$$R_u = \frac{8 \times M_u}{L^2} = \frac{8 \times 3.54 \times d^2 \times 10^{-3}}{2^2} = 7.08 \times d^2 \times 10^{-3} \text{ KN / m}$$

The elastic stiffness of the member is calculated by:

$$K_E = \frac{384EI}{L^4}$$

$$E_s = 2 \times 10^5 \text{ MPa}$$

$$E_c = 0.35 \times 10^5 \text{ MPa}$$

$$m = 5.714$$

For  $\frac{A_{st}}{bd} = 5 \times 10^{-3}$ , I is calculated from standard chart for type 2 section.

$$I = 0.021 \times 10^3 \times d^3 \text{ m}^4$$

$$K_E = \frac{384EI}{L^4} = 17.01 \times 10^{-3} \times d^3 \text{ KN / m / m}$$

The maximum deflection in elastic region is calculated as:

$$X_E = \frac{R_u}{K_E} = \frac{0.416}{d} \text{ m}$$

For protection category 2, maximum deflection is calculated as:

$$X_m = \frac{L}{2} \times \tan 4^\circ = 1.0 \times \tan 4^\circ = 69.92 \times 10^{-3} \text{ m}$$

The load mass factor for simply supported wall is;

$$K_{LM} = 0.78$$

Mass per unit height per metre width for the wall in terms of section depth:

$$m = 2400 \text{ Kg / m}^3 \times 1.0 \text{ m} \times d \times 10^{-3} \text{ m} = 2.4 \times d \text{ Kg / m}$$

Putting these quantities in to the basic impulse equation for blast loading:

$$\frac{i^2}{K_{LM} \times m} = \frac{R_u \times X_E}{2} + R_u \times (X_M - X_E)$$

$$i = 5800 \text{ Ns} / \text{m}^2$$

$$\frac{(5800 \text{ Ns} / \text{m}^2)^2}{0.78 \times 2.4 \times d \text{ Kg} / \text{m}} = \frac{(7.08 \times d^2 \times 10^{-3} \text{ KN} / \text{m}) \times \left(\frac{0.416}{d} \text{ m}\right)}{2} + (7.08 \times d^2 \times 10^{-3} \text{ KN} / \text{m}) \times \left( (69.92 \times 10^{-3} \text{ m}) - \left(\frac{0.416}{d} \text{ m}\right) \right)$$

With some rearrangement we get:

$$d^3 - 5.94d^2 + 38.85 \times 10^6 = 0$$

Solving for d, the only admissible solution is:

$$d = 340 \text{ mm}$$

Hence, provide a centre to centre distance between main reinforcing bars on tension and compression side as 340 mm.

$$\text{Area of steel} = 1700 \text{ mm}^2$$

Provide 20 mm diameter bars of yield strength 590MPa at 160 mm c/c on both faces equally.

### Design for shear

The shear force to be resisted by the section depends on the concrete resistance and is maximum at a section d away from the face of support:

$$V_u = R_u \times \left( \frac{L}{2} - d \right)$$

$$V_u = 7.08 \times 340^2 \times 10^{-3} \text{ KN} / \text{m} \times (1.0 - 0.34) \text{ m}$$

$$V_u = 540.175 \text{ KN}$$

The shear stress resisted by concrete alone is given by:

$$V_c = \tau_c \cdot b \cdot d = 0.51 \text{ N} / \text{mm}^2 \times 1000 \text{ mm} \times 340 \text{ mm} = 173.4 \text{ KN}$$

The design shear (for which shear reinforcement is designed) is provided for ultimate shear less shear strength of concrete:

$$V_d = V_u - V_c = 540.175 \text{ kN} - 173.4 \text{ kN} = 366.78 \text{ kN}$$

The cross section area of closed blast links (for shear is) given by:

$$A_{sv} = \frac{V_d \times s}{f_{ds} \times d}$$

$$s = 100 \text{ mm}$$

$$d = 340 \text{ mm}$$

$$f_{ds} = 1.1 \times 250 \text{ N/mm}^2 = 275 \text{ N/mm}^2$$

Takin the width of blast link as 320 mm:

$$A_{sv} = \frac{V_d \left( \frac{320}{1000} \right) \times s}{f_{ds} \times d} = \frac{(366.78 \times 10^3 \text{ N}) \times \left( \frac{320}{1000} \right) \times 100 \text{ mm}}{275 \text{ N/mm}^2 \times 340} = 125.52 \text{ mm}^2$$

Provide closed blast links of 10 mm diameter rebar and of width 320mm of yield strength 250 MPa at a spacing of 100mm c/c.

The overall depth of cross section will be:

$$D = d_c + 2 \times \frac{\phi_{main}}{2} + 2 \times \phi_{shear} + 2 \times \text{Clear cover}$$

$$D = 340 \text{ mm} + 2 \times \frac{20 \text{ mm}}{2} + 2 \times 10 \text{ mm} + 2 \times 35 \text{ mm} = 450 \text{ mm}$$

Hence, provide an overall depth of 450 mm.

#### 4.4 Aluminium foam sacrificial cladding

Design of aluminium foam sacrificial cladding involves finding the minimum required thickness of the foam to dissipate completely the impulse generated due to blast load. The details of the blast load and the foam cladding are:

Loads:

Charge weight of TNT = 180 kg

Standoff distance = 5.0 m

Type of burst = Hemispherical surface burst



Reflected impulse =  $I = 5800 \text{ Ns} / \text{m}^2$  (from curve given in figure 1-4)

Maximum reflected overpressure =  $p_0 = 11.2 \text{ MPa}$  (From curve given in figure 1-4)

Material properties of aluminium foam:

Density =  $\rho = 570 \text{ Kg} / \text{m}^3$

Plateau strength =  $\sigma_0 = 5 \text{ MPa}$

Modulus of elasticity =  $E = 1100 \text{ MPa}$

Densification strain =  $\varepsilon_D = 0.3$

Cover plate material = Mild steel

Cover plate thickness = 10 mm

Assumed thickness of foam = 100 mm

Mass of foam for  $1 \text{ m}^2$  area =  $M_0 = 57 \text{ Kg}$

Mass of cover plate for  $1 \text{ m}^2$  area =  $M_1 = 78 \text{ Kg}$

The minimum thickness of foam is given by L:

$$l \geq \frac{I^2}{(M_0 + 2M_1) p_0 A \varepsilon_D} \left\{ \frac{p_0}{\sigma_0} - \frac{4}{3} \right\}, \quad \frac{p_0}{\sigma_0} > 2$$

Putting the values of respective quantities:

$$l \geq \frac{(5800 \text{ Ns} / \text{m}^2)^2}{(57 \text{ Kg} + 2 \times 78 \text{ Kg}) \times (11.2 \times 10^6 \text{ Pa}) \times (1 \text{ m}^2) \times (0.3)} \left\{ \frac{11.2 \text{ MPa}}{5 \text{ MPa}} - \frac{4}{3} \right\}$$

$$l \geq 0.0426 \text{ m}$$

$$l \geq 42.6 \text{ mm}$$

Hence, the assumed thickness of 100 mm is OK.

## Chapter 5. Validation of material models used

In this chapter, the material models used in the work have been validated by using them in Abaqus models replicating the original experimental programme and comparing the results obtained in the experiments with the results of the numerical analysis in Abaqus.

### 5.1 Validation of material model for concrete and steel

#### 5.1.1 Experimental program

Wang et al (2012) [13] carried out blast loading tests on square one way fixed slab of dimensions 1000mm\*1000mm\*40mm with reinforcement of 6mm diameter at spacing of 75 mm c/c in both the directions. The reinforcement along major bending plane is at a clear cover of 10 mm from the bottom. The compressive strength of concrete was recorded as 39.5 MPa cylinder strength and the yield strength of rebars was 600 MPa. The blast load is applied by a TNT charge of 0.46 kg at a distance of 0.4 m from the top surface. The concrete damage and spalling for proximal and distal surfaces were observed and deflection at the centre of the slab was measured.

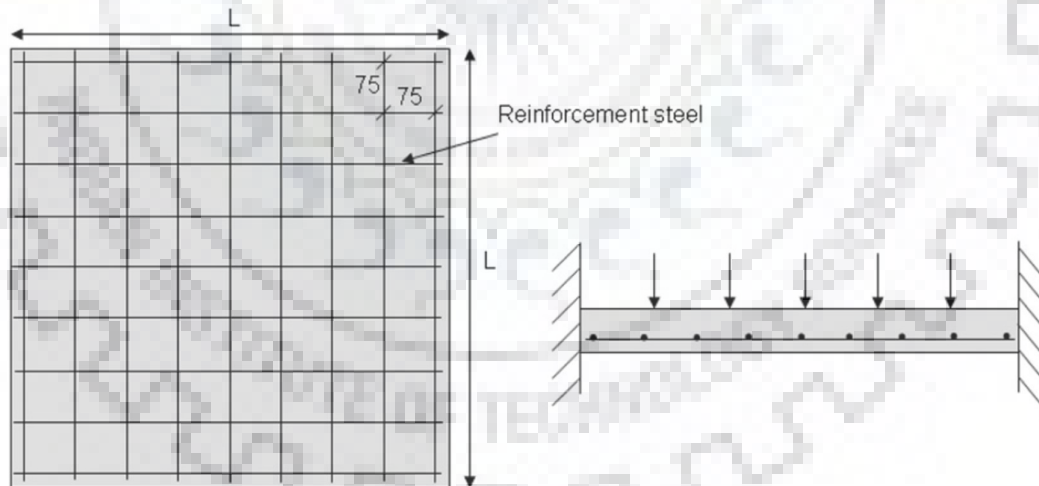


Figure 5-1: Wang et al. details of slab, reinforcement and support conditions

#### 5.1.2 Abaqus Model

An abaqus model replicating the experiment of Wang et al was made. The material models used in the model have been taken from literature. They are briefly described here.

### Concrete damaged plasticity (CDP) model for B50 concrete

Jankowiak and Lodygowski (2013) [15] identified the parameters for concrete damaged plasticity model for B50 grade of concrete (cube compressive strength of 50MPa). The laboratory tests used were presented. The identified parameters are mentioned here:

Table 5-1: CDP values for plasticity parameters

Dilation angle	Eccentricity	$f_{b0}/f_{c0}$	K	Viscosity parameter
38	0.1	1.16	0.67	1E-006

Table 5-2: CDP stress strain data for compression

Yield stress(N/mm <sup>2</sup> )	Inelastic strain	Rate of strain(s <sup>-1</sup> )
15	0	1E-006
20.197804	7.47307E-005	1E-006
30.000609	9.88479E-005	1E-006
40.303781	0.000154123	1E-006
50.007692	0.000761538	1E-006
40.23609	0.002557559	1E-006
20.23609	0.005675431	1E-006
5.257557	0.011733119	1E-006

Table 5-3: CDP damage data for compression

Inelastic strain	Compressive damage parameter
0	0
7.47307E-005	0
9.88479E-005	0
0.000154123	0
0.000761538	0
0.002557559	0.195402
0.005675431	0.596382

0.011733119	0.894865
-------------	----------

Table 5-4: CDP stress strain data for tension

Yield stress(N/mm <sup>2</sup> )	Cracking strain	Rate of strain(s <sup>-1</sup> )
1.99893	0	1E-006
2.842	3.333E-005	1E-006
1.86981	0.000160427	1E-006
0.862723	0.000279763	1E-006
0.226254	0.000684593	1E-006
0.056576	0.00108673	1E-006

Table 5-5: Damage data for tension

Inelastic strain	Compressive damage parameter
0	0
3.333E-005	0
0.000160427	0.406411
0.000279763	0.69638
0.000684593	0.920389
0.00108673	0.980093

### Johnson Cook model (J-C) model for DP-590 steel

Vedantam et al. (2006) [16] obtained tension stress strain data for mild steel and DP-590 steel using quasi static and split Hopkinson bar techniques at strain rates ranging from 10<sup>-3</sup>/s to 1800/s and used the data to identify the parameters of Johnson Cook strength model for mild steel and DP-590 steel. They are mentioned below:

Table 5-6: J-C strength parameters for DP-590 steel

A	B	C	m	n
430	823.6	0.0171	0	0.5071

Table 5-7: J-C strength parameters for mild steel

A	B	C	m	n
217	233.7	0.0756	0	0.6428

Table 5-8: J-C parameters common to both mild steel and DP-590 steel

$\dot{\epsilon}_0$ (Static yield strain rate)	$\theta_{transition}$ (Transition temperature)	$\theta_{melt}$ (Melting temperature)
$1 s^{-1}$	$700^{\circ}C$	$1400^{\circ}C$

Rest of the details of the Abaqus model are as follows:

Table 5-9: Partwise details of Abaqus model

Part	Type	Dimensions	Element	Mesh size
Concrete	Solid	$1000mm \times 1000mm \times 40mm$	C3D8R	$10mm \times 10mm \times 4mm$
	Deformable			
Steel Rebar	Wire	$Length = 1000mm$	T3D2	$Length = 10mm$
	Deformable			

- The assembly of parts is as per the experiment of Wang et al.
- Embedded constraint has been used for modelling bond between concrete and rebars.
- Fixed boundary condition has been provided along 2 side faces of the model.
- The blast load has been modelled as incident wave with CONWEP property corresponding to surface burst of 180 kg TNT charge and 0.4 m standoff distance from the face of slab.
- The blast load has been applied as an interaction in the explicit dynamic time step blast of step time 30 ms. Explicit solver has been used for analysing the system.

### 5.1.3 Comparison of experimental and numerical result

The following figure compares experimentally observed damage with the numerical damage in Abaqus. The graph of deflection vs time for the centre of the slab is also shown.

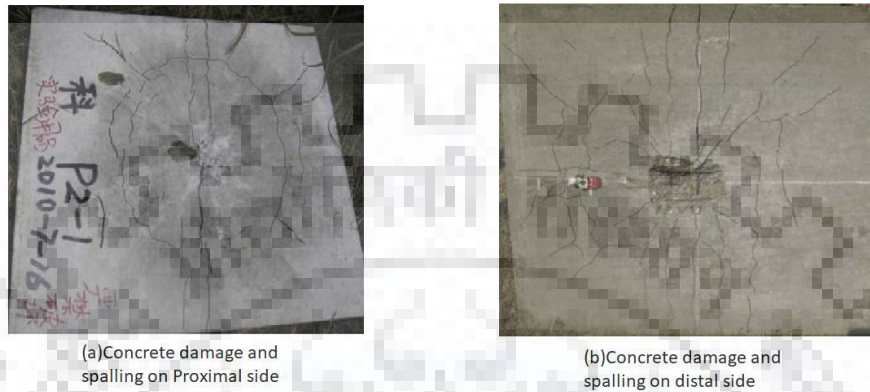


Figure 5-2: Experimentally observed damage on both faces of slab

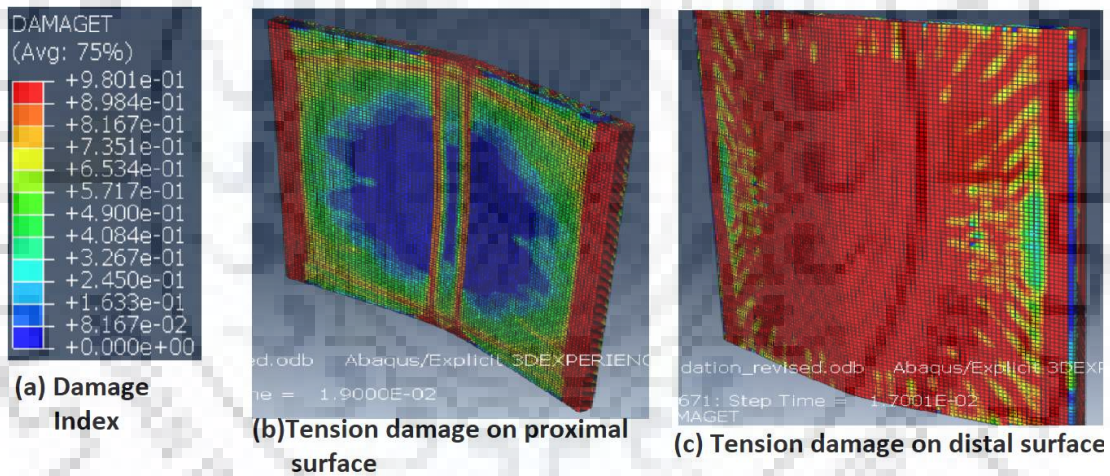


Figure 5-3: Numerically obtained Tension damage on both faces of slab

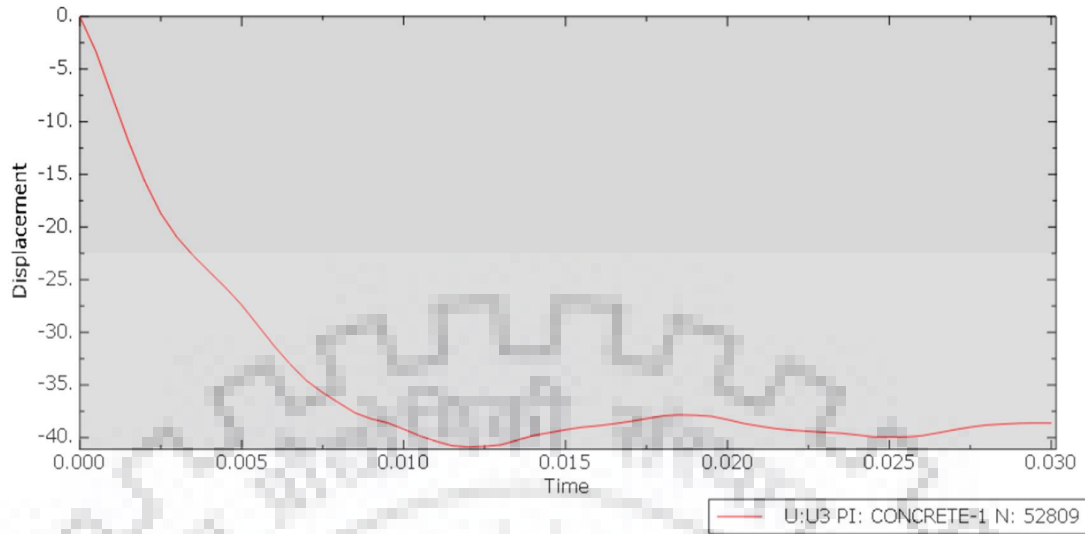


Figure 5-4: Deflection vs time curve for centre of slab

Table 5-10: Experimental Vs numerical deflection at centre of slab.

Experimental deflection	Numerical deflection	Percentage error
35 mm	38.75 mm	10.71%

The percentage error in the numerically obtained deflection from the experimental value is 10.71%. This is within the acceptable range of error. Hence, the material model for concrete and steel is validated.

## 5.2 Validation of material model for aluminium foam

### 5.2.1 Experimental programme

Langdon et al. (2009) [8] performed blast loading experiments on structure consisting of aluminium foam within a base plate and a cover plate all 105mm\*105mm. The material of base plate is 4mm and cover plate is 2mm and 4mm. aluminium foam of 3 different densities 10%, 15% and 20% are tested. The thickness of aluminium foam is 25 mm and 50mm. Two different case of cover plate bonded and unbonded with aluminium foam were tested.

Plastic explosive PE4 of charge weight between 4g and 20 g at a standoff distance of approximately 200 mm inside a blast shroud were used. The impulse generated as a

result of blast loads was measured using a ballistic pendulum. A total of 31 tests were conducted.

The crush percentage and cracks in aluminium foam were observed and the effect of foam thickness and density and cover plate thickness and bonding of plate with foam in the crack occurrence and foam crushing were observed. Figure shows the apparatus used for experiments.

The following two blast loading tests were selected for replication in Abaqus/Explicit:

*Table 5-11: Blast tests chosen to be replicated*

Foam density	Foam thickness	Cover to foam bond	Cover plate thickness	Charge weight (PE4)	Impulse	Final foam thickness	Percentage crush
10% Relative density	50 mm	Unbonded	4 mm	10g	12.9 Ns	27.2 mm	45.6%
20% Relative density	25 mm	Bonded	2 mm	6g	18.9 Ns	17.6 mm	29.6%



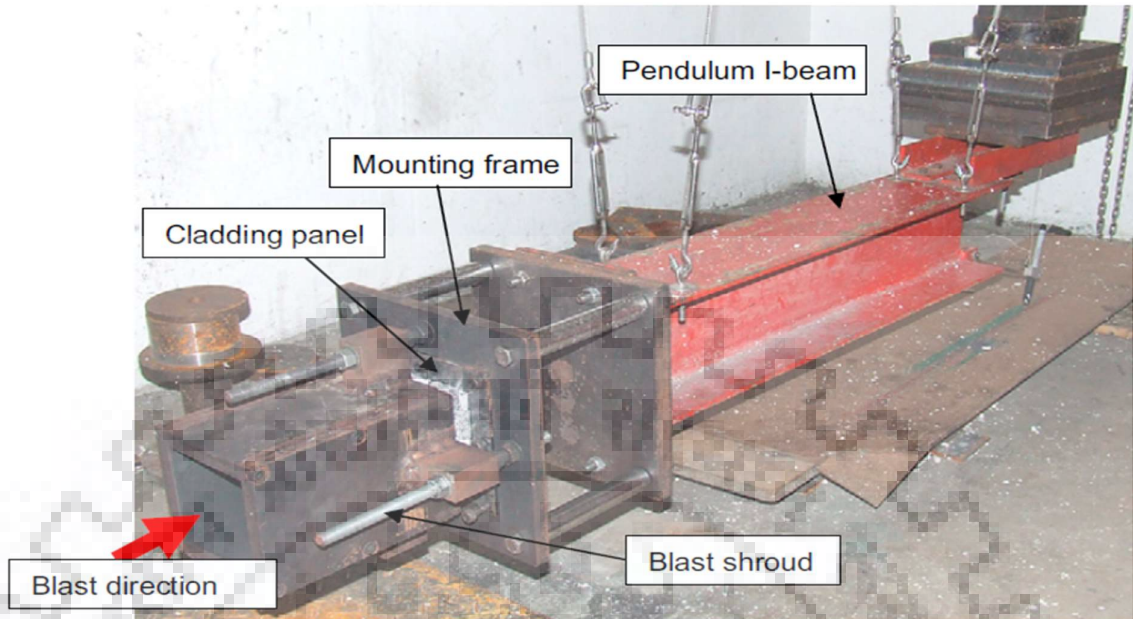


Figure 5-5: Apparatus used for experiments by Langdon et al.

### 5.2.2 Abaqus Model

The experiments performed by Langdon et al. were accompanied by numerical simulations in Abaqus/Explicit in which base plate was assumed as rigid and the cover plate was modelled as Johnson cook model for mild steel. The aluminium foam was modelled using crushable foam data for 10% and 20% relative density foams. These material models have been taken for this numerical study. They are briefly described below.

#### J-C data for mild steel

The following constants have been taken for mild steel of the cover plate:

Mechanical and elastic properties:

$$\rho = 7800 \text{ kg / m}^3$$

$$E = 200 \text{ GPa}$$

$$\nu = 0.3$$

Johnson Cook constants:

$$A = 190 \text{ MPa}, B = 400 \text{ MPa}, C = 0.135, n = 0.42 \text{ and } \dot{\epsilon}_0 = 0.001 \text{ s}^{-1}$$

## Crushable foam data for 10% and 20% relative density aluminium foam

The elastic and mechanical properties for this model are:

Table 5-12: Density and elasticity modulus for two foam densities

Foam type ↓	Properties →	Density ( $\rho$ )	Elasticity modulus (E)
10% Relative density		253kg / m <sup>3</sup>	450MPa
20% Relative density		570kg / m <sup>3</sup>	1100MPa

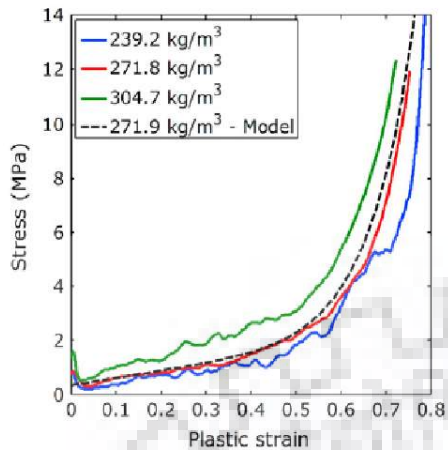
Crushable foam model uses a failure surface that evolves in a self-similar fashion. The shape factor  $\alpha$  depends on the ratio of yield stress in uniaxial compression to hydrostatic compression and the ratio of yield stress in uniaxial tension to hydrostatic tension.

$$k = \sigma_c^0 / p_c^0 = 1$$

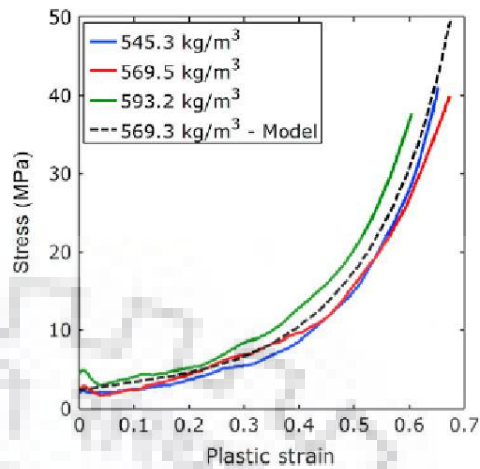
$$k_t = p_t / p_c^0 = 1$$

$$\alpha = 3k / \sqrt{(3k_t + k)(3 - k)}$$

The foam hardening data for 10% and 20% relative density foam is extracted in the tabular format from the graphs shown here.



**(a) 10% foam i.e. 272 kg/m<sup>3</sup>**



**(b) 20% foam i.e. 570 kg/m<sup>3</sup>**

Figure 5-6: Foam hardening data for 10% and 20% relative density foam

Rest of the details of the Abaqus model are as follows:

Table 5-13: Part details for bonded aluminium foam model

Part	Type	Dimensions	Element	Mesh size
Rigid Base	Discrete rigid Deformable	52.5mm × 52.5mm × 4mm	R3D4	4mm × 4mm × 4mm
Aluminium foam	Solid Deformable	52.5mm × 52.5mm × 25mm	C3D8R	0.5mm × 0.5mm × 0.5mm
Cover plate	Solid Deformable	52.5mm × 52.5mm × 2mm	C3D8R	1mm × 1mm × 1mm

- Axisymmetric boundary condition has been used along one X and Y boundary of the model to simulate a size double of the model i.e. 105mm\*105mm, the model is a quarter model to save simulation time.

Table 5-14: Part details for bonded aluminium foam model

Part	Type	Dimensions	Element	Mesh size
Rigid Base	Discrete rigid Deformable	52.5mm×52.5mm×4mm	R3D4	4mm×4mm×4mm
Aluminium foam	Solid Deformable	52.5mm×52.5mm×50mm	C3D8R	1mm×1mm×1mm
Cover plate	Solid Deformable	52.5mm×52.5mm×4mm	C3D8R	1mm×1mm×1mm

- Axisymmetric boundary condition has been used along one X and Y boundary of the model to simulate a size double of the model i.e. 105mm\*105mm, the model is a quarter model to save simulation time.
- The assembly of parts is replicating the experimental setup of Langdon et al.
- Rigid base has been given fixed boundary condition with the help of rigid body constraint.
- The bond between base plate and aluminium foam has been modelled as tie constraint
- The bond between cover plate and aluminium foam has been modelled as tie constraint in case of bonded foam and contact pair with normal behaviour hard contact and friction of 0.3 for tangential behaviour has been defined for unbonded foam.
- The blast load has been modelled as a uniform dynamic pressure on the cover plate with a peak pressure decaying exponentially with time  $P(t) = P_0 \exp(-2t/t_0)$ ,  $t_0 = 30\mu s$ . The peak pressure  $P_0$  is obtained by equating the impulse obtained with time integral of decaying pressure over the plate area.  $I = A \int P(t) dt$ . The peak pressure for bonded foam is thus obtained as 78MPa and for unbonded cladding it is 114.5MPa.
- The loads are applied in explicit dynamic step 'blast'. Step time for bonded foam is 0.5ms and that for unbonded foam is 1.5ms. Explicit solver is used for the analysis.

### 5.2.3 Comparison of experimental and numerical results

The following figures shows the displacement contours of bonded aluminium foam along with deflection vs time curve of its compression.

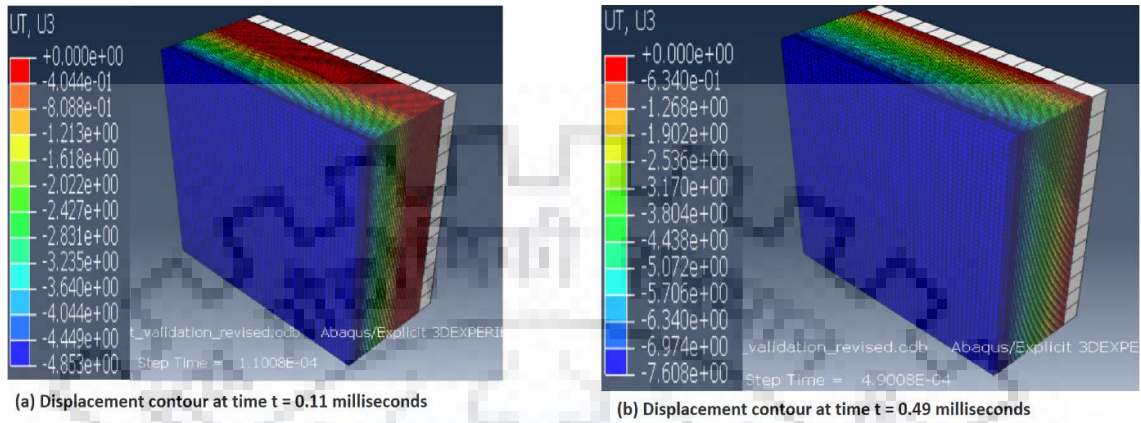


Figure 5-7: Displacement contours for bonded aluminium foam

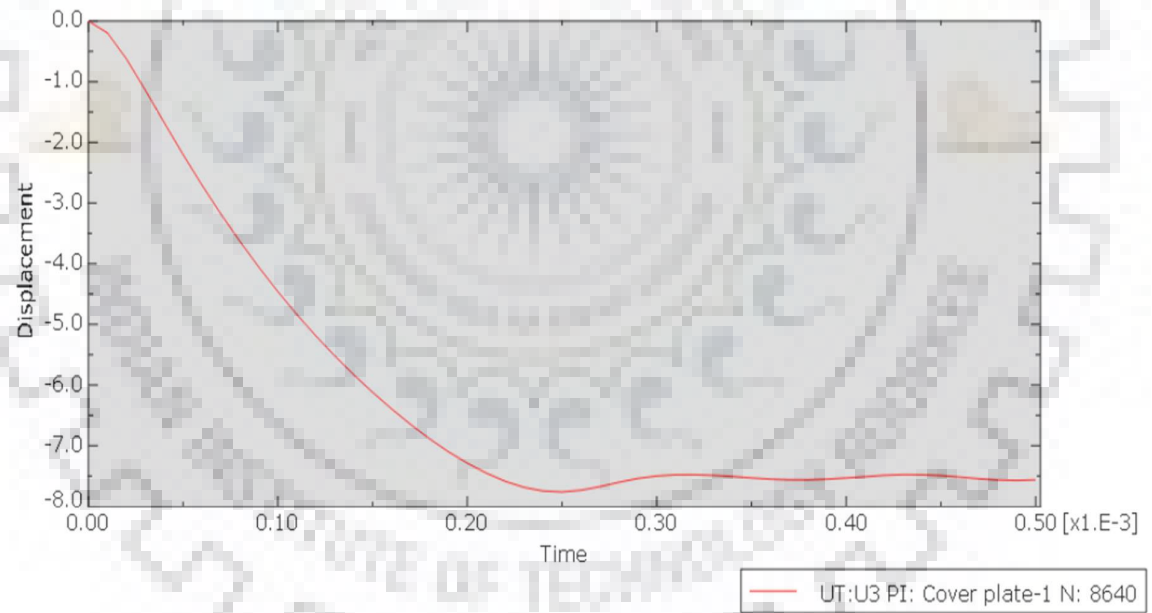


Figure 5-8: Displacement VS time curve for cover plate bonded with aluminium foam.

The following figures show the displacement contours for unbonded foam and displacement VS time curve for the top of unbonded aluminium foam. It may be observed that towards the end of step time the cover plate bounces off the aluminium foam.



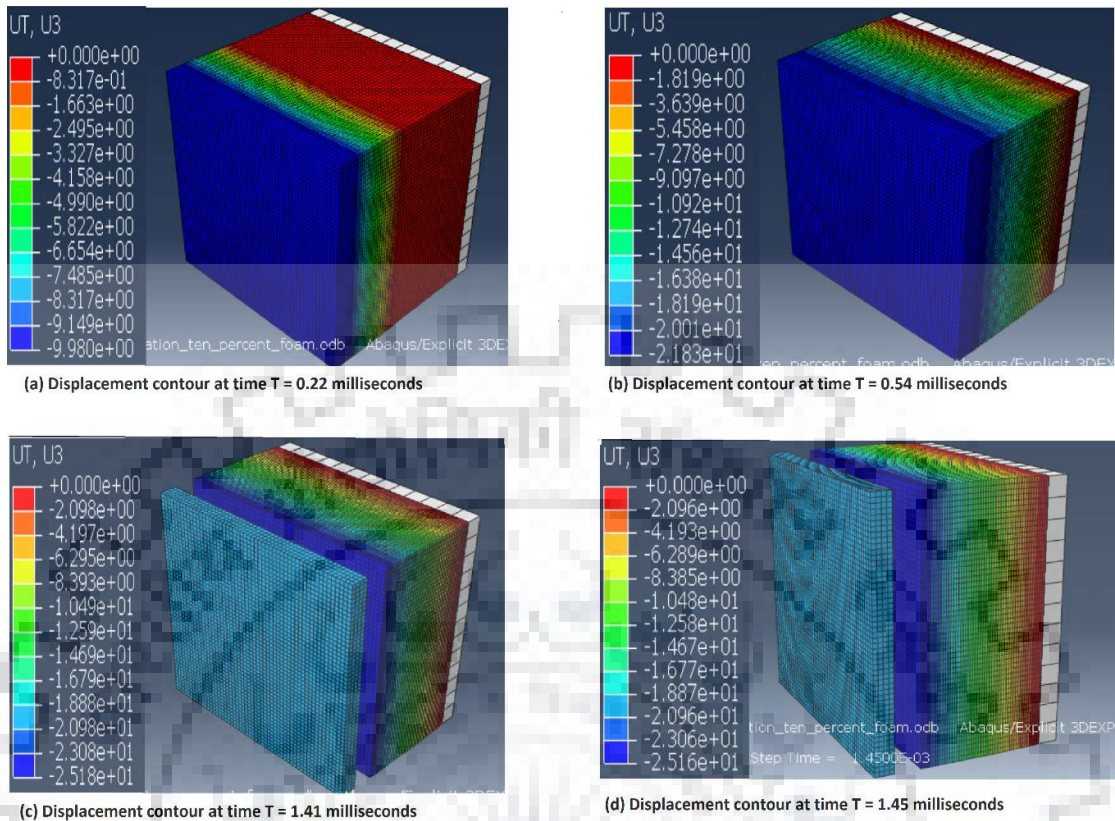


Figure 5-9: Displacement contours for unbonded aluminium and cover plate.

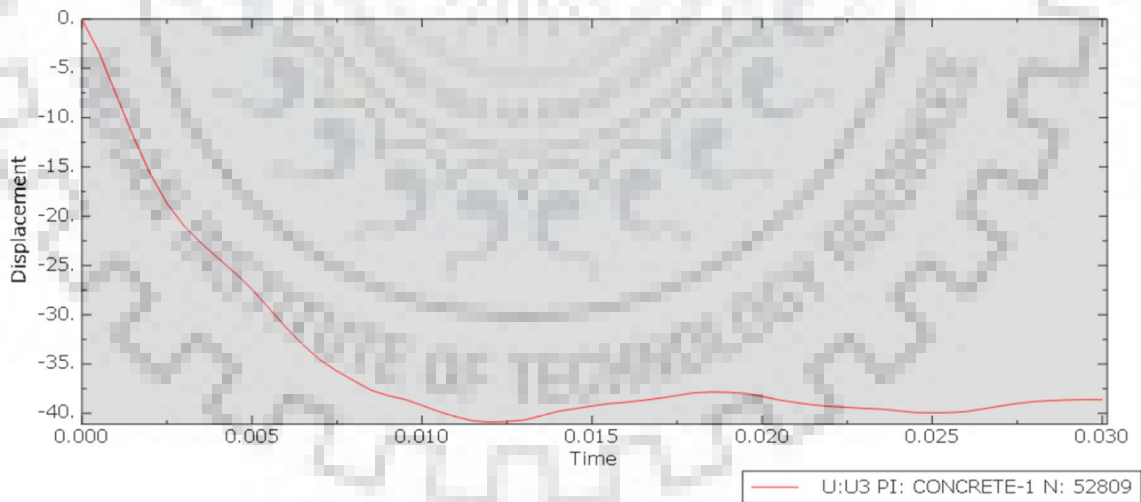


Figure 5-10: Displacement time curve for top of unbonded aluminium foam

The following table compares the crushed thickness for bonded and unbonded aluminium foam as obtained in the experimental program and numerical study.

Table 5-15: Comparison of experimental and numerical crushed thickness.

Type of foam	Original thickness	Crushed thickness obtained		Percentage error
		Experimental program	Numerical study	
Bonded	25 mm	17.6 mm	17.4 mm	1.14%
Unbonded	50 mm	27.2 mm	25.5 mm	6.25%

The errors in the numerical prediction of foam crushing is within acceptable range of error. Hence, the material models for aluminium foam and mild steel cover plate is validated.



## Chapter 6. Parametric study

In this chapter, a parametric study has been carried out to observe the effect of charge weight and standoff distance on damage to the concrete of an RC slab. A simulation in Abaqus is carried out where blast waves are made to impinge on a square RC slab simply supported in both directions. The damage to the concrete on proximal and distal face is recorded for different combinations of charge weight and standoff distance and trends of increase/decrease in damage with variation in charge weight and standoff distance is studied.

### 6.1 Abaqus model

An abaqus model of an RC slab of dimensions 1000mm\*1000mm\*120mm of M50 concrete reinforced with 10 mm diameter rebars of yield strength 590MPa at a spacing of 100 mm c/c in 2 mutually perpendicular layers with a clear cover of 50 mm is modelled. The partwise details of the model is presented in this table.

Table 6-1: Partwise details for Abaqus model

Part	Type of Part	Dimensions	Material	Element type	Mesh size
Concrete	Solid deformable	1000mm*1000mm*120mm	CDP/B50 concrete	C3D8R	Global seed size = 10mm
Rebars	Solid deformable	Cylinder, D=10mm, L= 1000mm	J-C/DP-590 steel	C3D8R	Global seed size = 10mm

Rest of the details of Abaqus model are:

- Simply supported boundary condition has been modelled in both directions.
- Embedded constraint has been used to model the bond between concrete and steel.
- The blast load has been modelled as incident wave with CONWEP property in the explicit dynamic step 'blast' with a step time of 100 milliseconds.
- Different combinations of charge weight and standoff distances were taken for the analysis. They are mentioned in this table.



Table 6-2: List of tests with different charge weight and standoff distance

Standoff distance	0.5 m	1.0 m	2.0 m
Charge weight			
0.5 Kg	✓		
10.0 Kg	✓		
50.0 Kg	✓		
200.0 Kg		✓	✓

## 6.2 Trends observed

The following trends were observed:

- It was observed that reduction in standoff distance caused the concrete damage to increase.

For example, shown here is the comparison of damage on proximal surface due to charge weight 200kg TNT and standoff distance 2.0 m and 1.0 m.

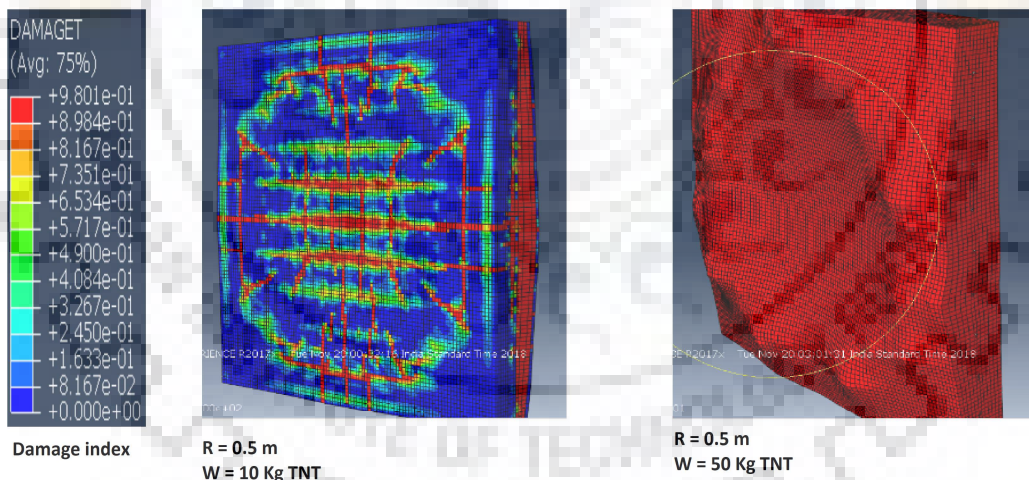


Figure 6-1: Effect of charge weight on concrete damage

- It was observed that increase in charge weight caused the concrete damage to increase.

For example, shown here is the comparison of damage on proximal surface due to charge weight 10kg and 50 kg TNT and standoff distance 0.5 m

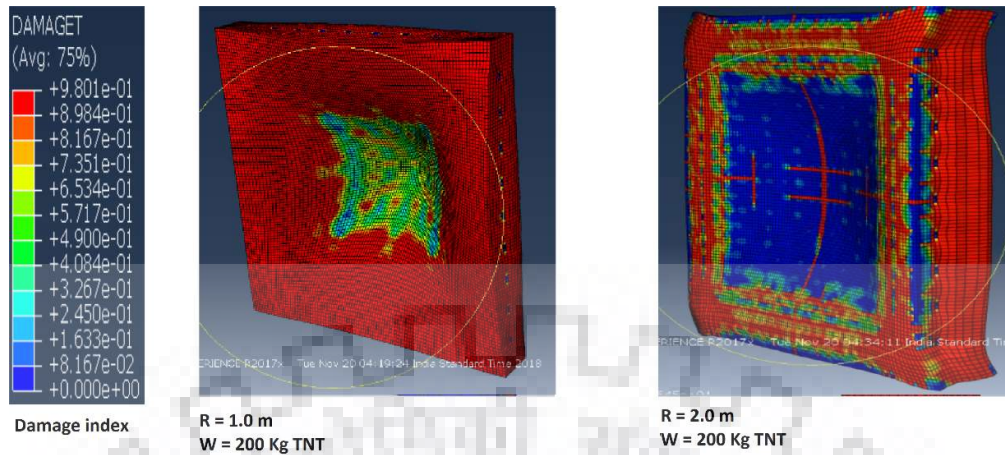


Figure 6-2: Effect of standoff distance on concrete damage

- It was observed that the reduction in standoff distance is more effective in causing an increase in concrete damage as compared to increase in charge weight.

For example, shown here is the comparison of damage on proximal surface due to weight of 200kg at 1.0m and 50 kg at 0.5 m.

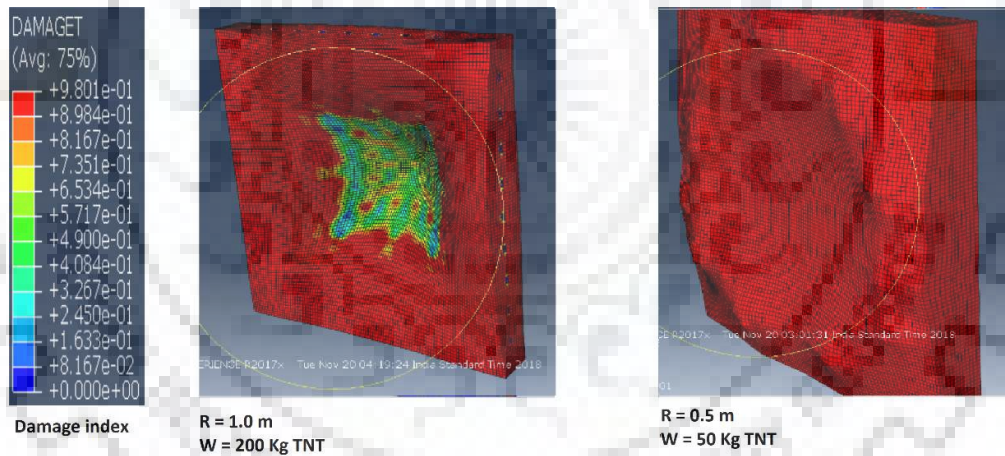


Figure 6-3: Effect of both charge weight and standoff distance on concrete damage.

## **Chapter 7. Sacrificial cladding in blast barriers**

---

In this chapter, the effect of presence of sacrificial cladding in blast barriers is investigated. Three blast barriers namely, type 1 cantilever, type 2 cantilever and type 2 fixed blast barrier for which design have been presented in chapter 3, have been modelled in Abaqus and are subjected to design blast loads in Abaqus simulations. Their performance under blast loading is assessed in terms of the permanent deformations and concrete damage accumulated. Hence, the same blast barriers are modelled with a sacrificial cladding of aluminium foam of design thickness for specified blast loads and the barriers are subject to blast loading in simulations and concrete damage and deformations assessed. A comparison of damage and deformation for with/without foam cases is made and the efficacy of sacrificial cladding in reducing damage to RC structures under blast load is assessed.

### **7.1 Type 1 cantilever blast barrier**

#### **7.1.1 Without aluminium foam sacrificial cladding**

An Abaqus model of the Type 1 cantilever blast barrier designed in section 3.1 is presented here. The design data for the wall, design values of thickness and reinforcement are mentioned here.

Blast load: Hemispherical surface burst due to 180 Kg TNT at ground level at 5.0 m standoff distance.

Height of wall = 3.0 m

Overall depth of section = 680 mm

Effective depth of section = 610 mm

Tension reinforcement = 20 mm dia bars of 590 MPa yield strength at 90 mm c/c

Compression reinforcement = 10 mm dia bars of 590 MPa yield strength at 90 mm c/c

Shear reinforcement = 10 mm dia bars bent into closed blast links of 90 mm width @ 300 mm c/c

Clear cover = 50 mm (tension side), 35 mm (compression side)

The partwise details of the Abaqus model are as follows:

Table 7-1: Part details of type 1 cantilever blast barrier

Part	Type of Part	Dimensions	Material	Element type	Mesh size
Concrete	Solid deformable	1180mm*680mm*3200mm	CDP/B50 concrete	C3D8R	Global seed size = 20mm
20 mm Rebar	Wire deformable	Length = 3200 mm, cross sectional area = $314\text{mm}^2$	J-C/DP-590 steel	T3D2	Global seed size = 20mm
10 mm Rebar	Wire deformable	Length = 3200 mm, cross sectional area = $78.5\text{mm}^2$	J-C/DP-590 steel	T3D2	Global seed size = 20mm
Shear blast link, 10mm $\varnothing$	Wire deformable	Chamfered rectangular closed loop, length=585 mm, width=120mm, CSA= $78.5\text{mm}^2$	J-C/Mild steel	T3D2	Global seed size = 10mm
Rigid base	Shell/Discrete rigid	300mm*1200mm*1180mm	-	R3D4	Global seed size=120mm

Rest of the details of the model are as follows:

- The parts have been assembled as per the design shown in chapter 3.
- Embedded constraint has been used to model the rebar concrete bond.
- Tie constraint has been used to model the fixity between rigid base and concrete part.
- Rigid body constraint has been used to model the fixity of rigid base by defining fixed boundary condition to reference point.
- The blast load is modelled as an interaction of incident wave of surface burst of 180 Kg TNT at a standoff of 5.0 m with the proximal surface of the barrier.
- The blast load has been applied in the dynamic explicit step 'blast' with a step time of 50 milliseconds and for with foam cladding case it is 60 milliseconds.
- Axisymmetric boundary condition has been used along one side face to simulate double the modelled length into study.

### 7.1.2 With sacrificial cladding

Abaqus model of type 1 blast barrier with aluminium foam sacrificial cladding is same as that without the sacrificial cladding except for the following extra details.

2 parts, namely the aluminium foam and cover plate are modelled. Their details are:

Table 7-2: Additional part details for foam cladding (type 1 cantilever)

Part	Type of Part	Dimensions	Material	Element type	Mesh size
Aluminium foam	Solid deformable	1180mm*3000mm*100mm	Crushable foam model/aluminium foam	C3D8R	20mm*20mm*5mm
Cover plate	Shell deformable	1180mm*3000mm Thickness = 10mm	J-C/Mild steel	S4R	20mm*20mm

- Tie constraint has been used to model the fixity between aluminium foam and concrete and between aluminium foam and cover plate.
- Rest of the details are same as the model without foam.

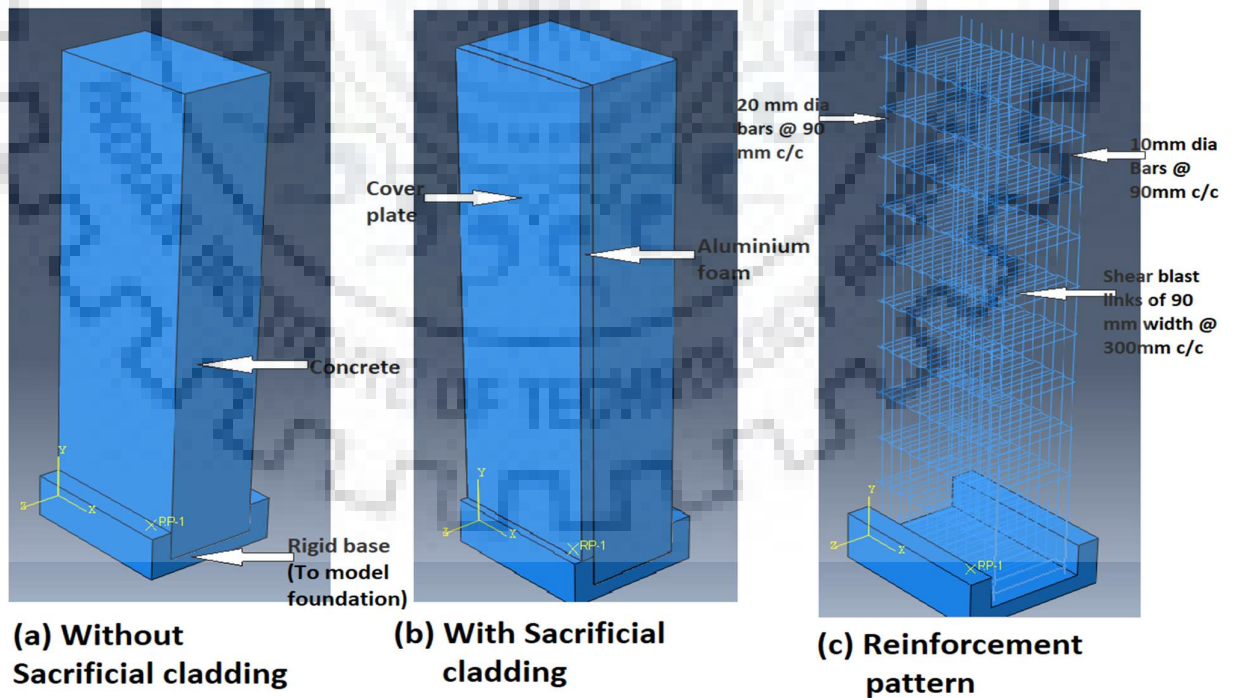


Figure 7-1: Assembly details of Type 1 blast barrier



### 7.1.3 Comparison of performance of barrier with/ without foam cladding

The performance of barrier with/without sacrificial cladding is assessed in terms of deflections induced and the damage sustained. The following figure shows a comparison of deflections in the barrier without and with aluminium foam cladding.

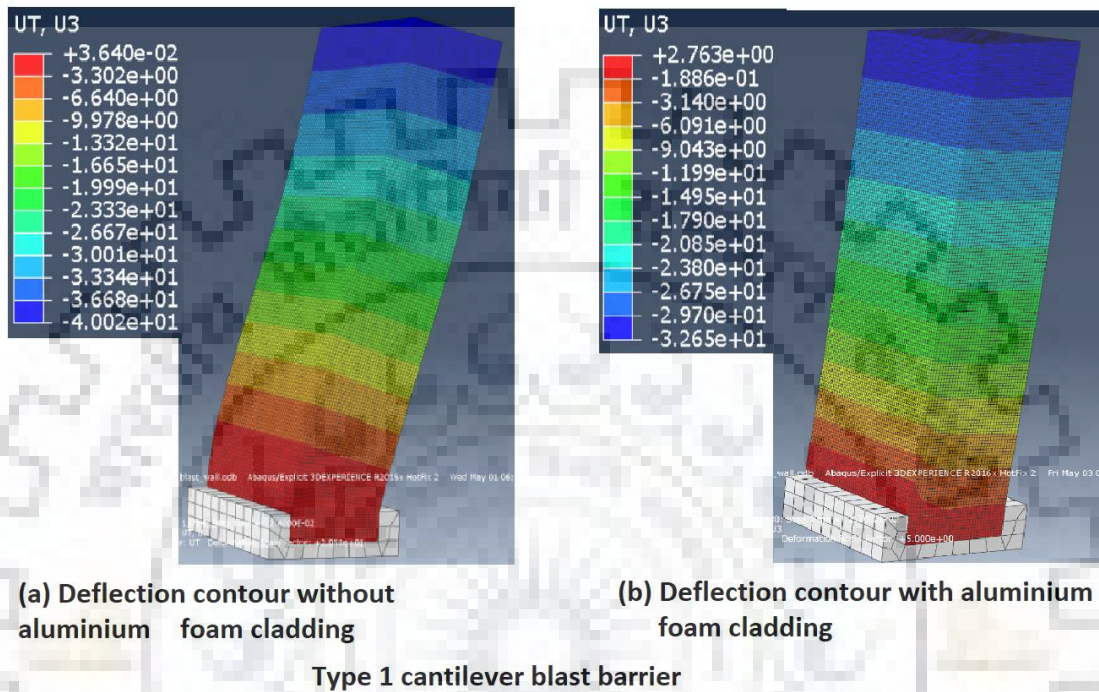


Figure 7-2: Deflection of type 1 blast barrier

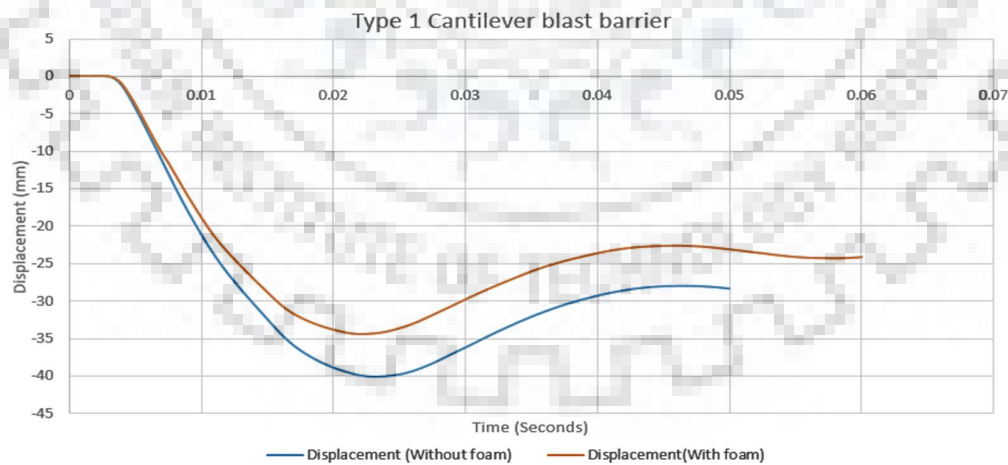


Figure 7-3: Comparative deflection vs time curve.

The tension damage sustained by the barrier on its distal and proximal face with and without foam cladding is shown.

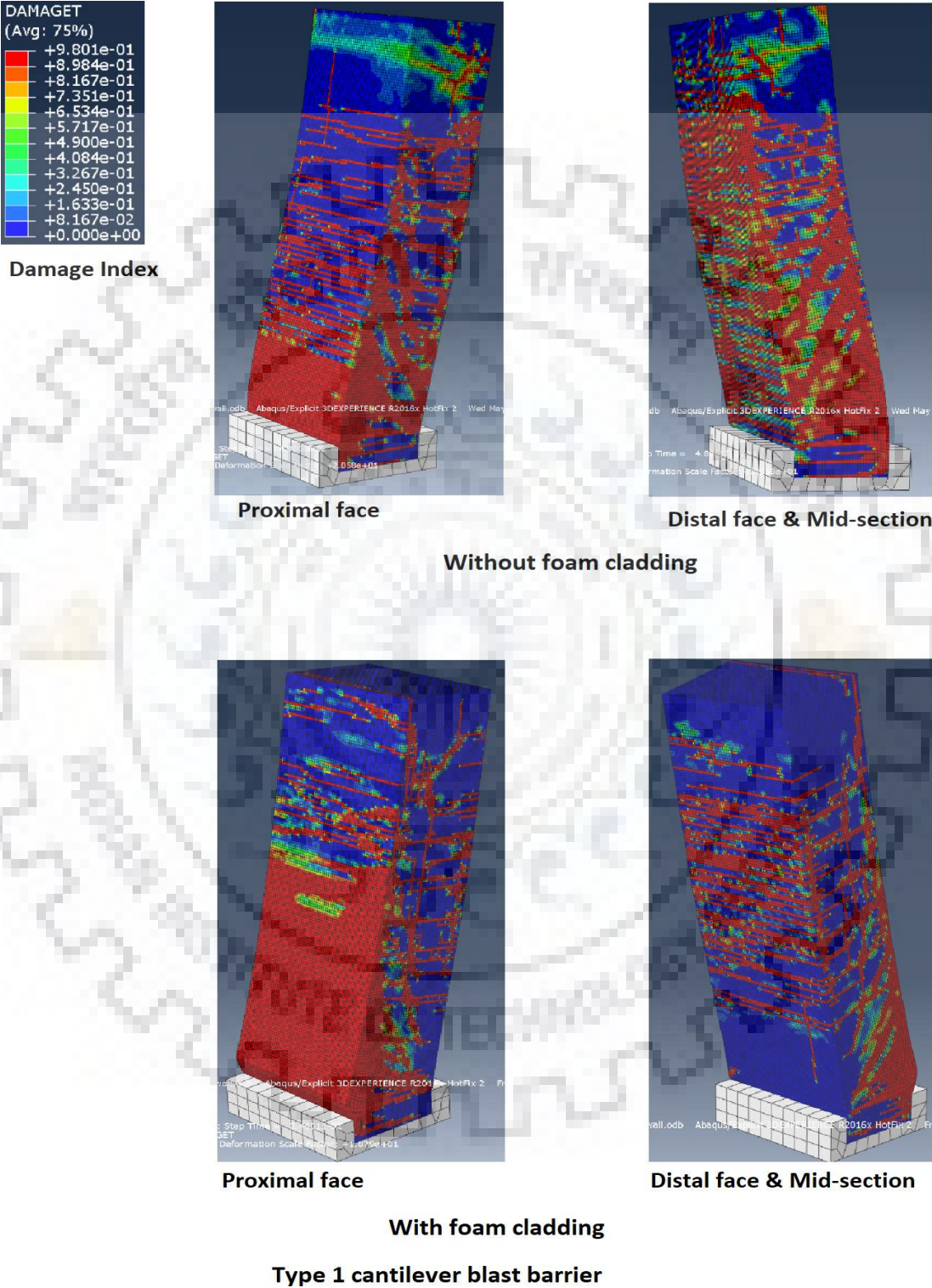


Figure 7-4: Concrete tension damage for type 1 cantilever blast barrier

The graph in figure 7-3 shows deflection of top edge of proximal side of the barrier with time for the two cases. It follows from the graph that the deflections are reduced for barrier with aluminium foam cladding. The deflection at the top edge on the proximal side at the end of the time step is shown in the following table.

*Table 7-3: Deflection reduction for Type 1 cantilever blast barrier*

Without foam cladding	With foam cladding	Percentage reduction
28.28 mm	24.07 mm	14.88%

## **7.2 Type 2 cantilever blast barrier**

### **7.2.1 Without aluminium foam sacrificial cladding**

An Abaqus model of the Type 2 cantilever blast barrier designed in section 3.2 is presented here. The design data for the wall, design values of thickness and reinforcement are mentioned here.

Blast load: Hemispherical surface burst due to 180 Kg TNT at ground level at 5.0 m standoff distance.

Height of wall = 3.0 m

Overall depth of section = 540 mm

C/C distance between reinforcing bars on both faces = 400 mm

Tension reinforcement = 20 mm dia bars of 590 MPa yield strength at 150 mm c/c

Compression reinforcement = 20 mm dia bars of 590 MPa yield strength at 150 mm c/c

Shear reinforcement = 10 mm dia bars bent into closed blast links of 150 mm width @ 300 mm c/c

Clear cover = 50 mm (tension side), 50 mm (compression side)



The partwise details of the Abaqus model are as follows:

Table 7-4: Part details for type 2 cantilever blast barrier

Part	Type of Part	Dimensions	Material	Element type	Mesh size
Concrete	Solid deformable	1180mm*540mm*3200mm	CDP/B50 concrete	C3D8R	Global seed size = 20mm
20 mm Rebar	Wire deformable	Length = 3200 mm, cross sectional area = $314mm^2$	J-C/DP-590 steel	T3D2	Global seed size = 20mm
Shear blast link, 10mm $\varnothing$	Wire deformable	Chamfered rectangular closed loop, length=430 mm, width=180mm, CSA= $78.5mm^2$	J-C/Mild steel	T3D2	Global seed size = 10mm
Rigid base	Shell/Discrete rigid	300mm*1000mm*1180mm	-	R3D4	Global seed size=120mm

Rest of the details of the model are as follows:

- The parts have been assembled as per the design shown in chapter 3.
- Embedded constraint has been used to model the rebar concrete bond.
- Tie constraint has been used to model the fixity between rigid base and concrete part.
- Rigid body constraint has been used to model the fixity of rigid base by defining fixed boundary condition to reference point.
- The blast load is modelled as an interaction of incident wave of surface burst of 180 Kg TNT at a standoff of 5.0 m with the proximal surface of the barrier.
- The blast load has been applied in the dynamic explicit step 'blast' with a step time of 75 milliseconds.
- Axisymmetric boundary condition has been used along one side face to simulate double the modelled length into study.

### 7.2.2 With sacrificial cladding

Abaqus model of type 2 blast barrier with aluminium foam sacrificial cladding is same as that without the sacrificial cladding except for the following extra details.

2 parts, namely the aluminium foam and cover plate are modelled. Their details are:

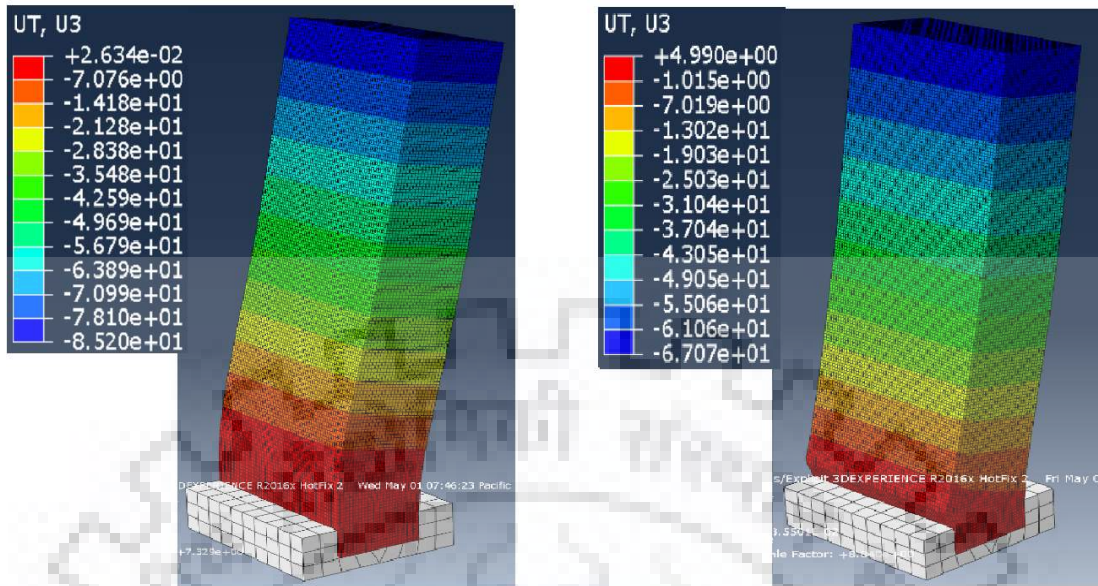
Table 7-5: Additional part details for foam cladding (type 2 cantilever)

Part	Type of Part	Dimensions	Material	Element type	Mesh size
Aluminium foam	Solid deformable	1180mm*3000mm*100mm	Crushable foam model/aluminium foam	C3D8R	20mm*20mm*5mm
Cover plate	Shell deformable	1180mm*3000mm Thickness = 10mm	J-C/Mild steel	S4R	20mm*20mm

- Tie constraint has been used to model the fixity between aluminium foam and concrete and between aluminium foam and cover plate.
- Rest of the details are same as the model without foam.

### 7.2.3 Comparison of performance of barrier with/ without foam cladding

The performance of barrier with/without sacrificial cladding is assessed in terms of deflections induced and the damage sustained. The following figure shows a comparison of deflections in the barrier without and with aluminium foam cladding.



(a) Deflection contour without aluminium foam cladding

(b) Deflection contour with aluminium foam cladding

Type 2 cantilever blast barrier

Figure 7-5: Deflection contours for type 2 blast barrier

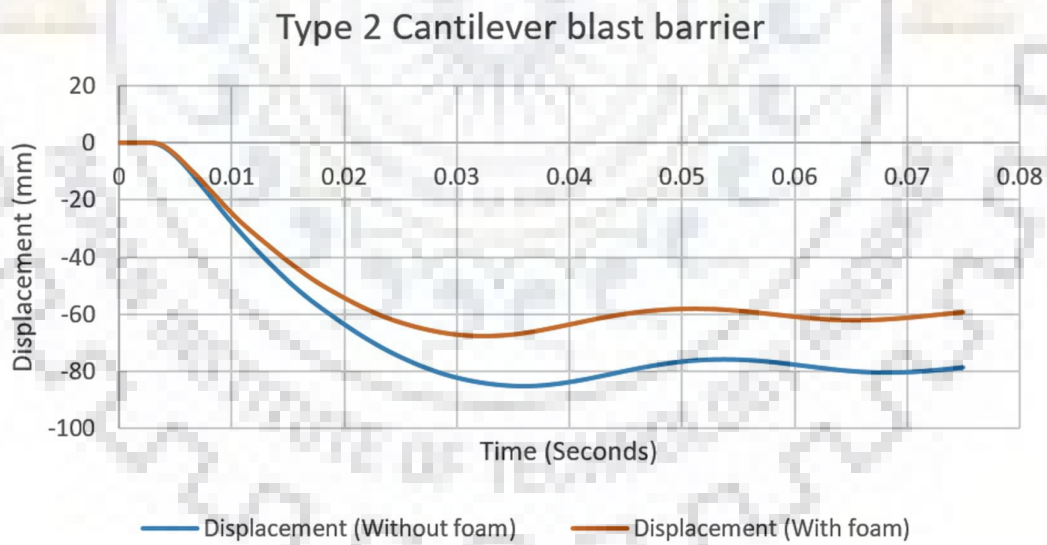
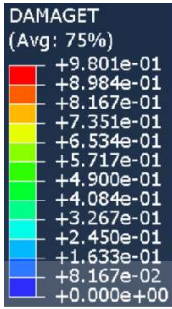
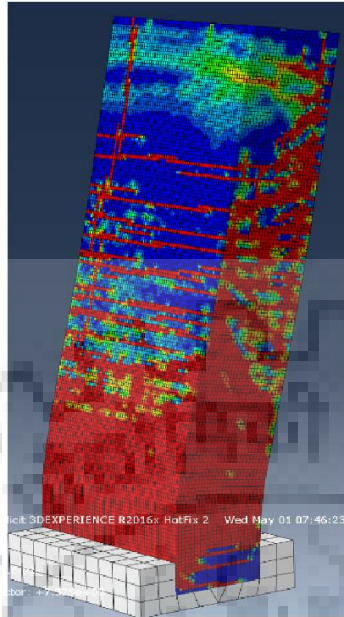


Figure 7-6: Deflection VS time curve for type 2 cantilever blast barrier

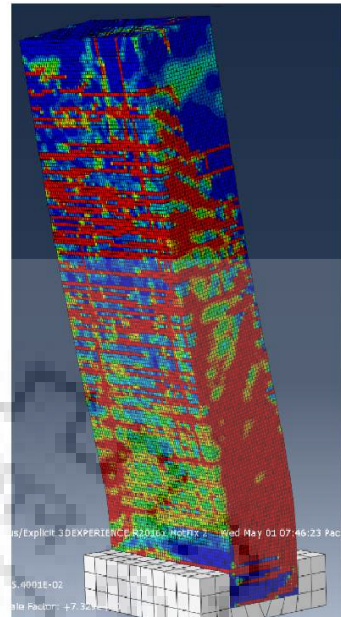
The tension damage sustained by the barrier on its distal and proximal face with and without foam cladding is shown.



**Damage Index**

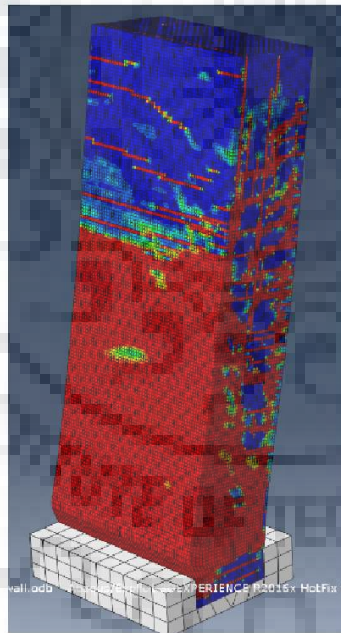


**Proximal face**

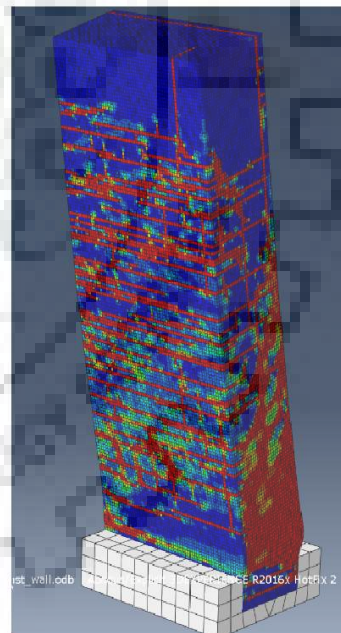


**Distal face & Mid-section**

**Without foam cladding**



**Proximal face**



**Distal face & Mid-section**

**With foam cladding**

**Type 2 cantilever blast barrier**

*Figure 7-7: Concrete tension damage for type 2 cantilever blast barrier.*

The graph in figure 7-6 shows deflection of top edge of proximal side of the barrier with time for the two cases. It follows from the graph that the deflections are reduced for barrier with aluminium foam cladding. The deflection at the top edge on the proximal side at the end of the step time is shown in the following table.

*Table 7-6: Deflection reduction due to foam cladding (Type 2 fixed barrier)*

Without foam cladding	With foam cladding	Percentage reduction
78.70 mm	59.14 mm	24.85%

### **7.3 Type 2 fixed blast barrier**

#### **7.3.1 Without aluminium foam sacrificial cladding**

An Abaqus model of the Type 2 fixed blast barrier with rigid counterfort blast barrier designed in section 3.2 is presented here. The design data for the wall, design values of thickness and reinforcement are mentioned here.

Blast load: Hemispherical surface burst due to 180 Kg TNT at ground level at 5.0 m standoff distance.

Height of wall = 3.0 m

Clear distance between support = 2.0 m

Overall depth of section = 450 mm

C/C distance between reinforcing bars on both faces = 340 mm

Tension reinforcement = 20 mm dia bars of 590 MPa yield strength at 160 mm c/c

Compression reinforcement = 20 mm dia bars of 590 MPa yield strength at 160 mm c/c

Shear reinforcement = 10 mm dia bars bent into closed blast links of 320 mm width @ 100 mm c/c

Clear cover = 45 mm (tension side), 45 mm (compression side)



The partwise details of the Abaqus model are as follows:

Table 7-7: Part details for fixed blast barrier

Part	Type of Part	Dimensions	Material	Element type	Mesh size
Concrete	Solid deformable	1200mm*450mm*3000mm	CDP/B50 concrete	C3D8R	Global seed size = 20mm
20 mm Rebar	Wire deformable	Length = 1200 mm, cross sectional area = $314\text{mm}^2$	J-C/DP-590 steel	T3D2	Global seed size = 20mm
Shear blast link, 10mm $\varphi$	Wire deformable	Chamfered rectangular closed loop, length=370 mm, width=350 mm, CSA= $78.5\text{mm}^2$	J-C/Mild steel	T3D2	Global seed size = 10mm
Rigid Counterfort	Shell/Discrete rigid	Height=3000mm, Thickness=400mm, length L1=600mm, L2=2000mm	-	R3D4	Global seed size=200mm

Rest of the details of the model are as follows:

- The parts have been assembled as per the design shown in chapter 3.
- Embedded constraint has been used to model the rebar concrete bond.
- Tie constraint has been used to model the fixity between rigid counterfort and concrete part.
- Rigid body constraint has been used to model the fixity of rigid base by defining fixed boundary condition to reference point.
- The blast load is modelled as an interaction of incident wave of surface burst of 180 Kg TNT at a standoff of 5.0 m with the proximal surface of the barrier.
- The blast load has been applied in the dynamic explicit step 'blast' with a step time of 15 milliseconds.
- Axisymmetric boundary condition has been used along one side face to simulate double the modelled length into study.

### 7.3.2 With sacrificial cladding

Abaqus model of type 2 blast barrier with aluminium foam sacrificial cladding is same as that without the sacrificial cladding except for the following extra details.

2 parts, namely the aluminium foam and cover plate are modelled. Their details are:

Table 7-8: Additional part details for foam cladding (type 2 fixed blast barrier)

Part	Type of Part	Dimensions	Material	Element type	Mesh size
Aluminium foam	Solid deformable	1000mm*3000mm*100mm	Crushable foam model/aluminium foam	C3D8R	20mm*20mm*5mm
Cover plate	Shell deformable	1000mm*3000mm Thickness=10mm	J-C/Mild steel	S4R	20mm*20mm

- Tie constraint has been used to model the fixity between aluminium foam and concrete and between aluminium foam and cover plate.
- The step time of 'blast' is increased from 15 milliseconds to 20 milliseconds.
- Rest of the details are same as the model without foam.

The following figure shows the assembly of type 2 fixed cantilever blast barrier with rigid counterfort both with foam cladding and without foam cladding. A suppressed concrete part also reveals the reinforcement pattern of the model.

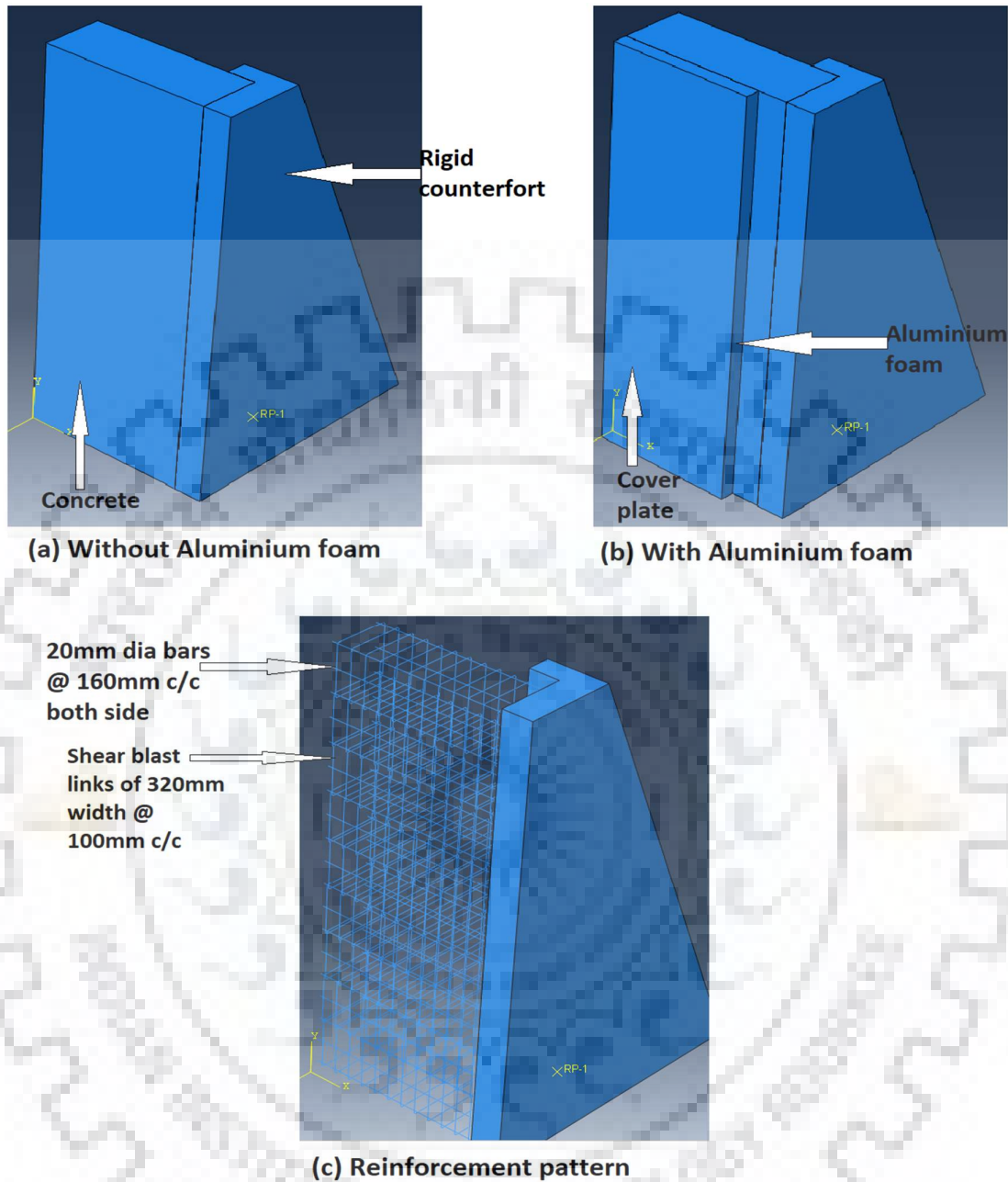
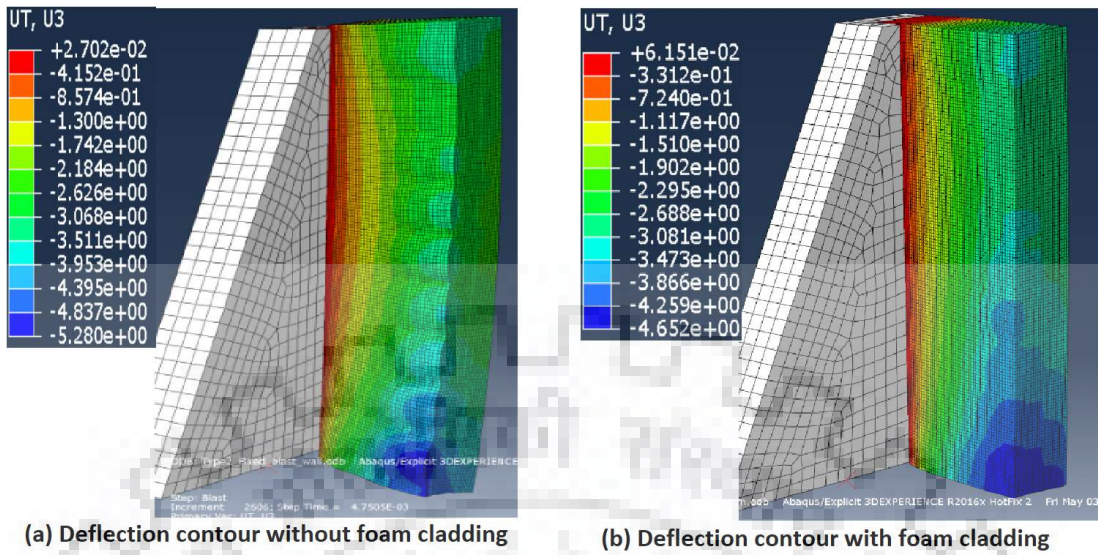


Figure 7-8: Assembly of type 2 fixed blast barrier.

### 7.3.3 Comparison of performance of barrier with/ without foam cladding

The performance of barrier with/without sacrificial cladding is assessed in terms of deflections induced and the damage sustained. The following figure shows a comparison of deflections in the barrier without and with aluminium foam cladding.





Type 2 Fixed blast barrier

Figure 7-9: Deflection contours of fixed blast wall

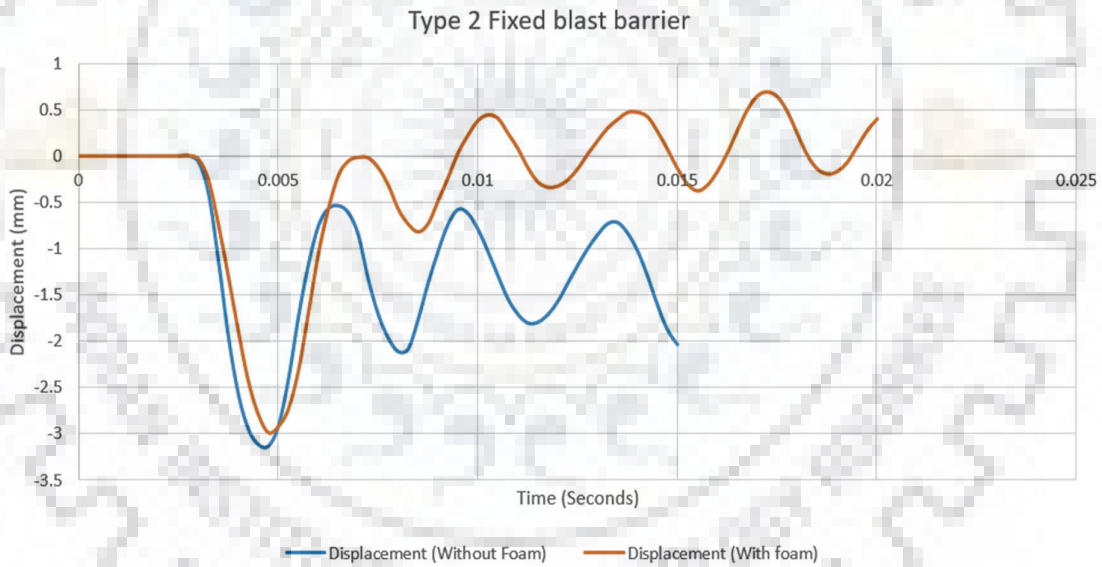


Figure 7-10: Deflection VS time curve for fixed blast barrier

The tension damage sustained by the barrier on its distal and proximal face with and without foam cladding is shown.

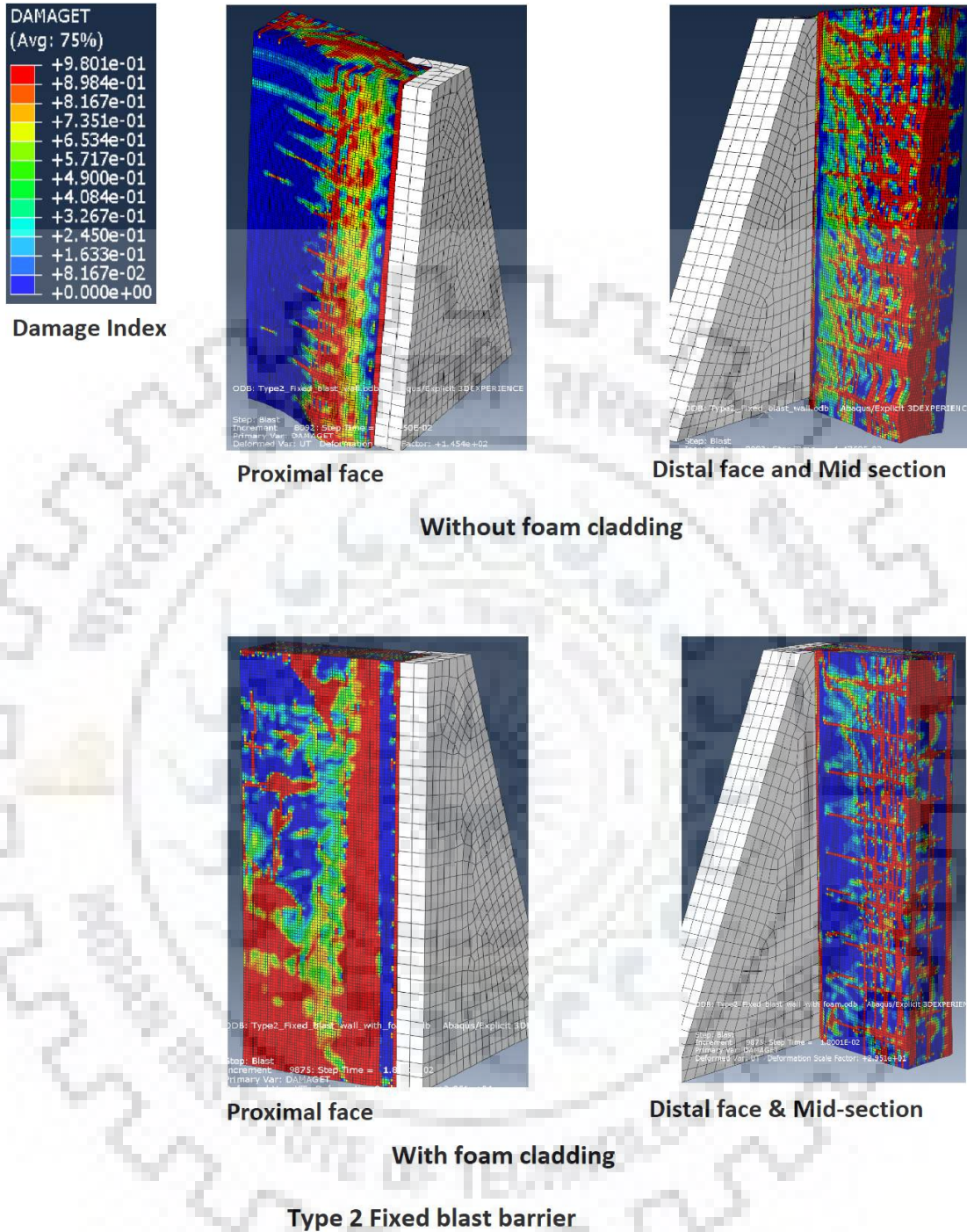


Figure 7-11: Concrete tension damage contours for fixed blast barrier

The graph in figure 7-10 shows deflection of bottom most point of middle of proximal side of the barrier with time for the two cases. It follows from the graph that the deflections are reduced for barrier with aluminium foam cladding. The deflection at

the bottom most point of the middle of the barrier on the proximal side at the end of the step time is shown in the following table.

*Table 7-9: Deflection reduction for type 2 fixed blast barrier*

Without foam cladding	With foam cladding	Percentage reduction
2.032 mm	0.376 mm	81.5%



## Chapter 8. Efficacy of sacrificial foam cladding

In this chapter, numerical studies have been presented wherein the properties of the sacrificial aluminium foam cladding applied to type 2 cantilever blast wall have been varied and the results compared. The properties varied are the foam thickness and relative density of the foam. The cases for foam thickness taken are 100mm and 200mm while the relative density are 20% and 10% relative density.

### 8.1 Effect of increasing thickness of foam cladding

#### 8.1.1 Model details for revised foam cladding thickness

Numerical studies for blast loading of 180 kg TNT surface hemispherical burst at a standoff distance of 5.0 m on type 2 cantilever blast barrier are shown with and without sacrificial aluminium foam cladding in chapter 7. The details of the model, parts and numerical studies for 100mm thick cladding is taken from chapter 7. Here, additional details for 200 mm thick aluminium foam cladding are presented.

Table 8-1: Revised part details for foam cladding

Part	Type of Part	Dimensions	Material	Element type	Mesh size
Aluminium foam	Solid deformable	1180mm*3000mm*200mm	Crushable foam model/aluminium foam	C3D8R	20mm*20mm*5mm
Cover plate	Shell deformable	1180mm*3000mm Thickness = 20mm	J-C/Mild steel	S4R	20mm*20mm

- Thickness of aluminium foam has been increased to from 100 mm to 200 mm and that of cover plate has increased from 10 mm to 20 mm.
- Rest of the details are same as mentioned in section 7.2.

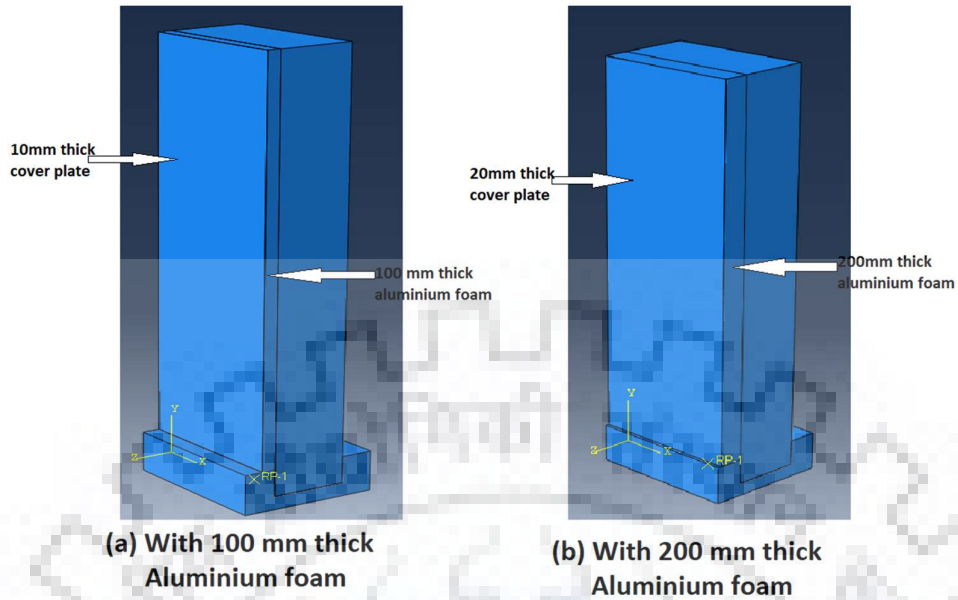


Figure 8-1: Assembly details of model with different foam cladding thicknesses (type 2 cantilever blast barrier)

### 8.1.2 Comparison of performance of barrier for 200mm/100mm thick foam cladding

The performance of barrier with 200mm/100mm sacrificial cladding is assessed in terms of deflections induced and the damage sustained.

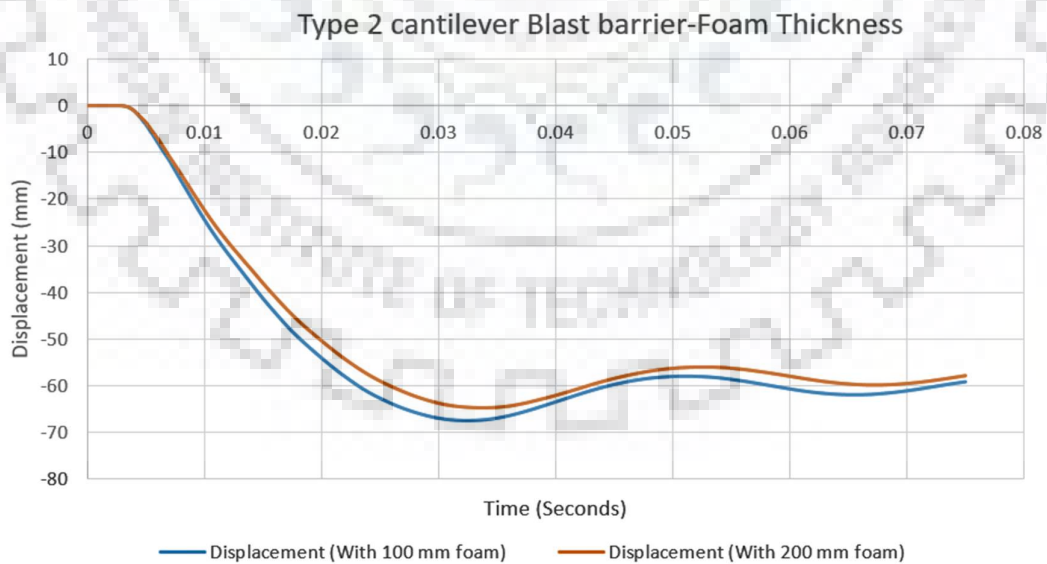


Figure 8-2: Deflection VS time curve for 2 thicknesses (type 2 cantilever blast barrier)



The tension damage sustained by the barrier on its distal and proximal face with and without foam cladding is shown.

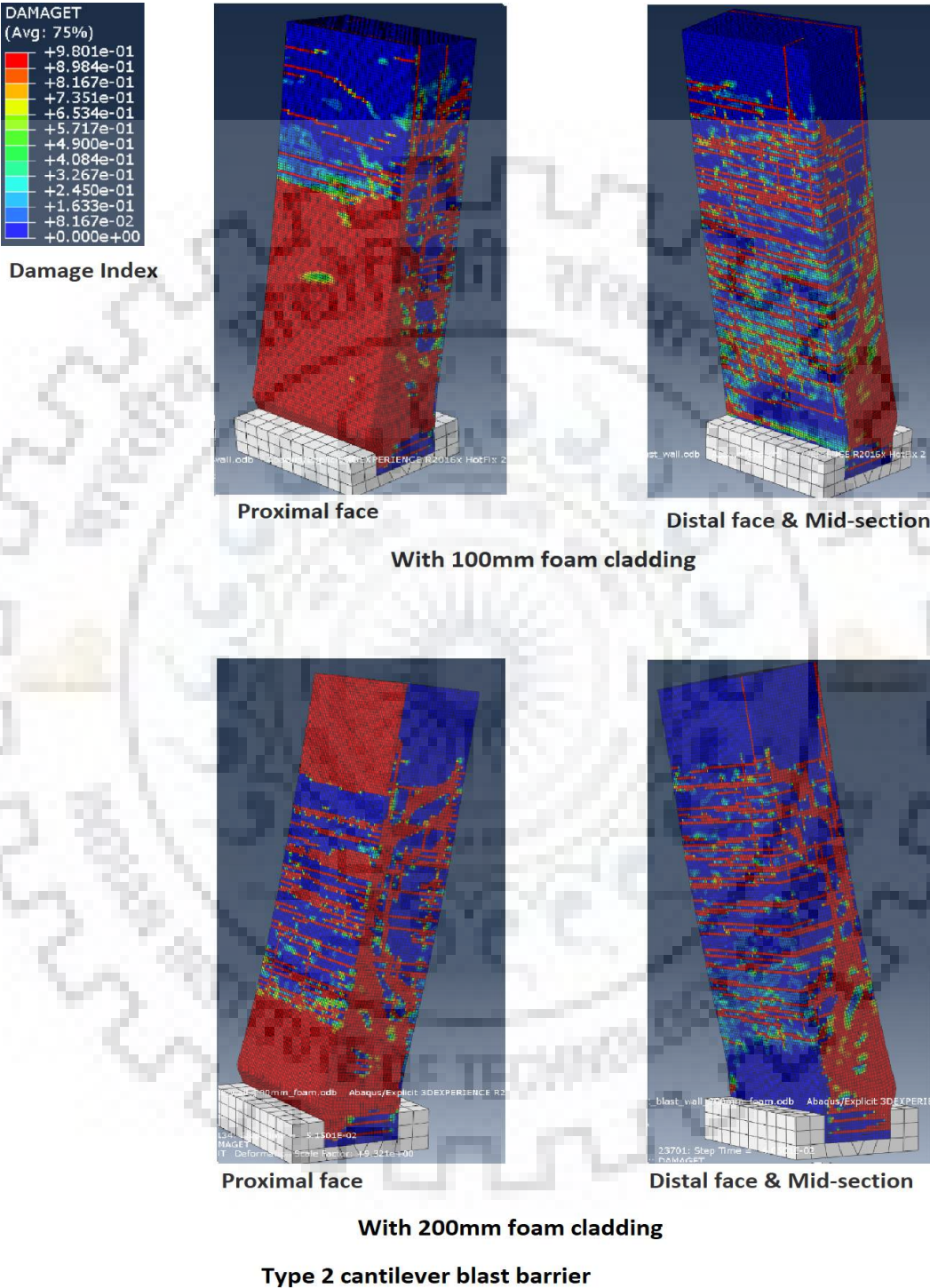


Figure 8-3: Concrete damage for type 2 cantilever blast barrier (effect of thickness of foam)

The graph in figure 8-2 shows deflection of midpoint of top edge of proximal side of the barrier with time for the two cases. It follows from the graph that the deflections are slightly reduced for barrier with 200mm thick aluminium foam cladding as compared to 100 mm thick aluminium foam cladding.

The comparison of deflection of the top edge of proximal side of the barrier at the end of the step time is shown in the following table.

Table 8-2: Deflection for different foam thicknesses (type 2 cantilever blast barrier)

With foam cladding thickness of 100mm	With foam cladding thickness of 200mm	Percentage reduction
59.13 mm	57.88 mm	2.11%

## 8.2 Effect of decreasing density of foam cladding

### 8.2.1 Foam cladding densities tested

For all the numerical studies performed above, the foam was of relative density 20%, or  $\rho = 570 \text{Kg} / \text{m}^3$ , here foam cladding of 200 mm thickness used above is replaced with material properties of 10% relative density foam, or  $\rho = 272 \text{Kg} / \text{m}^3$ , was performed and the performance of the type 2 blast barrier for the two foam densities and cladding thickness of 200 mm was compared. The table below summarises the cladding details for the two cases.

Table 8-3: Foam cladding density and thickness used

Case	Foam cladding Thickness	Foam material density
Case 1	200 mm	$\rho = 570 \text{Kg} / \text{m}^3$
Case 2	200 mm	$\rho = 272 \text{Kg} / \text{m}^3$

- The material model used, element type and mesh size for both the cases is same, i.e. crushable foam model, C3D8R and 20mm\*20mm\*5mm respectively.
- The properties of both the foams are described in chapter 5: Validation of material models, section 5.2

### 8.2.2 Comparison of performance for 20%/10% relative density foam cladding

The performance of type 2 blast barrier under 20% and 10% relative density foam is comparatively assessed in terms of permanent deflection and concrete damage sustained.

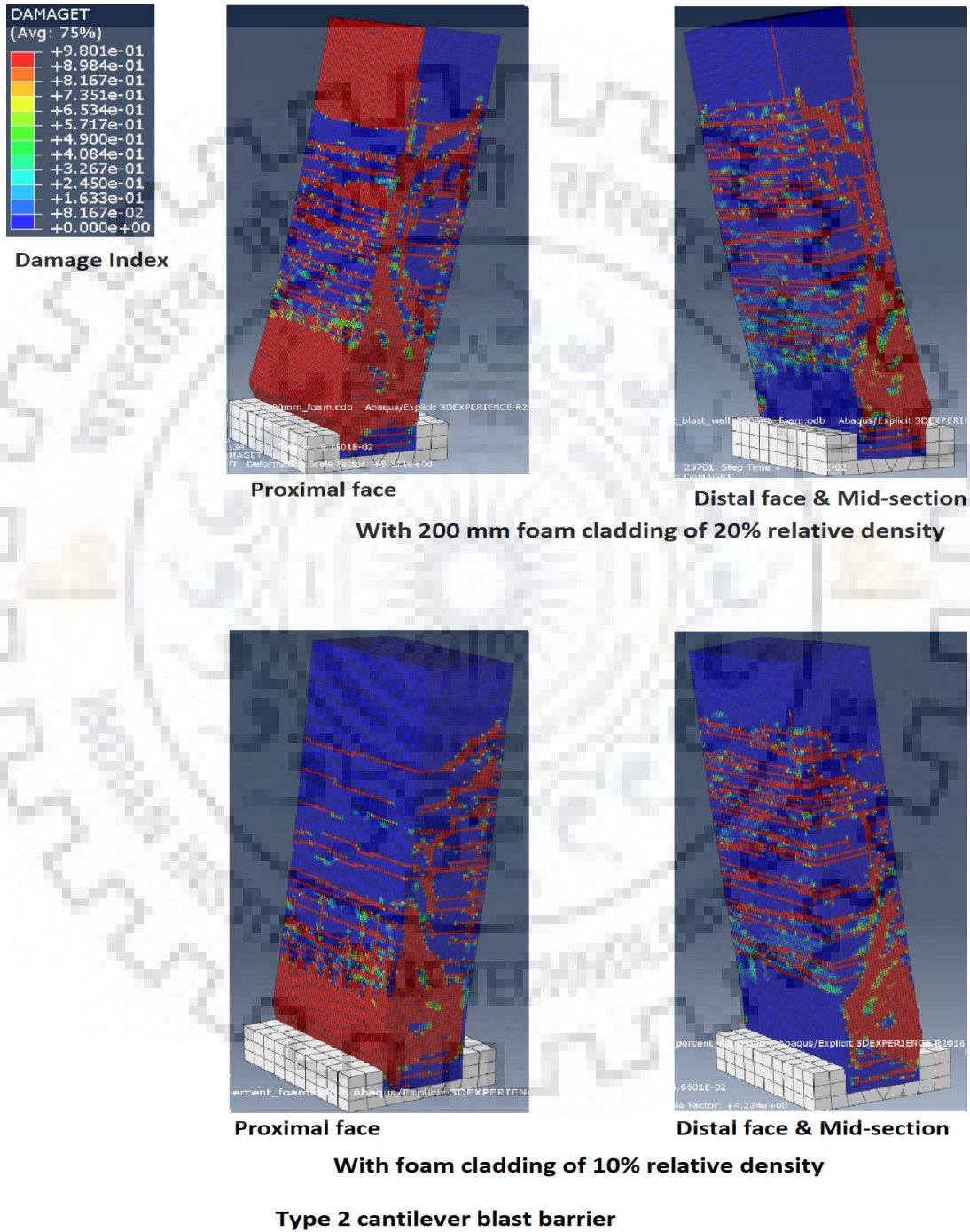


Figure 8-4: Concrete damage for different foam density (Type 2 cantilever blast barrier)



The following graph shows the deflection Vs time curve for the two cases:

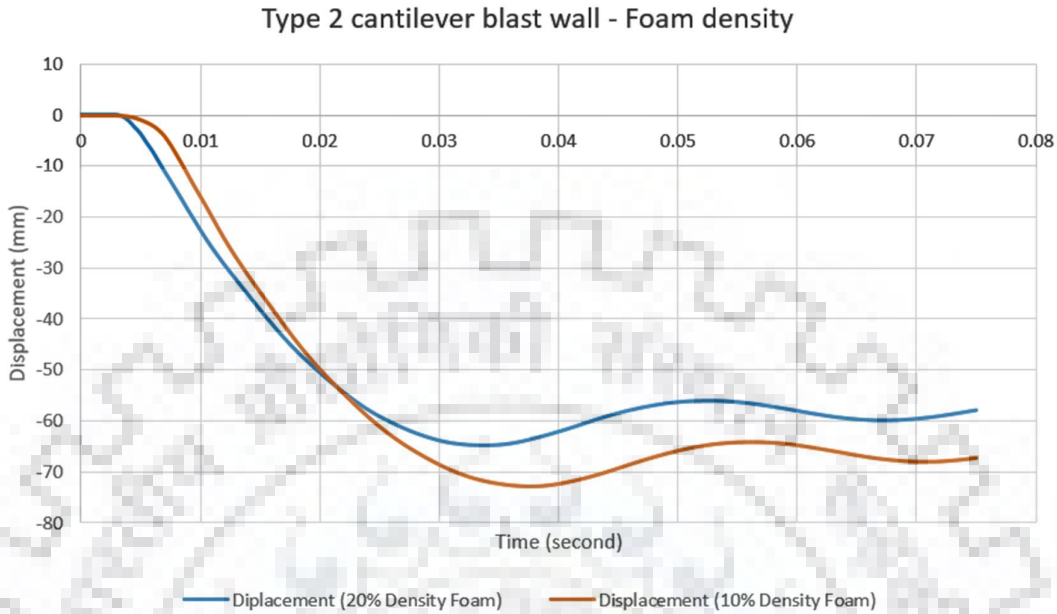


Figure 8-5: Deflection vs time curve for different densities (type 2 cantilever blast barrier)

As seen from the curve, the rate of deflection is more for 20% foam initially, but final deflection is more for 10% foam.

Table 8-4: Deflection for 2 foam densities (type 2 cantilever blast barrier)

With 20% foam cladding	With 10% foam cladding	Percentage increase
57.88	67.22	16.14%

## Chapter 9. Interpretation of Results

---

In this chapter discussions and interpretation of the results obtained on the investigations of presence and efficacy of aluminium foam sacrificial claddings in blast barriers are provided. Possible mechanisms of the observed phenomenon are discussed. Based on these discussions, conclusions and recommendations are provided.

### 9.1 Sacrificial cladding in Blast barrier

#### 9.1.1 Type 1 cantilever blast barrier

The compression damage accumulated by the blast barrier is minimal both with and without the application of foam cladding, hence it is of no consequence and hasn't been discussed.

The tension damage, though is significant. Without the sacrificial foam cladding applied to the proximal face, the damage pattern observed is as follows. On the proximal face, very severe tension damage is concentrated at the bottom portion. On the distal face severe tension damage is evenly distributed from the bottom to the top. The damage seen on the side face and mid-section is also severe and widespread indicating complete structural failure of the blast barrier making it unserviceable and needing replacement.

With a sacrificial foam cladding applied to the proximal face, the damage pattern observed is as follows. On the proximal face, the damage pattern becomes much more severe and widespread than what it had been without the foam cladding. On the distal face the tension damage is visibly reduced both in intensity and spread. The tension damage seen on the side face and mid-section has also reduced to moderate and less widespread. This indicates that the damage to the proximal surface has increased but it has significantly reduced in rest of the barrier. In other words, the damage has localised to the proximal surface. But there is significant damage along the depth of the section at the bottom indicating an unserviceable structure not capable of withstanding further moments. Excessive element distortions are also seen at the bottom on the proximal side.

Also, the deflection vs time curve for the two cases shows that foam cladding has reduced the final permanent deflection of the top by about 15%. This shows the efficacy of foam cladding in energy absorption.

The following possible mechanisms are suggested.

The addition of foam cannot reduce the global structural damage in flexure and shear. This is because foam cannot reduce the impulse transferred to the barrier, it can only reduce the rate at which the impulse is transferred. In an impulsive loading regime, the impulse transferred is more of a consequence than the force. Blast loads of decay time of around 2-3 ms on type 1 blast barrier, with a natural time period of around 25 ms is an impulsive loading regime. With a foam cladding added, the decay time of impulse transfer increase by 3-4 times but the structure still remains in impulsive loading regime, where total impulse decided maximum deflections and damage.

It appears from the deflected shape of the barriers with and without foam cladding that the mode of vibration for the barrier is different in the two cases. Without the foam cladding, the barrier deflects in a contra flexure while with the foam cladding a rotation about a hinge at the bottom is seen. This may explain the reduction in tension damage on the distal side and excessive element distortion and damage at the bottom on the proximal side in the case of foam cladding present.

Blast loads, or any other high impact loads create strong stress waves which travel inside a solid at sonic speeds and cause huge disruptions. When blast waves impinge on the proximal side, they produce compression waves of amplitudes sometimes higher than strength of concrete causing rupture. These waves get reflected from the distal face and become tension waves causing much more cracking in brittle concrete. These stress waves are a reason of widespread damage to concrete apart from global flexural and shear failure. Foam cladding does a good job in attenuating these stress waves in concrete. It appears that the reduction of widespread damage to concrete is because of weakening of these stress waves in foam cladding barrier as compared to barrier without cladding. Also, the localised damage on the proximal face may be a result of the effect of these stress waves being restricted to the vicinity of proximal face.

### **9.1.2 Type 2 cantilever blast barrier**

The damage pattern seen in case of type 2 cantilever blast barrier is same as the type 1 barrier except that the damage is more intense and pronounced in this case.

Without the sacrificial foam cladding applied to the proximal face, the damage pattern observed is as follows. On the proximal face, very severe tension damage is concentrated at the bottom portion. On the distal face severe tension damage is evenly distributed from the bottom to the top. The damage seen on the side face and mid-section is also severe and widespread indicating complete structural failure of the blast barrier making it unserviceable and needing replacement. The damage intensity and spread are more than what they were in type 1 cantilever blast barrier.

With a sacrificial foam cladding applied to the proximal face, the damage pattern observed is as follows. On the proximal face, the damage pattern becomes much more severe and widespread than what it had been without the foam cladding. On the distal face the tension damage is visibly reduced both in intensity and spread. The tension damage seen on the side face and mid-section has also reduced to moderate and less widespread. This indicates that the damage to the proximal surface has increased but it has significantly reduced in rest of the barrier. In other words, the damage has localised to the proximal surface. But there is significant damage along the depth of the section at the bottom indicating an unserviceable structure not capable of withstanding further moments. Excessive element distortions are also seen at the bottom on the proximal side. The damage reduction in case of type 2 cantilever blast barrier though, is less than that of type 1 blast barrier.

The deflection of the top plotted against time for the two cases shows that foam cladding reduces permanent deflection by about 25% in case of type 2 blast barrier.

The mechanism of damage discussed for type 1 cantilever blast barrier seem to be valid for type 2 barrier as well.

The damage pattern and deflections obtained for type 1 and type 2 blast barriers are in agreement with experimental findings of the full scale blast tests conducted by Schenker et al, (2008) [19] where he noted that the damage of the backside for protected slab was much less than that for unprotected slab, aluminium foam cladding

being used as a protection. They also noted that the maximum deflections sustained by the slab were more for the unprotected case than the protected case.

### **9.1.3 Type 2 fixed blast barrier**

The motive behind designing the fixed blast barrier was developed from the experimental conclusions made by Hansen et al, (2002) [7] in his paper on close range blast loading of aluminium foam panels. He remarked that aluminium foam sacrificial cladding can reduce the local damage by arresting and attenuating stress waves, but a global reduction in response (flexure and shear) is unlikely to be achieved. This is so because, most structural components have time periods of natural vibration much longer than the decay time of blast waves so that the blast loading regime is essentially impulsive. Even with addition of foam cladding, though the response intensity is reduced and the response prolonged, the regime is still likely to remain an impulsive where the total impulse is of significance which essentially does not change by addition of foam cladding.

By designing a stiffer and lighter fixed blast barrier as compared to cantilever, an attempt has been made to verify this logical hypothesis. While type 2 cantilever blast barrier has a time period of free vibration of around 50 ms, the type 2 fixed blast barrier has a time period of around 6ms. Hence, in case of fixed blast barrier it is expected that the increase in time duration of impulse transfer to the barrier due to foam cladding is likely to change the loading regime from impulsive loading regime to dynamic loading regime and some reduction in global response is expected.

The results obtained are mixed in the sense that the phenomena described above could not be verified in its entirety but some promising results were obtained.

Without the sacrificial foam cladding the damage pattern recorder was as follows. On the proximal face tension damage was seen near the fixed ends and gradually decreased towards the centre whereas on the distal face the damage was concentrated at the centre and reduces towards the fixed ends. The mid-section showed damage toward the distal face. The deflected shape was in accordance with the usual deflected shape for fixed beams and slabs.

The deflection vs time curve at the bottom of proximal face in the centre revealed some permanent deflection about which the wall oscillated.

With the sacrificial foam cladding in place the damage pattern varied greatly. The damage on the distal face was reduced drastically with only a few damage lines visible. The damage seen through the mid-section has visibly reduced and concentrated in certain pockets. The extent of damage on the proximal side, though, increased. The observations of the deflection time contour of the bottom centre line on proximal side, as before, revealed interesting trends. One is that no permanent deflection is recorded. The curve though plunges at first, later recovers all of its deflection and oscillates about the point of zero deflection, indicating that either no damage has occurred or the little damage sustained is not enough to produce permanent deformations, unlike the case of type 1 and type 2 cantilever blast barriers. This indicated that the flexural capacity (indicating global damage) has not suffered the effect of blast load in the case of foam cladding present, unlike in the case of type 1 and type 2 cantilever blast barriers, where the flexural capacity (indicated by permanent deformations and widespread damage) has evidently suffered.

The possible mechanisms are discussed:

The reduction of global response due to spreading out of the blast impulse by the foam cladding is evidenced.

Though the increase in the extent of damage at the proximal face is unexplained by the spreading out of the blast impulse by foam cladding and the global structural response. Here, the mechanism of stress wave attenuation seems logical. It appears that the stress waves are being altered by the presence of foam cladding in their intensity and behaviour so that most of the damage they cause is localised at and near the proximal face, while bulk of the structure is shielded from their effect.

These findings prove the hypothesis of Hansen et al, (2002) wherein they have indirectly asserted that if the foam helps in changing loading regime from impulsive to dynamic, global response is likely to change (reduce).

## **9.2 Efficacy of sacrificial foam cladding**

### **9.2.1 Effect of increasing thickness of foam cladding**

Comparative assessment of damage pattern observed for foam claddings of 2 different thickness 200mm and 100mm for type 2 cantilever blast wall is made. Comparing the



performance of 200 mm foam cladding barrier with that of 100mm, the following trends are observed.

Minimal change in damage pattern is observed. The damage on the distal face is almost the same, albeit very slightly reduced in severity. The same is true of the mid-section and side face which tells about the bulk of concrete. On the proximal face the damaged is distributed in 2 parts with some damage collected at the top as well.

A very slight reduction in deformation is observed from the deflection time curve of the 2 cases indicating slightly better energy absorption in the thicker foam.

The following are possible mechanisms.

A slightly better energy absorption and larger thickness for impact dissipation has caused a marginally better weakening of stress waves induced in the barrier causing the damage accumulated to very slightly reduce. The change in damage pattern on proximal face is probably because of change in the mode of deflection of the barrier.

It may be noted that the design thickness for this blast load is 100 mm and an addition of 100mm thickness to this design thickness doesn't add as much value in terms of damage reduction. Given that aluminium foam is a costly material, it is noted that increasing thickness beyond an optimum value is not economically viable.

### **9.2.2 Effect of decreasing density of foam cladding**

Comparative assessment of damage pattern observed for foam claddings of 2 different relative densities 20% and 10% and thickness 200 mm for type 2 cantilever blast wall is made. Comparing the performance of 10% density foam cladding barrier with that of 20%, the following trends are observed.

The damage pattern recorded for 10% density foam cladding showed improvement over the 20% density foam cladding. On the proximal side, the extent of damage was contained to a small area at the bottom. The distal side also showed improvement with very few fine tension damage contours appearing there. The side face and mid-section also showed improvements in the damage pattern with the extent and severity of tension damage reduced and restricted to bottom front half portion, the entire barrier except for this small region suffered minimal damage, lesser than in the case of 20% foam.



The deflection time curve shows that the rate of deflection is initially lesser in case of 10% foam as compared to 20% foam but the final deflections are more.

The possible mechanisms are:

Lower density foam has lower plateau stress causing a better time spread of sudden impulse of blast with lower overpressures. This has worked in weakening the stress waves and reduced damage due to stress waves wherever they caused damage except for the bottom part of proximal face and its proximity where the damage is due to global response (flexure) and not stress waves.

The trends in deflection prove that initially the impulse transfer in 10% foam is lesser than that in 20% foam hence a lower rate of deflection is seen initially but the final deflection of 10% foam cladding is higher meaning that the energy absorbed by 10% foam is lesser than that which is absorbed by 20% foam.

## Chapter 10. Conclusions and recommendations

---

### 10.1 Conclusions

From the numerical studies performed and the analysis of the results obtained, the following conclusions are drawn.

1. It was found that aluminium foam claddings were effective as sacrificial claddings in improving the performance of blast barriers because they reduced the concrete damage and deformation to the barrier in every case tested.
2. Two main mechanisms of improving the performance of blast barriers by sacrificial foam claddings were identified. One is the ability to reduce the global response of the barrier to blast loads such as flexure and shear. The other is its ability to attenuate the stress waves that are set up and propagate in solids on which blast waves impinge.
3. An understanding of the mechanism by which foam claddings can effect the reduction in global response was developed. Close range blast waves are short duration extreme loading events with a positive phase duration of a few milliseconds, much lesser than the time period of natural vibration of most structural systems. Hence, blast loading is invariably an impulsive loading regime wherein the global damage to structures is a result of the total impulse transferred rather than the shape of impulse time curve. A foam cladding reduces peak force of impulse transfer and increases the time spread of impulse time curve. This can help in lessening the global response only if the increase in time spread (which is around 3-4 times without cladding) brings about a change in loading regime from impulsive to dynamic. This happens only when the natural time period of free vibration of the structure is comparable with the Modified positive phase duration of blast wave.
4. Accordingly, in order to take advantage of foam cladding in global damage reduction, the blast barriers should be designed with lesser thickness and stiffer support conditions so that their natural time period of vibration is within a range of 3-4 times of the positive phase duration of blast waves.
5. An understanding of the exact mechanism by which foam cladding reduces the intensity and amplitude of stress waves generated in concrete was not

developed in this work. But it was noted that in all cases, foam claddings reduced the widespread damage due to blast waves and concentrated them to the proximal face of the barrier. This also suggests that in some way foam claddings reduced not only the intensity and amplitude of the blast waves but also reduced or localised the extent of their damage.

6. Comparison of two different density foams showed that better damage reduction with lower density foam is achieved. Hence, it was found that in order to attain better attenuation of stress waves, foam cladding of lower relative density is better suited. This is because lower density foam also has lower plateau stress and the impulse transfer to the barrier is dependent on the plateau stress of the foam. The lower the plateau stress of the foam, the lower the peak force transferred. Hence, better attenuation of stress waves is attained.
7. Also, lower density foams, because of their lower plateau stresses, cause a better peak force reduction and increase the time spread of blast waves and may be better utilised in reducing the global response of the barrier as well. A disadvantage of using lower density foam, though, is that more thickness is required for the same blast wave as compared to higher density foam.
8. In the comparative study of two different foam types, it was found that deformations slightly increased for lower density foams signifying that higher density foams have better energy absorption capabilities as compared to lower density foams. Still lower density foams are better suited from the point of view of design because they achieve significant reduction in concrete damage and cracks due to stress waves which cause spalling and scabbing on distal face and sometimes debris and fragments flying at high speeds from the distal side which may injure occupants or equipment protected by the barrier.
9. It was found that increasing the thickness of foam beyond a minimum design thickness does not improve the damage reduction. The deformations reduced marginally and energy absorption improved marginally for doubling the foam thickness. Hence, foam cladding thickness should not be selected much more than design thickness. Also, aluminium foam is a costly material, so selecting excessively thick foam cladding is economically unviable.
10. Sacrificial foam claddings are effective in damage reduction but they cannot eliminate the damage to concrete barriers completely. The work presented in

this thesis and experimental programs by various researchers has shown that under no condition will the foam cladding make the RC barrier damage proof. In the event of blast loading, the RC barrier, even with a foam cladding, will suffer damage and become unserviceable to the point where it cannot take one more blast impact necessitating its replacement. Foam claddings can only improve the performance of blast barriers by reducing concrete damage, deformation, spalling and scabbing and flying fragments on the distal side. In other words they improve they margin of safety for a RC barrier or improve the blast loading capability of the barrier, but cannot make the barrier damage proof in any way. The design objectives for RC barrier with foam cladding should be set accordingly.

## **10.2 Recommendations**

### **10.2.1 Recommendations for design**

Recommendations for design of RCC blast barrier with foam cladding that follow from this work are:

1. RC blast barriers with foam cladding should be designed with an objective to improve performance and margin of safety from conventional blast barriers.
2. The design objective should not be to make the arrangement damage proof or capable of withstanding more than one blast loading event. The barriers should be designed to withstand blast loading for a single event after which they may be replaced.
3. The barrier should be designed with lighter and stiffer support conditions to reduce the time period of free vibration so that foam cladding causes the blast loading to change from impulsive to dynamic regime and significantly reduces global response in flexure.
4. Foam cladding of lower relative density should be chosen as it helps in better attenuating stress waves in concrete which causes significant damage, cracks, spalling and scabbing on distal face and flying fragments and debris.
5. The thickness of foam cladding should not be increased much beyond design thickness because it has no effect on damage reduction and negligible effect on energy absorption. On the other hand, aluminium foam is an expensive material and unnecessarily using larger thickness foam is economically unviable.

### 10.2.2 Recommendations for further research

Recommendations for further research in RC blast barriers with foam cladding following from this work are:

1. The presented work investigates the effect of presence and efficacy of sacrificial foam cladding in improving the performance of RCC blast barrier. The mechanisms of global response reduction and stress wave attenuation are identified.
2. An insight is developed into the mechanism by which foam cladding can help in reducing the global flexural response and a method to incorporate it in design is presented. But the mechanism of stress wave attenuation, apart from suitability of density and thickness is weakly understood.
3. An understanding of the mechanism of stress wave attenuation by foam claddings is desirable. Research focussed on this aspect may result in an insight that may be incorporated in optimising the design for reducing damaging effect of stress waves.
4. The presented work and experiments by researchers has demonstrated that foam claddings cannot be expected to completely eliminate damage from blast waves and make the RC blast barriers damage proof. Hence, foam claddings have a limited utility for RC blast barriers. The utility and efficacy of foam claddings for other promising materials for blast barriers such as UHPC and prestressed concrete may be investigated.

## References

- [1] T. d. Ngo, P. Mendis and A. Gupta, "Blast loading and blast effect on structures," *Electronic journal of structural engineering*, no. Special issue, pp. 76-91, 2007.
- [2] K. Ramamurthi, "Lecture Series on Blast Wave in an Explosion," NPTEL, 2014.
- [3] V. Karlos, G. Solomos and M. Larcher, "Analysis of the blast wave decay coefficient using the Kingery-Bulmash data," *International Journal of Protective Structures*, vol. 7, no. 3, 2016.
- [4] D. Cormie, G. May and P. Smith, Blast effect on buildings, Thomas Telford publishing, 2009.
- [5] M. D. Goel and V. Matsagar, "Blast resistant design of structures," *Practice periodical on structural design and construction*, pp. 1-9, 2014.
- [6] S. C. K. Yuen, G. Nurick, M. Theobald and G. Langdon, "Sandwich Panels Subjected to Blast Loading," in *Dynamic Failure of Materials and Structures*, Springer US, 2009, pp. 297-325.
- [7] A. Hanssen, L. Enstock and L. M., "Close-range blast loading of aluminium foam panels," *International Journal of Impact Engineering*, vol. 27, no. 7, pp. 593-618, 2002.
- [8] G. Langdon, D. Karagiozova, M. Theobald, G. Nurick, G. Luc and R. Merrett, "Fracture of aluminium foam core sacrificial cladding subjected to air-blast loading," *International journal of impact engineering*, vol. 37, no. 6, pp. 638-651, 2010.
- [9] ABAQUS Documentation, Simulia, 2016.
- [10] P. Smith, "Blast Walls for Structural Protection against high explosive threats: A Review," *International journal of protective structures*, vol. 1, no. 1, pp. 67-84, 2010.

- [11] T. Rose, P. Smith and G. Mays, "The effectiveness of walls designed for the protection of structures against air blasts of high explosives," *Structures and buildings*, vol. 110, no. 1, pp. 78-85, 1995.
- [12] A. Erdik and V. Uçar, "On evaluation and comparison of blast loading methods used in numerical simulations," *Sakarya University Journal of Science*, vol. 22, no. 5, pp. 1385-1391, 2018.
- [13] W. Wang, D. Zhang, F. Lu, S.-c. Wang and F. Tang, "Experimental study on scaling the explosion resistance of a one-way square reinforced concrete slab under a close-in blast loading," *International journal of impact engineering*, vol. 49, no. 11, pp. 158-164, 2012.
- [14] W. Wang, D. Zhang, F. Lu, S.-c. Wang and F. Tang, "Experimental study and numerical simulation of the damage mode of a square reinforced concrete slab under close in explosion," *Engineering Failure Analysis*, vol. 27, no. 1, pp. 41-51, 2013.
- [15] T. Jankowiak and T. Lodygowski, "Identification of Parameters of Concrete Damage Plasticity Constitutive Model," *Foundations of Civil and Environmental Engineering*, vol. 6, 2005.
- [16] K. Vedantam, D. Bajaj, N. Brar and S. Hill, "Johnson - Cook Strength Models For Mild and DP 590 Steels," *American Institute of Physics*, 2006.
- [17] S. Guruprasad and A. Mukherjee, "Layered sacrificial claddings under blast loading, Part 1 - Analytical studies," *International Journal of Impact Engineering*, vol. 24, no. 10, pp. 957-973, 2000.
- [18] S. Guruprasad and A. Mukherjee, "Layered sacrificial claddings under blast loading Part 2 - Experimental Studies," *International Journal of Impact Engineering*, vol. 24, no. 10, pp. 975-984, 2000.
- [19] R. Cook, D. Malkus, M. Phelsha and R. Witt, *Concepts and applications of finite element analysis*, WILEY, 2007.



[20] H. Kolsky, Stress waves in solids, Dover publications, 1963.

[21] A. Schenker, I. Anteby, E. Gala, Y. Kivity, E. Nizria and O. Sadota, "Full-scale field tests of concrete slabs subjected to blast loads," *International Journal of Impact Engineering*, vol. 35, no. 3, pp. 184-198, 2008.

